NASA/TM-20250004725

Testing of Sunscreen-Protected Silicone Seals From MISSE–12 and MISSE–13 On-Orbit Flights

Janice L. Mather
The University of Akron, Akron, Ohio

Kim K. de Groh and Henry C. de Groh III
Glenn Research Center, Cleveland, Ohio

May 2025

NASA STI Program Report Series

Since its founding, NASA has been dedicated to the advancement of aeronautics and space science. The NASA scientific and technical information (STI) program plays a key part in helping NASA maintain this important role.

The NASA STI program operates under the auspices of the Agency Chief Information Officer. It collects, organizes, provides for archiving, and disseminates NASA's STI. The NASA STI program provides access to the NTRS Registered and its public interface, the NASA Technical Reports Server, thus providing one of the largest collections of aeronautical and space science STI in the world. Results are published in both non-NASA channels and by NASA in the NASA STI Report Series, which includes the following report types:

- TECHNICAL PUBLICATION.
  Reports of completed research or a major significant phase of research that present the results of NASA programs and include extensive data or theoretical analysis. Includes compilations of significant scientific and technical data and information deemed to be of continuing reference value. NASA counterpart of peer-reviewed formal professional papers but has less stringent limitations on manuscript length and extent of graphic presentations.

- TECHNICAL MEMORANDUM.
  Scientific and technical findings that are preliminary or of specialized interest, e.g., quick release reports, working papers, and bibliographies that contain minimal annotation. Does not contain extensive analysis.

- CONTRACTOR REPORT.
  Scientific and technical findings by NASA-sponsored contractors and grantees.

- CONFERENCE PUBLICATION.
  Collected papers from scientific and technical conferences, symposia, seminars, or other meetings sponsored or cosponsored by NASA.

- SPECIAL PUBLICATION.
  Scientific, technical, or historical information from NASA programs, projects, and missions, often concerned with subjects having substantial public interest.

- TECHNICAL TRANSLATION.
  English-language translations of foreign scientific and technical material pertinent to NASA's mission.

Specialized services also include organizing and publishing research results, distributing specialized research announcements and feeds, providing information desk and personal search support, and enabling data exchange services.

For more information about the NASA STI program, see the following:

- Access the NASA STI program home page at http://www.sti.nasa.gov

NASA/TM-20250004725

Testing of Sunscreen-Protected Silicone Seals From MISSE–12 and MISSE–13 On-Orbit Flights

Janice L. Mather
The University of Akron, Akron, Ohio

Kim K. de Groh and Henry C. de Groh III
Glenn Research Center, Cleveland, Ohio

National Aeronautics and
Space Administration

Glenn Research Center
Cleveland, Ohio 44135

May 2025

Acknowledgments

The authors are grateful to the NASA Flight Opportunities program, the International Space Station Program Office, and Aegis Aerospace for making these flight opportunities possible. We would also like to thank Richard Martin of HX5, LLC at NASA Glenn for performing the SEM imaging of the MISSE–13 flight and control samples. This work was funded under NASA contract numbers NNC13TA85T.01 and 80GRC020D0003.

Level of Review: This material has been technically reviewed by technical management.

This report is available in electronic form at https://www.sti.nasa.gov/ and https://ntrs.nasa.gov/

NASA STI Program/Mail Stop 050
NASA Langley Research Center
Hampton, VA 23681-2199

Testing of Sunscreen-Protected Silicone Seals From MISSE–12 and MISSE–13 On-Orbit Flights

Janice L. Mather
The University of Akron
Akron, Ohio 44325

Kim K. de Groh and Henry C. de Groh III*
National Aeronautics and Space Administration
Glenn Research Center
Cleveland, Ohio 44135

Summary

In a continued investigation of the effects of space environments, silicone S0383–70 test articles were flown as part of the Materials International Space Station Experiment–12 (MISSE–12) and MISSE–13 Polymers and Composites Experiments–3 (PCE–3) and PCE–4, respectively, on the exterior of the International Space Station (ISS). The effects of simultaneous exposure to space environments (temperature, vacuum pressure, atomic oxygen (AO), and ultraviolet (UV) radiation) on the silicone compound were explored for test articles fabricated from S0383–70 with and without coatings applied to the surface. The following three coatings were evaluated: Braycote® 601EF grease (BP Lubricants USA Inc.), Braycote® 601EF plus Z–COTE® zinc oxide powder (BASF Corp.) (BZ coating), and Dow Corning® 7 (DC7) grease (Dow Corning Corp.) plus Z–COTE® (DCZ coating). In addition, tests articles fabricated from a reformulated silicone compound of S0383–70 with titanium dioxide (TiO_2) were part of the investigation. The Braycote® 601EF-coated test articles represented the current-use configuration of the S0383–70 material as a docking seal. The other two coatings were sunscreens developed at the NASA Glenn Research Center to prevent damage to the elastomer from UV radiation. Like the sunscreen coatings, the reformulated compound was designed to minimize the effects of UV radiation. The primary objective of this study was to compare the effectiveness of the countermeasures designed to protect silicone seals from the space environment. Physical properties of color, mass, and durometer hardness and the performance property of leak rate were evaluated to determine the effectiveness of these protective measures. Evidence of changes or damage to the surfaces was observed in the photographs and scanning electron microscopy (SEM) images of the test articles, and the change in fluorescence indicated some change at the molecular level. The leak rates measured for test articles fabricated with the baseline S0383–70 compound and the reformulated compound significantly increased to unacceptable levels, indicating the concentration of the TiO_2 particles was not great enough to protect the material. However, the leak rates of the test articles with surface coatings were no different than those of the ground control (i.e., unexposed) test articles, indicating the coating provided protection to the underlying material. Overall, the coatings provided protection to the S0383–70 elastomer from the damaging effects of space environments. The coatings were durable and still intact at the end of the mission. The positive results obtained from the MISSE–12 and MISSE–13 test articles will aid in the continued advancement of the BZ and DCZ coatings as viable options for silicone space seals.

*Currently retired.

Acronyms

AO	atomic oxygen
BZ	Braycote® 601EF plus Z–COTE®
DC7	Dow Corning® 7
DCZ	DC7 grease plus Z–COTE®
DSLR	digital single-lens reflex
ELC	Express Logistics Carrier
ESH	equivalent Sun hours
FOD	foreign object debris
ID	identification
ISS	International Space Station
MISSE	Materials International Space Station Experiment
MISSE–FF	MISSE Flight Facility
MSC	MISSE Sample Carrier
PCE	Polymers and Composites Experiments
SEM	scanning electron microscope/microscopy
UV	ultraviolet
UVA	ultraviolet A
UVB	ultraviolet B
UVC	ultraviolet C

1.0 Introduction and Background

Silicone elastomer seals are used on space vehicles in docking and hatch systems, in part due to their large operating temperature range. When exposed to space environments, the silicone material can be damaged from vacuum, atomic oxygen (AO), and ultraviolet (UV) radiation exposure. For this reason, NASA has been investigating ways of protecting the seals from these exposures. Some solutions for protecting the silicone material include covers, coatings, or a reformulation of the elastomer compound to withstand or attenuate the damage. Each solution comes with its own challenges—covers require additional mass, logistics, and operations; coatings can attract or retain debris or may need to be reapplied; and reformulating the compound could modify the desirable material properties. Several studies of silicone seals coated with a UV-radiation-blocking material containing zinc oxide (ZnO) have shown promising results (Refs. 1 to 4). In a continued investigation of the effects of space environments, silicone S0383–70 test articles were flown as part of the Materials International Space Station Experiment–12 (MISSE–12) and MISSE–13 Polymers and Composites Experiments–3 (PCE–3) and PCE–4, respectively, on the exterior of the International Space Station (ISS) (Refs. 5 and 6). In addition to the coated test articles, test articles of the baseline S0383–70 material and a reformulated material were included for comparison. The reformulated compound contained titanium dioxide (TiO_2), another mineral used to block UV radiation. The MISSE–12 test articles were on MISSE Sample Carrier (MSC) 4 and MSC 6, oriented in the ram-facing and wake-facing directions, respectively. The wake-facing MSC 6 was not opened; therefore, the wake-facing test articles were reflown on MISSE–15 on MSC 10. The MISSE–13 test articles were on MSC 5 and MSC 19, oriented in the wake-facing and zenith-facing directions, respectively.

2.0 Objectives

The primary objective of this study was to compare the effectiveness of countermeasures designed to protect silicone seals from the space environment. The S0383–70 baseline material was compared with coated S0383–70 test articles and test articles fabricated from a reformulated silicone compound. Three coatings were tested: Braycote® 601EF grease (BP Lubricants USA Inc.), Braycote® 601EF grease mixed with Z–COTE® (BASF Corp.), and Dow Corning® 7 (DC7) grease (Dow Corning Corp.) mixed with Z–COTE®. Z–COTE® is an extremely fine (nanometer-sized) ZnO powder. The reformulated silicone compound was S0383–70 with 1.5 wt% TiO_2. Specifically, the physical properties of color, mass, and durometer hardness and the performance property of leak rate were evaluated to determine the effectiveness of these protective measures. The test articles were simultaneously exposed to the space environments of temperature, vacuum, AO, UV radiation, and ionizing and electromagnetic radiation while on the ISS MISSE Flight Facility (MISSE–FF) as part of PCE–3 and PCE–4. Exposures to ionizing and electromagnetic radiation were not reported and were not included in this study. The durability of the coatings was qualitatively evaluated through visual observation.

3.0 Test Article Description

The test articles for both MISSE–12 and MISSE–13 began with the baseline silicone material S0383–70. The MISSE–12 test articles were made by first punching a 1-in. circle from a 0.08-in.-thick sheet of material and then manually cutting the circle into two semicircle pieces (Figure 1). The MISSE–13 test articles were cut from 0.22-in.-thick sheets of material, either S0383–70 or S0383–70 with 1.5 wt% TiO_2 (herein referred to as "1.5% TiO_2"). The MISSE–13 test article assembly consisted of an outer ring, a flat ring, and a button (Figure 2). Using a laser cutter (Epilog® Laser Fusion system, Epilog Corp.), the three diameters in the test article assembly (1.0, 0.835, and 0.040 in.) were cut into the sheet material to a depth of approximately 0.1 in. The test article assemblies were then removed from the sheet material using a punch, leaving the three components of the assembly attached. Isopropyl alcohol was the solvent used to remove the soot from the outside of the test article assembly and from the remaining cut diameter grooves.

Four categories of test articles were prepared for MISSE–12 and five for MISSE–13. The first category was the baseline S0383–70 material. The next three categories consisted of different coatings applied to the baseline material. Braycote® 601EF grease from Castrol® (Castrol Corp.) was selected because it is a typical grease applied to space seals to aid in installation. A perfluorinated, polyether-based grease, Braycote® 601EF is space rated and has been shown to reduce adhesion between the seal and the mating surface. The other two coatings were options being explored to mitigate the harmful effects of UV radiation on the elastomer. Both coatings contained 17% by weight of Z–COTE®, which consists of ZnO nanoparticles that block both ultraviolet A (UVA) (315 to 400 nm) and ultraviolet B (UVB) (280 to 315 nm) radiation (Ref. 7). In one coating, the Z–COTE® was mixed with Braycote® 601EF grease; this coating is referred to as "BZ." In the other coating, Z–COTE® was mixed with DC7 grease, a dimethyl silicone compound used as a mold release agent as well as a lubricant. This coating is referred to as "DCZ." These four categories (baseline plus baseline coated test articles) were categories for both MISSE–12 and MISSE–13. The additional category for MISSE–13 was a reformulated compound of S0383–70 with 1.5% TiO_2 blended into the compound. Similar to ZnO, TiO_2 is a mineral that reflects UV rays. Blending TiO_2 into the baseline compound has the potential benefit of mitigating the effects of UV radiation without introducing a coating that could degrade, be removed, or act as a foreign object debris (FOD) collector; however, as the TiO_2 particle size decreases, the mineral's effectiveness in blocking UVA radiation also decreases.

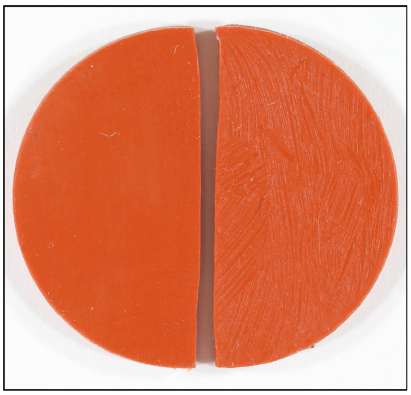

Figure 1.—MISSE–12 test articles.

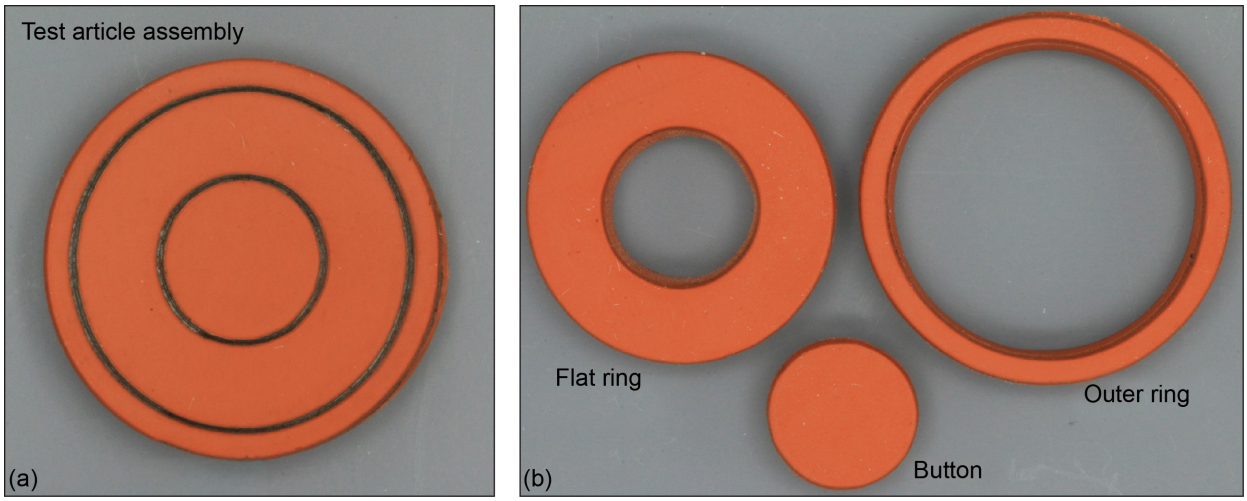

Figure 2.—MISSE–13 baseline S0383–70 test articles. (a) Test article assembly. (b) Separated into individual parts.

The five categories of test articles fell into one of two groups, uncoated or coated, as listed here:

1. Uncoated: Baseline material S0383–70, Figure 3(a) (MISSE–12) and Figure 4(a) (MISSE–13).
2. Uncoated: Reformulated baseline material with 1.5% TiO_2 added to the compound, Figure 4(b) (MISSE–13).
3. Coated: Baseline material with Braycote® 601EF grease applied to top surface, Figure 3(b) (MISSE–12) and Figure 4(c) (MISSE–13).
4. Coated: Baseline material with a mixture of Braycote® 601EF grease and Z–COTE® applied to the top surface (BZ), Figure 3(c) (MISSE–12) and Figure 4(d) (MISSE–13).
5. Coated: Baseline material with a mixture of DC7 and Z–COTE® applied to the top surface (DCZ), Figure 3(d) (MISSE–12) and Figure 4(e) (MISSE–13).

There were five sets of MISSE–12 test articles; each set contained one test article from each category for a total of 20 test articles. Two of the sets were flight test articles, two sets were flight backup test articles, and the fifth set remained at the NASA Glenn Research Center as a ground control set. The flight test articles were part of the PCE–3 experiment, with one set oriented in the ram-facing direction and the other set in the wake-facing direction. After integration, the two backup sets were returned to Glenn and stored at the Center.

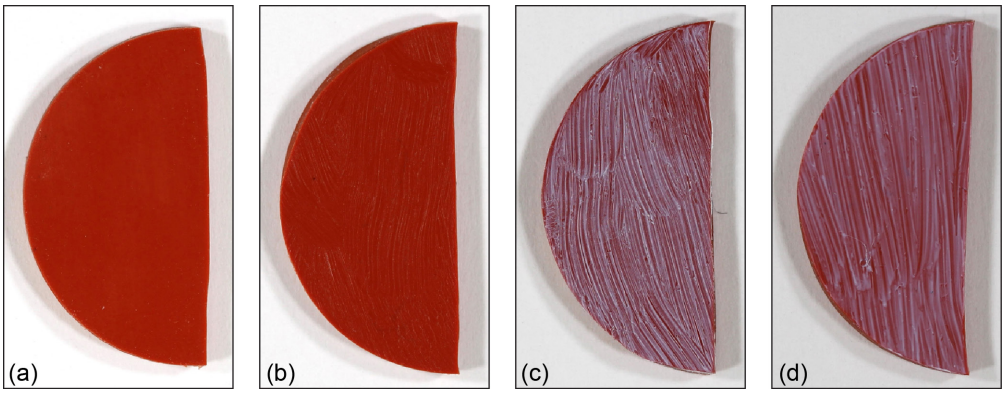

Figure 3.—MISSE–12 test articles. (a) Baseline material S0383–70. (b) Baseline material with Braycote® 601EF coating. (c) Baseline material with Braycote® 601EF plus Z–COTE® coating (BZ). (d) Baseline material with DC7 plus Z–COTE® coating (DCZ).

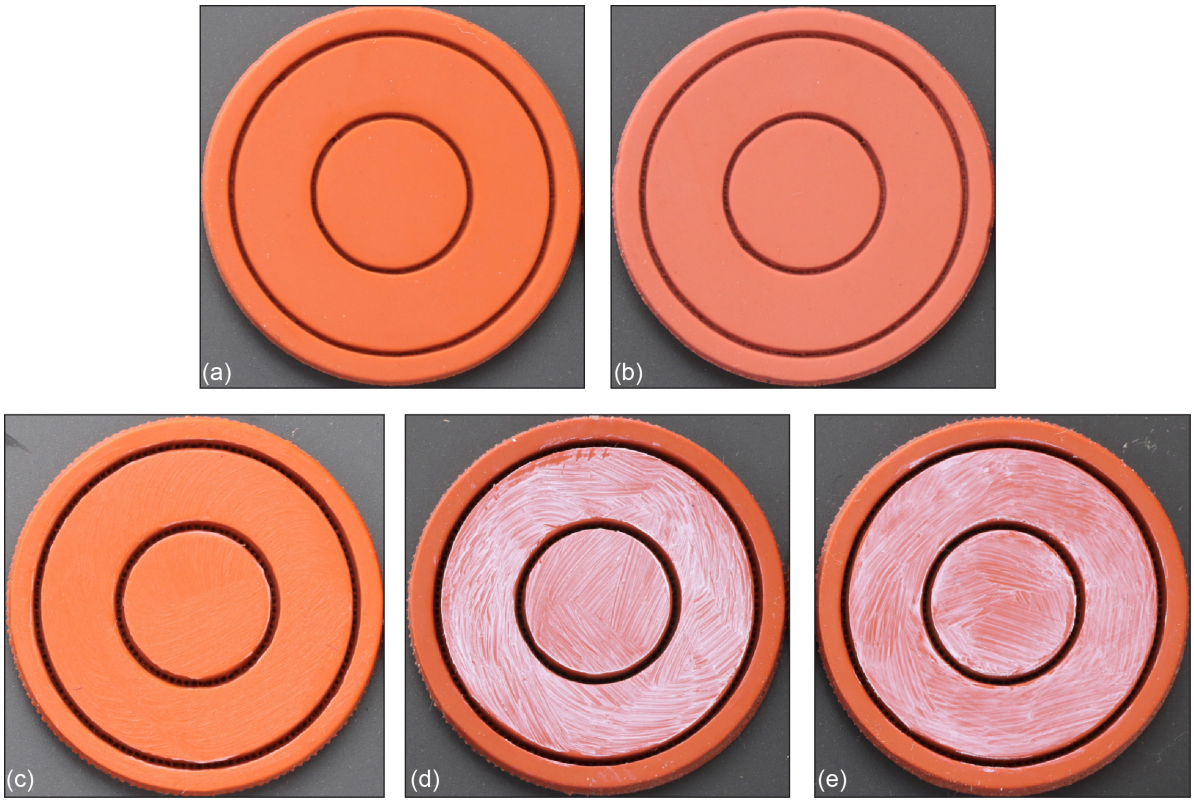

Figure 4.—MISSE–13 test article assemblies. (a) Baseline material S0383–70. (b) Baseline material with 1.5% TiO_2. (c) Baseline material with Braycote® 601EF coating. (d) Baseline material with BZ coating. (d) Baseline material with DCZ coating.

Thirty-five MISSE–13 test article assemblies were cut out, 26 from the baseline material and 9 from the 1.5% TiO_2 material. Of the 26, 7 were uncoated S0383–70 baseline material, 7 were coated with Braycote® 601EF grease, 6 were coated with the BZ mixture, and 6 were coated with the DCZ mixture. Four each of the baseline, Braycote® 601EF, BZ, and DCZ test articles were provided to the PCE–4 experiment along with six of the nine 1.5% TiO_2 assemblies as flight and backup test articles. The remaining test article assemblies were classified as ground control test articles that stayed at Glenn. Like the MISSE–12 backups, the MISSE–13 backup test article assemblies were returned to Glenn after integration.

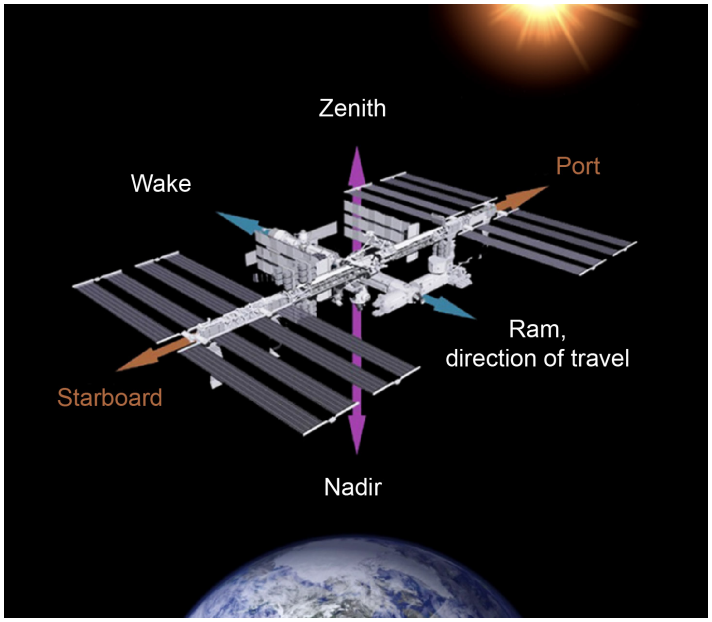

Figure 5.—Orientations with respect to ISS.

There are six orientations with respect to the ISS: starboard, port, nadir (Earth facing), zenith (space facing), ram (direction of travel), and wake (opposite direction of ram), as shown in Figure 5. The MISSE–12 test articles were installed on carrier trays for the ram-facing and wake-facing directions, and the MISSE–13 test articles were installed in the zenith-facing and wake-facing orientations.

All of the test articles for MISSE–12 and MISSE–13 are listed in Table I and Table II, sorted by test article category. Along with the test article identification (ID) number, the flight orientation and corresponding flat ring and button ID numbers for the MISSE–13 assemblies are given. The test article ID is based on the PCE sample ID, which provides the MISSE mission number (M12 or M13), the flight orientation (ram (R), wake (W) or zenith (Z)), the sample's shape (i.e., circular (C)), and the ID number. For example, M13W–C9 was a circular sample (no. 9) flown on the MISSE–13 mission in the wake direction. The MISSE–12 test article ID is the PCE sample ID with additional terms that describe the test article (ram (R), wake (W), uncoated (U), Braycote® 601EF (B), BZ coating (ZB), and DCZ coating (ZDC7)). A "B" preceding the "R" or "W" indicates the test article was a backup. The MISSE–13 flight and backup test article IDs are the same as the PCE sample IDs. The MISSE–13 ground control test article ID provides the mission number (M13), the designation for ground control (GC), the test article category (S for baseline, T for 1.5% TiO_2, or B for Braycote® 601EF), and the serial number. Figure 6 through Figure 9 are sample map diagrams that show the location of each test article installed on its respective carrier tray. Figure 10 and Figure 11 are photographs of the preflight installed test articles. For MISSE–12, the semicircular test articles were separated with an aluminum spacer bar. As shown in Figure 11, the outer ring of the MISSE–13 test article assembly was covered, leaving the top surfaces of the flat ring and button uncovered. While on flight, the entire test article was exposed to the vacuum pressures and temperatures of space, but only the top surfaces of the flat ring and button were exposed to UV radiation and AO. The outer edges of the MISSE–12 test articles were covered in the same way. Figure 12 shows the MISSE–FF on the ISS, and Figure 13 shows the location of carrier tray MSC 19 on the MISSE–FF (as seen from the top of the carrier).

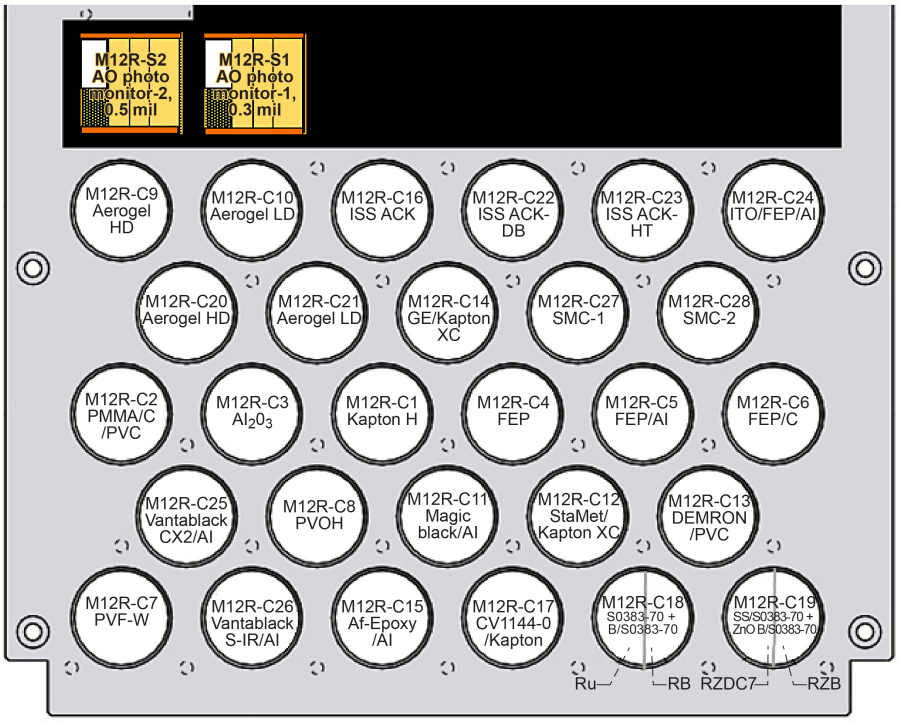

Figure 6.—MISSE–12 test article positions on ram tray (MSC 4).

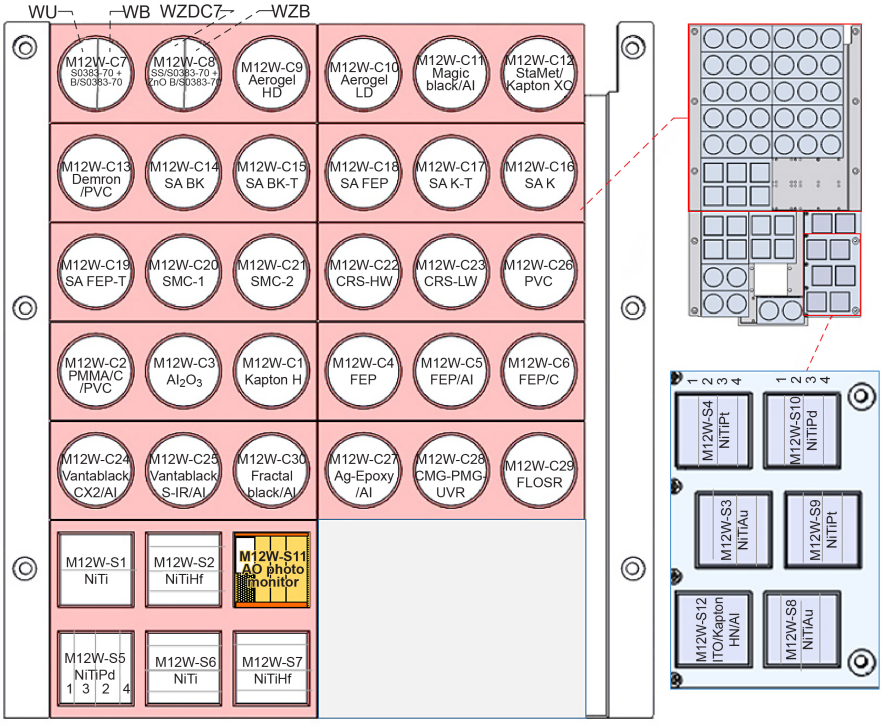

Figure 7.—MISSE–12 test article positions on wake tray (MSC 6); reflown on MISSE–15 wake tray (MSC 10).

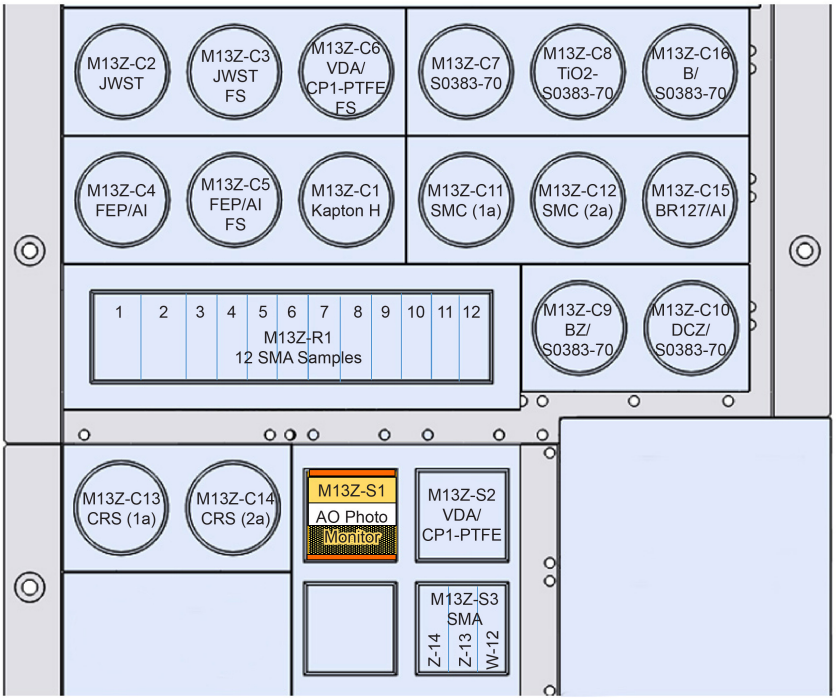

Figure 8.—MISSE–13 test article positions on zenith tray (MSC 19).

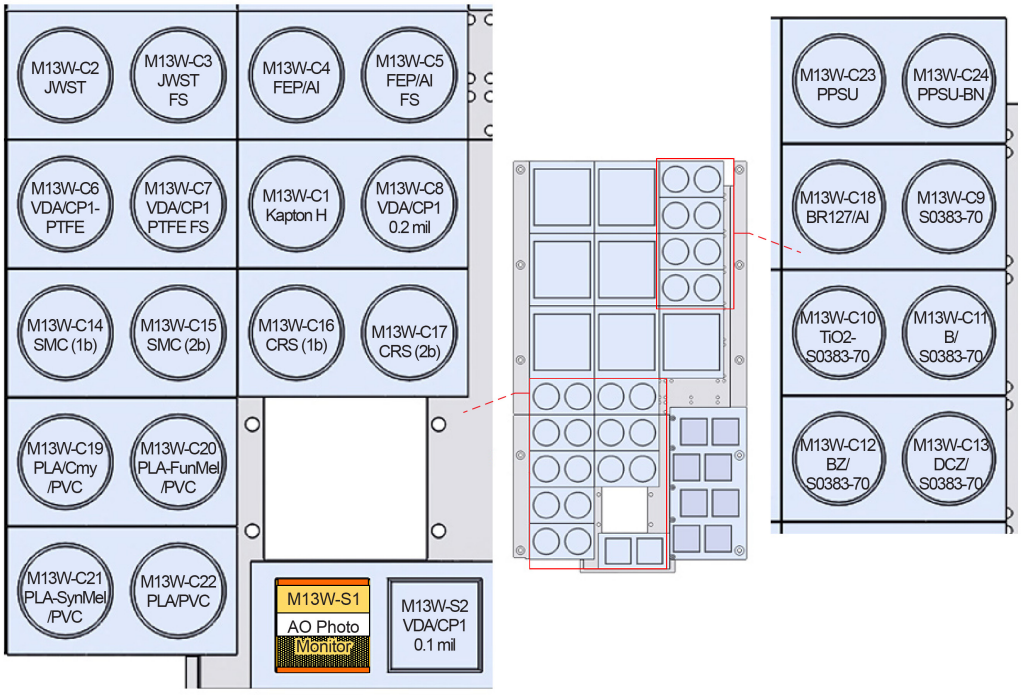

Figure 9.—MISSE–13 test article positions on wake tray (MSC 5).

Figure 10.—Carrier trays preflight with MISSE–12 test articles installed. (a) Ram. (b) Wake.

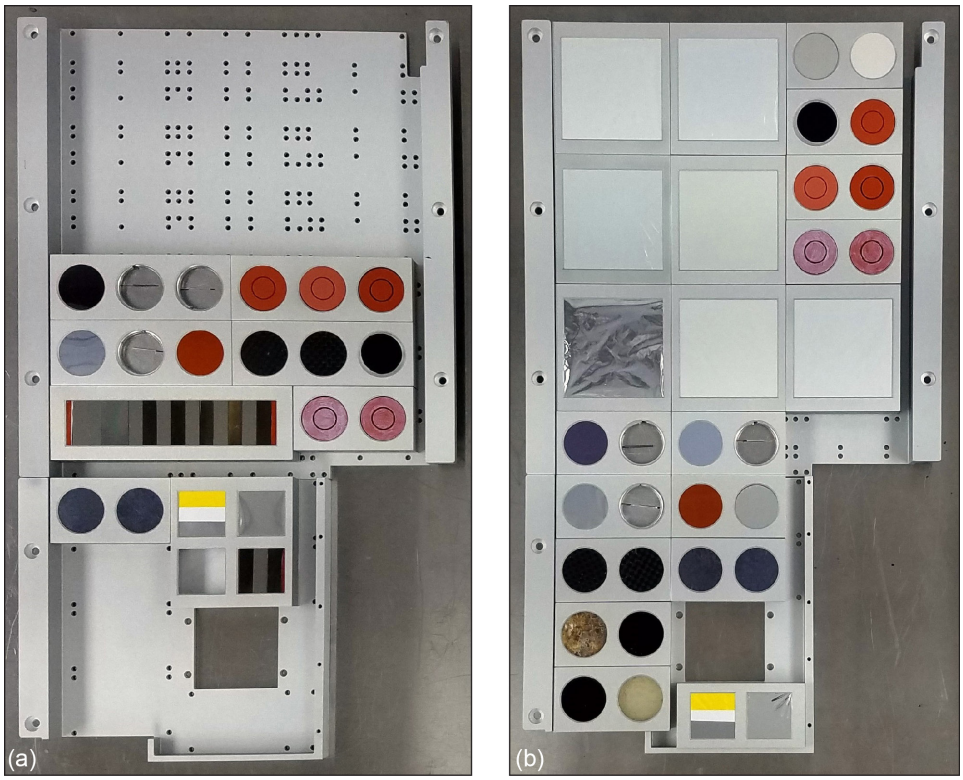

Figure 11.—Carrier trays preflight with MISSE–13 test articles installed. (a) Zenith. (b) Wake.

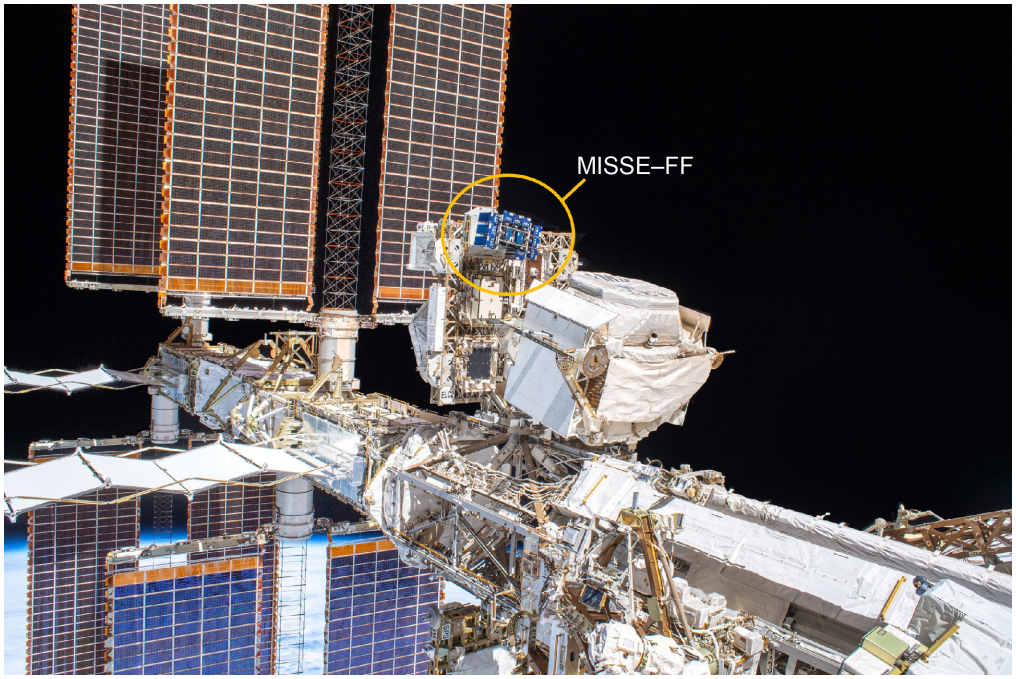

Figure 12.—MISSE–FF on ISS.

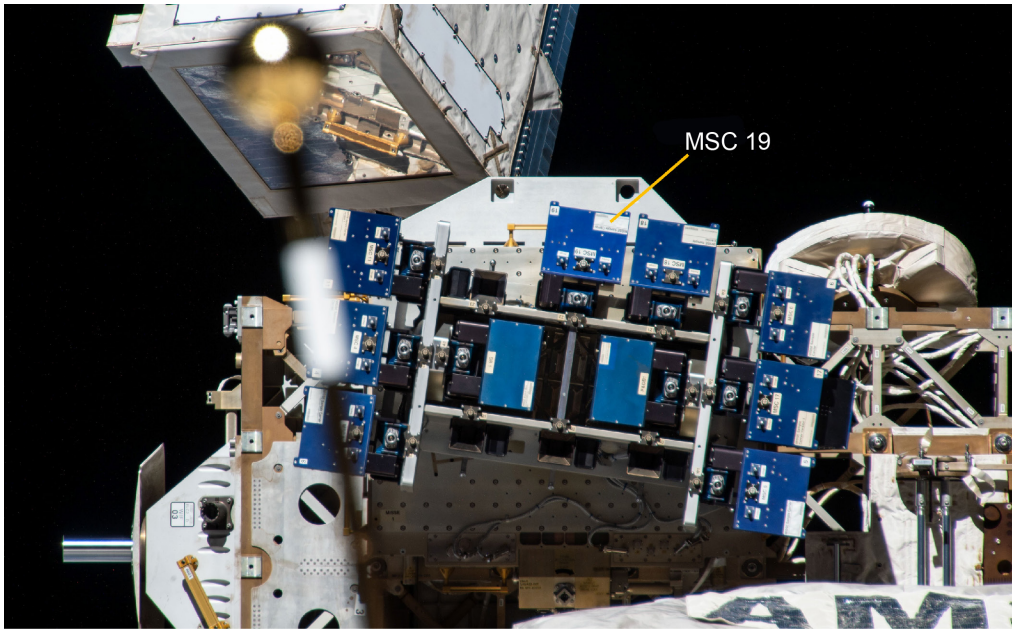

Figure 13.—MSC 19 (zenith-facing) location on MISSE–FF.

TABLE I.—FLIGHT AND BACKUP TEST ARTICLES

Description	Test article ID	Flat ring ID	Button ID	Orientation
Baseline material S0383–70	M12R–C18 Part 1 RU	NA	NA	Ram facing
	M12W–C7 Part 1 WU	NA	NA	Wake facing
	M13W–C9	19–59	19–60	Wake facing
	M13Z–C7	19–63	19–64	Zenith facing
	M12R–C18 Part 1 BRU	NA	NA	Backup
	M12W–C7 Part 1 BWU	NA	NA	
	M13W–C9R	19–61	19–62	
	M13Z–C7R	19–65	19–66	
Baseline material with 1.5% TiO_2	M13W–C10	19–45	19–46	Wake facing
	M13Z–C8	19–49	19–50	Zenith facing
	M13W–C7	19–41	19–42	Backup
	M13W–C7R	19–43	19–44	
	M13W–C10R	19–47	19–48	
Baseline material top surface coated with Braycote® 601EF	M12R–C18 Part 2 RB	NA	NA	Ram facing
	M12W–C7 Part 2 WB	NA	NA	Wake facing
	M13Z–C8R	19–51	19–52	Wake facing
	M13Z–C16	19–77	19–78	Zenith facing
	M12R–C18 Part 2 BWB	NA	NA	Backup
	M12W–C7 Part 2 BWB	NA	NA	
	M13W–C11R	19–75	19–76	
	M13Z–C16R	19–79	19–80	
Baseline material top surface coated with BZ mixture	M12R–C19 Part 2 RZB	NA	NA	Ram facing
	M12W–C8 Part 2 WZB	NA	NA	Wake facing
	M13W–C12	BZW–C12 FR	BZW–C12 B	Wake facing
	M13Z–C9	BZZ–C9 FR	BZZ–C9 B	Zenith facing
	M12R–C19 Part 2 BRZB	NA	NA	Backup
	M12W–C8 Part 2 BWZB	NA	NA	
	M13W–C12R	BZW–C12R FR	BZW–C12R B	
	M13Z–C9R	BZZ–C9R FR	BZZ–C9R B	
Baseline material top surface coated with DCZ mixture	M12R–C19 Part 1 RZDC7	NA	NA	Ram facing
	M12W–C8 Part 1 WZDC7	NA	NA	Wake facing
	M13W–C13	DCZW–C13 FR	DCZW–C13 B	Wake facing
	M13Z–C10	DCZZ–C10 FR	DCZZ–C10 B	Zenith facing
	M12R–C19 Part 1 BRZDC7	NA	NA	Backup
	M12W–C8 Part 1 BWZDC7	NA	NA	
	M13W–C13R	DCZW–C13R FR	DCZW–C13R B	
	M13Z–C10R	DCZZ–C10R FR	DCZZ–C10R B	

TABLE II.—GROUND CONTROL TEST ARTICLES

Description	Test article ID	Flat ring ID	Button ID
Baseline material S0383–70	M12W–C7 Part 1 CWU	NA	NA
	M13GC–S–1	19–67	19–68
	M13GC–S–2	19–69	19–70
	M13GC–S–3	19–71	19–72
Baseline material with 1.5% TiO_2	M13GC–T–1	19–53	19–54
	M13GC–T–2	19–55	19–56
	M13GC–T–3	19–57	19–58
Baseline material top surface coated with Braycote® 601EF	M12W–C7 Part 2 CWB	NA	NA
	M13GC–B–1	19–81	19–82
	M13GC–B–2	19–83	19–84
	M13GC–B–3	19–85	19–86
Baseline material top surface coated with BZ mixture	M12W–C8 Part 2 CWZB	NA	NA
	BL–1	BL–1	B5
	BL–2	BL–2	B6
Baseline material top surface coated with DCZ mixture	M12W–C8 Part 1 CWZDC7	NA	NA
	BL–3	BL–3	B7
	BL–4	BL–4	B8

4.0 Flight Missions

On November 2, 2019, the MISSE–12 carrier trays were launched to the ISS aboard the Northrup Grumman Cygnus NG–12 mission. The carriers were subsequently installed on the MISSE–FF on November 11, 2019. The MISSE–12 ram carrier was opened and closed between December 3, 2019, and November 25, 2020. On March 6, 2020, the MISSE–13 carrier trays were launched to the ISS aboard the SpaceX–20 mission. The carriers were subsequently installed on the MISSE–FF on March 18, 2020. Figure 14 shows carriers MSC 5 and MSC 19 on the ISS in preparation for deployment of the MISSE–13 flight. The MISSE–13 carriers were opened and closed between March 20, 2020, and September 3, 2020. The zenith-facing carrier, MSC 19, was retrieved from the flight facility on November 26, 2020, and the wake-facing carrier, MSC 5, was retrieved the following day (November 27, 2020). The MISSE–12 carriers were retrieved from the MISSE–FF a year after installation on November 25, 2020 (MSC 4, ram facing) and on November 27, 2020 (MSC 6, wake facing). All carriers were repressured on December 1, 2020, and returned to Earth aboard the SpaceX–21 mission on January 13, 2021 (January 14, 2021 (UTC)). The 22 MISSE–13 test article assemblies were received on April 27, 2022, for postflight evaluations.

The wake-facing carrier for MISSE–12 was not opened during the flight. Therefore, these test articles were reflown during the MISSE–15 mission. On August 29, 2021, the MISSE–15 carrier trays were launched aboard the SpaceX–23 mission. The MISSE–15 wake carrier tray (MSC 10) was installed on the MISSE–FF on December 28, 2021, and retrieved on August 2, 2022. The test articles returned to Earth on August 20, 2022, with the SpaceX–25 mission. The 20 MISSE–12/MISSE–15 wake test articles were received on June 15, 2023, for postflight evaluations.

Details of these missions can be found in NASA/TM-20240000755 (Ref. 5).

Figure 14.—MSC 5 and MSC 19 on ISS prior to deployment to MISSE–FF.

4.1 Vacuum Pressure and Space Exposure Durations

The test article assemblies were exposed to space vacuum pressure while in the transfer tray and while on the MISSE–FF. The total time on the MISSE–FF was 1.04 yr (MISSE–12 ram facing), 1.65 yr (MISSE–12/MISSE–15 wake facing), and 0.70 yr (MISSE–13 wake facing and zenith facing). Of the 1.65 yr, 1.05 yr was during the MISSE–12 flight and 0.60 yr was during the MISSE–15 flight. The overall total exposure time to space vacuum pressure was 1.07 yr (MISSE–12 ram facing), 1.78 yr (MISSE–12/ MISSE–15 wake facing), and 0.72 yr (MISSE–13).

The carriers needed to be open to have direct space exposure (i.e., exposure to AO and UV radiation). Carrier MSC 4 (MISSE–12 ram-facing carrier) had 0.89 yr of direct space exposure, carrier MSC 10 (MISSE–12/MISSE–15 wake-facing carrier) and carrier MSC 5 (MISSE–13 wake-facing carrier) each had 0.44 yr of direct space exposure, and carrier MSC 19 (MISSE–13 zenith-facing carrier) had 0.46 yr of exposure.

4.2 Temperature

The temperature of the MSCs depends on the orientation of the ISS and the Sun's beta angle. Temperature sensors measure the anodized aluminum deck of the MSCs, and typical temperature ranges are –30 to 45 °C, –26 to 45 °C, and –20 to 50 °C for ram-facing, wake-facing, and zenith-facing directions, respectively (Ref. 5). It was assumed that the temperatures of the test articles and test article assemblies were within the typical ranges throughout the duration of the flights.

4.3 Atomic Oxygen and Ultraviolet Radiation Exposure

For a given period, test articles installed in ram-facing MSCs will have the greatest exposure to AO; AO exposure values for the other orientations will be orders of magnitudes less than the ram-facing value. The ram-facing MISSE–12 test articles (MSC 4) received 2.97×10^{20} atoms/cm^2 of AO exposure, whereas the AO exposure for the MISSE–12 wake-facing and MISSE–13 wake- and zenith-facing carriers was two orders of magnitude less (Ref. 5). The MISSE–12 wake-facing test articles (MSC 10) were exposed to an AO fluence of 4.77×10^{18} atoms/cm^2 (during the MISSE–15 mission) (Ref. 5). The MISSE–13 wake-facing and zenith-facing test articles received similar AO exposure during flight. The test articles on the wake-facing MSC (MSC 5) had an AO fluence of 2.65×10^{18} atoms/cm^2, and the zenith-facing MSC (MSC 19) had an AO fluence of 2.24×10^{18} atoms/cm^2 (Ref. 5).

The amount of UV radiation exposure a test article receives depends on several factors. These factors include

- The direction the test article was facing (ram, wake, zenith, or nadir)
- The angle or orientation of the test article surface with respect to the Sun
- The surface geometry of the test article (e.g., flat or curved)
- Reflections from other surfaces (e.g., ISS, visiting vehicles, and Earth's albedo)
- Shadowing from other surfaces
- The number of hours exposed

A UV radiation sensor was placed on each MSC to determine the UV radiation equivalent Sun hours (ESH) exposure of the mounted test articles; however, the sensor only operated when the MSC was powered. Because the MSC can be open without being powered, thus exposing the test articles to UV radiation, the UV radiation sensor does not provide the total ESH exposure. Therefore, Aegis Aerospace, Inc., calculated the ESH for each MSC orientation based on the number of hours the MSC was open and the equivalent solar irradiance for UV wavelengths 100 to 400 nm (Ref. 8). The calculated ESH values were then reported to NASA (Ref. 9). In the wake direction, the MISSE–13 wake MSC 5 was open for 3,861 h with a reported ESH exposure of 515.6, and the MISSE–12/MISSE–15 wake MSC 10 was open for 3,833 h with a reported ESH exposure of 511.7. MSC 19, in the MISSE–13 zenith-facing direction, was open for a longer period, 4,005 h, with a reported ESH of 467.9. The MISSE–12 ram MSC had the longest duration of exposure at 7,810 h open, with a corresponding ESH of 1,104.

The ESH values computed by Aegis Aerospace indicate that the wake samples received more solar exposure than the zenith samples for similar exposure duration (i.e., MISSE–13 wake and zenith). This is not consistent with expected zenith and wake exposures in low Earth orbit or with past MISSE environment exposure data. For example, for the MISSE–7 mission, which was also located at Express Logistics Carrier–2 (ELC–2) Site 3, the estimated solar exposures were 2,000 ESH for the wake direction and 4,300 ESH for the zenith direction for a 1.5-yr direct space exposure mission (Ref. 10). Thus, for MISSE–7, the estimated ESH was 2.15 times greater for zenith than for wake.

Recent analyses of thin-film tensile samples flown as part of the PCE–1 and PCE–4 experiments on MISSE–9 (wake and zenith) and MISSE–13 (wake), respectively, indicate that the zenith samples received significantly higher solar exposures than wake samples of similar exposure duration (Ref. 11). The PCE–1 and PCE–4 tensile results indicate that the ESH computations provided by Aegis Aerospace are not accurate. Thus, ESH estimates have been made based on ESH values computed for the MISSE–7 and MISSE–8 missions. Table III provides the ESH and ESH/yr for the MISSE–7 and MISSE–8 missions provided in References 10 and 12, respectively. Using the MISSE–8 ESH/yr provided in Table III, the

ESH estimates are as follows: 587 for MISSE–13 wake MSC 5; 587 for MISSE–12/MISSE–15 wake MSC 10; 1,311 for MISSE–13 zenith MSC 19; and 1,424 for MISSE–12 ram MSC 4. These MISSE–8-based ESH values are more consistent with expected flight-orientation-based solar exposures and with the PCE–1 and PCE–4 tensile results provided in Reference 11. The MISSE–8-based ESH values provide slightly higher wake ESH, higher ram ESH, and significantly higher zenith ESH. As stated in Reference 5, the MISSE–8-based ESH values are the best ESH estimates available for the PCE 1 to 4 missions. It should be kept in mind, however, that these values are lower than rough theoretical values for the wake orientation (~18% lower) and higher than rough theoretical values for the zenith orientation (~21% higher).

Table IV lists the exposure type and value for the ram-, wake-, and zenith-facing test articles. Overall, the space exposures for MSC 4 (the MISSE–12 ram-facing test articles) were greater than the space exposures for the other three MSCs (MSC 10, MSC 5, and MSC 19). The AO exposure was two orders of magnitude greater, and the UV radiation exposure was approximately 2.25 to 2.5 times as great. The two wake-facing MSCs (10 and 5) were similar with respect to the amount of time the MSC was open and the range of UV radiation exposure. The AO exposures for these two were not the same. MSC 10 (MISSE–15) received approximately twice as much AO exposure compared to MSC 5 (MISSE–13). The zenith-facing MSC for MISSE–13 (MSC 19) was open longer (144 h) than the wake-facing MSC (MSC 5) and received a similar amount of AO exposure. However, the range of UV radiation exposure was significantly greater, up to 2.5 times.

TABLE III.—MISSE–7 AND MISSE–8 SOLAR EXPOSURES

Flight Orientation	MISSE–7 exposure, yr	MISSE–7 ESH[a]	MISSE–7 ESH/yr	MISSE–8 exposure, yr	MISSE–8 ESH[b]	MISSE–8 ESH/yr
Zenith	1.5	4,300	2,867	2.14	6,100[c]	2,850
Ram	1.5	2,400	1,600	2.00	3,200[d]	1,600
Wake	1.5	2,000	1,333	2.00	2,700[d,e]	1,333
Nadir	1.5	<<2,000		2.14	800[f]	374

[a]Reference 10.

[b]Reference 12.

[c]Naval Research Laboratory computation (Ref. 12).

[d]Computed based on MISSE–7 ESH/yr (Ref. 12).

[e]Rounded up from 2,667 ESH.

[f]NASA Marshall Space Flight Center estimate (Ref. 12).

TABLE IV.—SPACE EXPOSURE PARAMETERS FOR RAM-, WAKE-, AND ZENITH-FACING MSCS ON MISSE–12/MISSE–15 AND MISSE–13 MISSIONS

	Ram-facing MISSE–12 (MSC 4)	Wake-facing		Zenith-facing MISSE–13 (MSC 19)
		MISSE–12/MISSE–15 (MSC 10)	MISSE–13 (MSC 5)	
Time MSC open	7,810 h	3,833 h	3,861 h	4,005 h
Temperature range	–30 to 45 °C	–26 to 45 °C		–20 to 50 °C
AO	2.97×10^{20} atoms/cm^2	4.77×10^{18} atoms/cm^2	2.65×10^{18} atoms/cm^2	2.24×10^{18} atoms/cm^2
UV radiation	1,104 to 1,424 ESH	511.7 to 587 ESH	515.6 to 587 ESH	467.9 to 1,311 ESH

5.0 Results—Physical Appearance

Upon return to Earth, the test article assemblies were deintegrated from the carrier trays. Figure 15 and Figure 16 are postflight photographs of the carrier trays prior to deintegration. First inspection of the MISSE–12 carrier trays showed that the coatings of the ram-facing BZ test article (ID RZB) and the wake-facing DCZ test article (ID WZDC7) were disturbed, as if something had contacted and moved across the surface (Figure 17). The disturbance of the DCZ coating was visible in a preflight photograph from Aegis Aerospace of the MISSE–15 deck, confirming the disturbance occurred prior to exposure. On the MISSE–13 carrier trays, the BZ-coated assembly in the zenith tray appeared darker in color than the BZ-coated assembly in the wake tray. Figure 18 shows side-by-side photographs of the MISSE–13 BZ-coated postflight assemblies. In this photograph, the color difference can easily be seen. Closer inspections of all test articles were conducted, and the results are summarized in the following subsections.

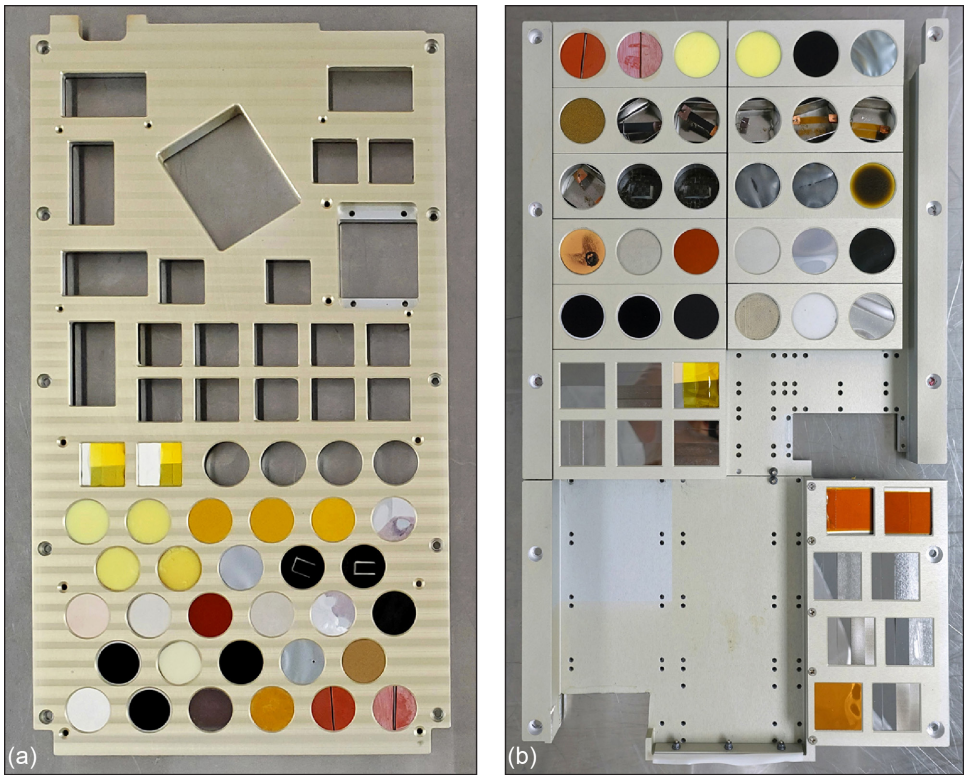

Figure 15.—Postflight PCE–3 carrier trays with MISSE–12 test articles installed. (a) Ram. (b) Wake.

Figure 16.—Postflight PCE–4 carrier trays with MISSE–13 test articles installed. (a) Zenith. (b) Wake.

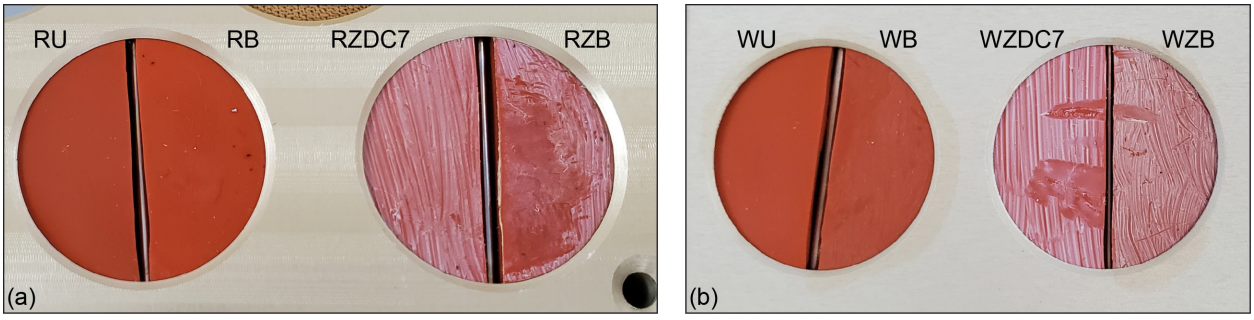

Figure 17.—MISSE–12 postflight test articles in carrier trays showing disturbed coatings of (a) RZB and (b) WZDC7 test articles.

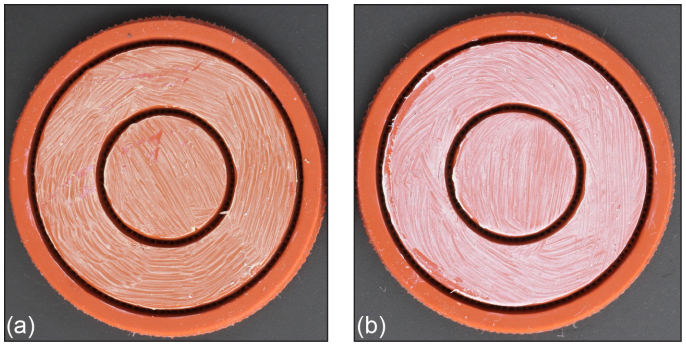

Figure 18.—MISSE–13 postflight test article assemblies with BZ coating. (a) Zenith-facing tray. (b) Wake-facing tray.

5.1 Inspection of the Exposed Surface

The top surface of each test article and test article assembly was visually inspected, and photographs were taken using a Canon® (Canon Kabushiki Kaisha) digital single-lens reflex (DSLR) camera to compare exposed flight surfaces with unexposed nonflight surfaces (i.e., controls) (Figure 19 through Figure 26). Within each category of test article, the unexposed nonflight top surface was examined first to establish a reference. For the S0383–70 baseline material, narrow parallel lines on the surface were observed from the tooling marks on the mold in which the sheet material had been formed. These features were uniformly located across the surface on the MISSE–12 baseline material and, except around the regions near the laser-cut paths, the MISSE–13 baseline material. As shown in Figure 19, the baseline material was smoothed next to the laser-cut paths (sheet material cut with a punch or razor did not have smoothed regions at the cut lines). These smoothed areas on the MISSE–13 test articles were considered heat-affected zones that resulted from the elastomer being exposed to high temperatures during the laser-cutting process. The top surfaces of the unexposed nonflight test articles laser cut from the reformulated S0383–70 compound with 1.5% TiO_2 were void of the visible tooling mark features even though the sheet material from which the test articles were cut had visible mold lines. The lack of mold lines was attributed to a larger heat-affected zone created during the laser-cutting process. The parameters for the laser cuts in the reformulated 1.5% TiO_2 material were the same as the parameters for the S0383–70 baseline material. Why the heat-affected zone was greater on the TiO_2 test articles than on the baseline test articles is unknown.

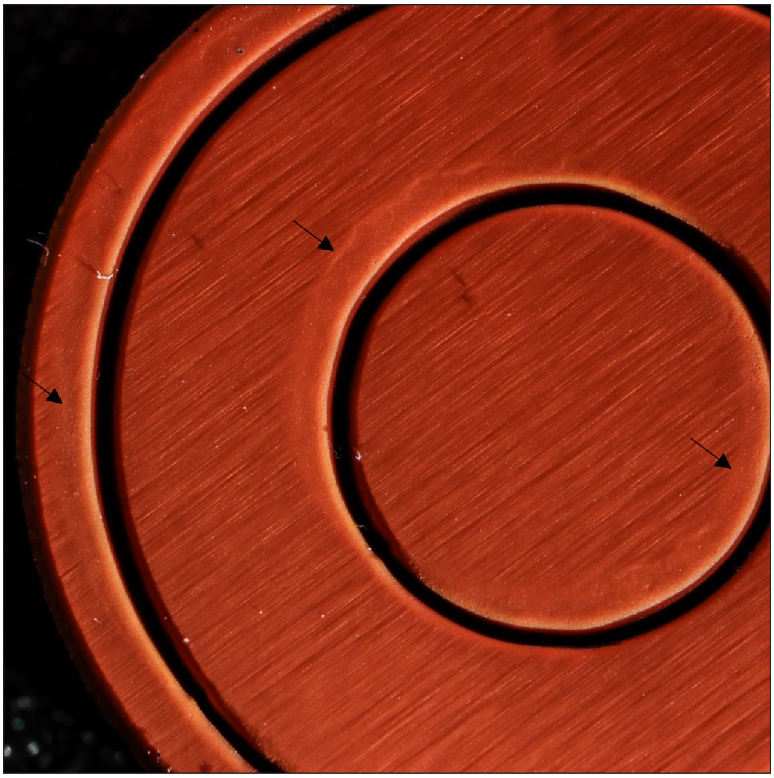

Figure 19.—Surface of S0383–70 baseline material showing smoothed material regions near laser-cut paths, indicated by arrows.

The surfaces of the uncoated exposed test articles (S0383–70 and 1.5% TiO_2) were different than those of the unexposed materials. Under close examination, the surfaces of the S0383–70 baseline material on the wake-facing and zenith-facing test articles appeared to have a faint, translucent-whitish thin film in the areas where the tooling mark features were observed, shown in Figure 20. The thin film was not observed in the heat-affected zones or on the outer ring. For the 1.5% TiO_2 material, the color of the exposed surfaces was different than that of the unexposed surface. As shown in Figure 21, the unexposed test article (Figure 21(a)) and the outer ring of the wake-facing and zenith-facing test articles (Figure 21(b) and Figure 21(c), respectively) were a salmon color, and the exposed surfaces (flat ring and button) had more of an orange hue. The outer rings did not change color, indicating that the color change was a result of exposure to UV radiation and/or AO, not temperature or vacuum pressure.

The coated test articles also showed differences between the unexposed and flight-exposed surfaces. For the test articles coated with Braycote® 601EF grease, the unexposed surface was glossy and the same orange color as the S0383–70 baseline material (Figure 22(a) and Figure 23(a)). The nonuniformity of the application of the coating was visible as swirls and lines, along with a few locations of white where excess coating accumulated (Figure 22(a)). The heat-affected zone was more visible on the MISSE–13 wake-facing surface than on either of the unexposed or zenith-facing surfaces. On both wake-facing test articles, the Braycote® 601EF coating appeared dry and the surface had a matte finish (Figure 22(b) and Figure 23(b)); however, a difference in color was observed. The MISSE–13 wake-facing test article had a

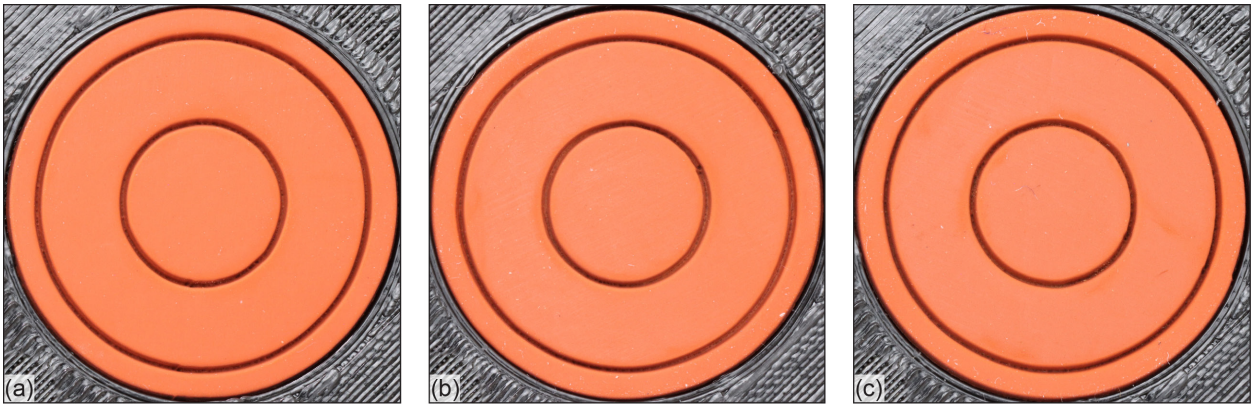

Figure 20.—Postflight MISSE–13 baseline material S0383–70 test article assemblies. (a) Unexposed. (b) Wake facing. (c) Zenith facing.

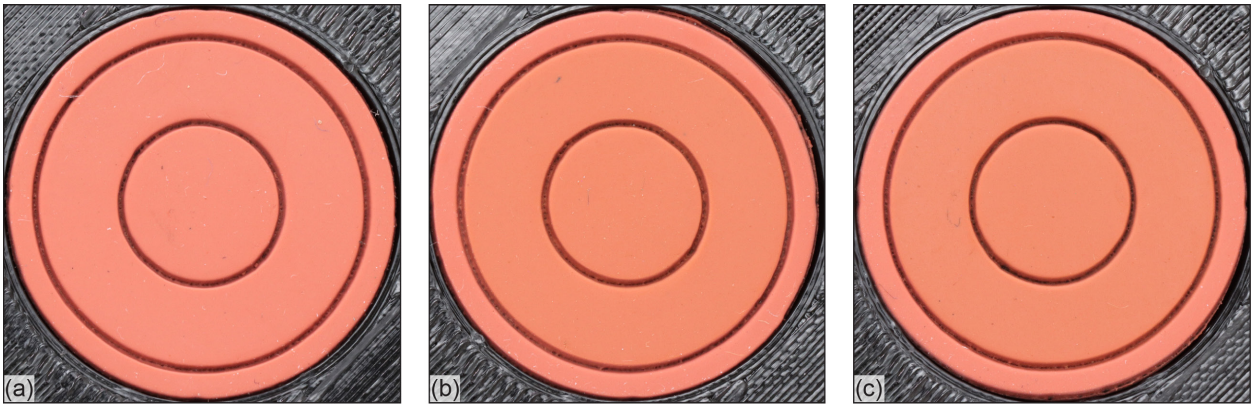

Figure 21.—Postflight MISSE–13 1.5% TiO_2 test article assemblies. (a) Unexposed. (b) Wake facing. (c) Zenith facing.

pink hue where the surface was exposed (flat ring and button) and remained orange where the surface was covered (outer ring) (Figure 22(b)). Similarly, the outer unexposed edge of the MISSE–12 wake-facing test article was distinctly different from the exposed surface area, but the color of the exposed surface was not pink like the MISSE–13 surface; it was still orange (Figure 23(b)). The MISSE–13 zenith-facing test article, which had more UV radiation exposure than the wake-facing test articles and a similar amount of AO exposure, also appeared dry with a matte finish, and some of the coating on the edge of the button appeared flaky. The color remained orange, although it was a lighter shade than the unexposed surface of the outer ring and unexposed test article (Figure 22(c)). On the MISSE–12 ram-facing test article, the contrast of color between the covered surface and the exposed surface was greater than that of wake-facing surface, with the exposed surface a darker orange color than the covered outer edge (Figure 23(c)).

The BZ coating of the unexposed test article was opaque white and glossy in appearance, with visible swirls and lines from the application process (Figure 24(a) and Figure 25(a), right semicircle). The coating on the MISSE–13 wake-facing test article surface was still opaque white, but it was less glossy than the unexposed coating and appeared drier (Figure 24(b)). In contrast, the MISSE–13 zenith-facing coating was not as white as the wake-facing coating, making the surface darker. Overall, the coating appeared more translucent in areas where the coating was not as thick, allowing more of the S0383–70 color to be seen, whereas thicker portions of the coating were still white (Figure 24(c)). The heat-affected zone of the S0383–70 material was not visible in either of the MISSE–13 BZ-coated test articles. The MISSE–12 BZ-coated test articles showed a difference in color between the outer edge that was covered and the exposed surface. The exposed surfaces were darker than the outer edge (right semicircles of Figure 24(b) and Figure 24(c)). In addition, the coating was not as glossy as the unexposed BZ coating. The BZ coating on the MISSE–12 ram-facing test article was disturbed, with a significant portion wiped away, making it challenging to assess the condition of the exposed coating (Figure 25(c)).

Like the other coated flight-test articles, the DCZ coating on the wake-, zenith-, and ram-facing test articles appeared drier and a little less glossy than the unexposed test article (Figure 25 (left semicircles) and Figure 26). No color changes were observed with the DCZ wake-facing and zenith-facing test articles. A color change was observed on the ram-facing test article; the exposed area was darker than the unexposed outer edge (Figure 25(c), left semicircle).

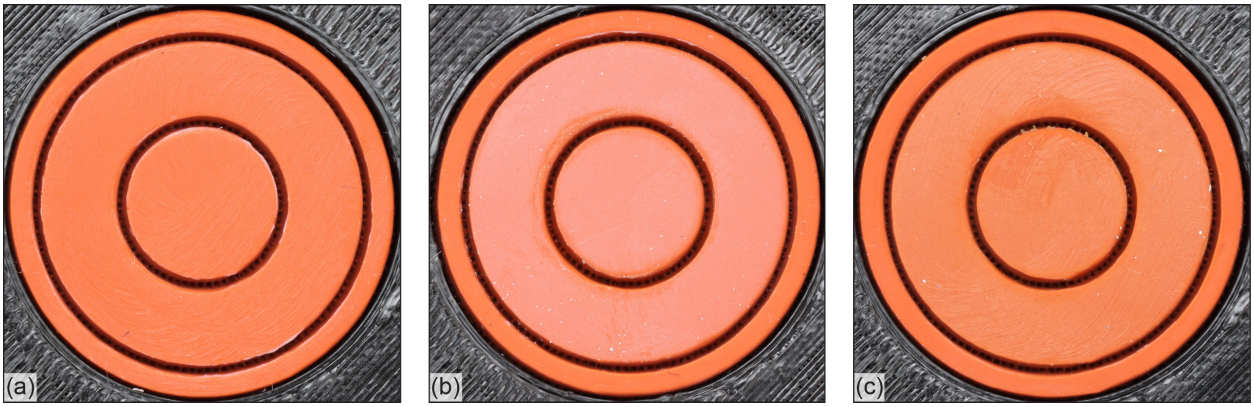

Figure 22.—Postflight MISSE–13 Braycote® 601EF-coated test article assemblies. (a) Unexposed. (b) Wake facing. (c) Zenith facing.

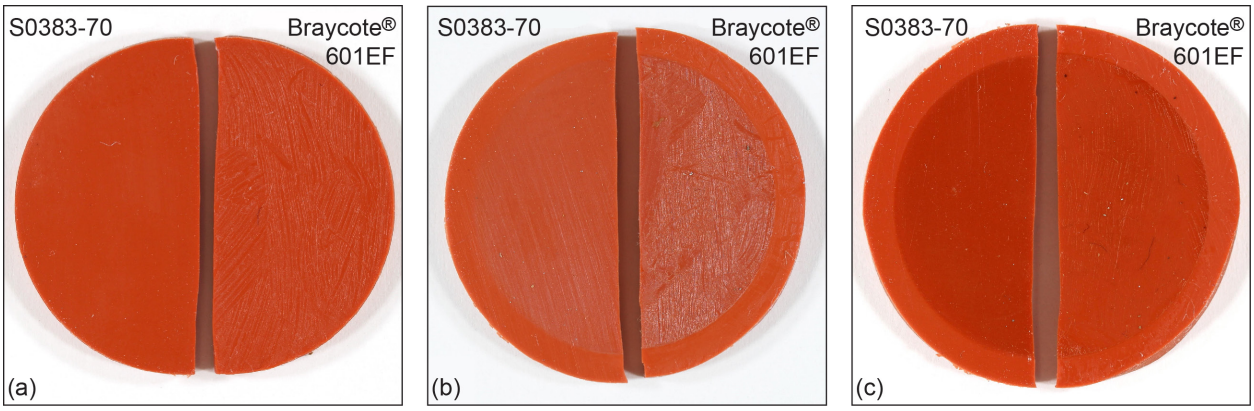

Figure 23.—Postflight MISSE–12 uncoated S0383–70 baseline material (left half) and Braycote® 601EF-coated test articles (right half). (a) Unexposed. (b) Wake facing. (c) Ram facing.

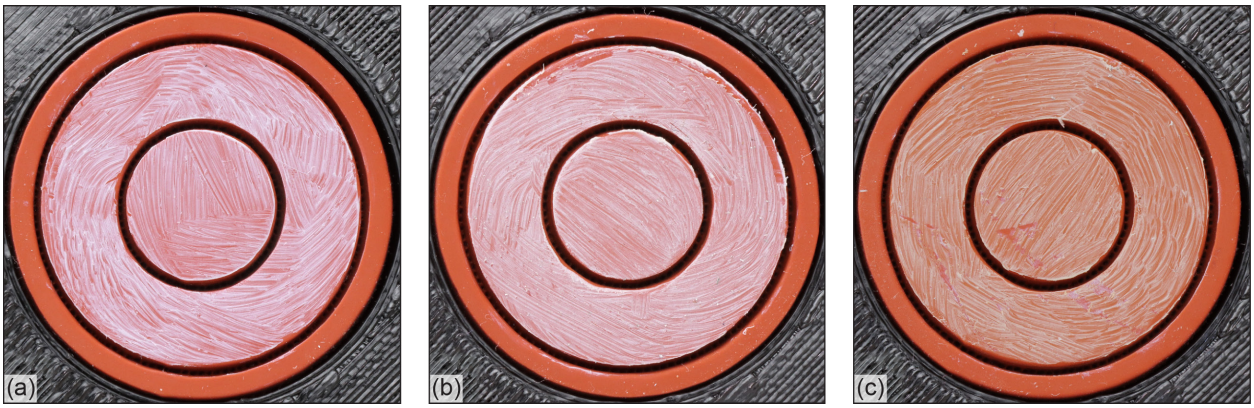

Figure 24.—Postflight MISSE–13 BZ-coated test article assemblies. (a) Unexposed. (b) Wake facing. (c) Zenith facing.

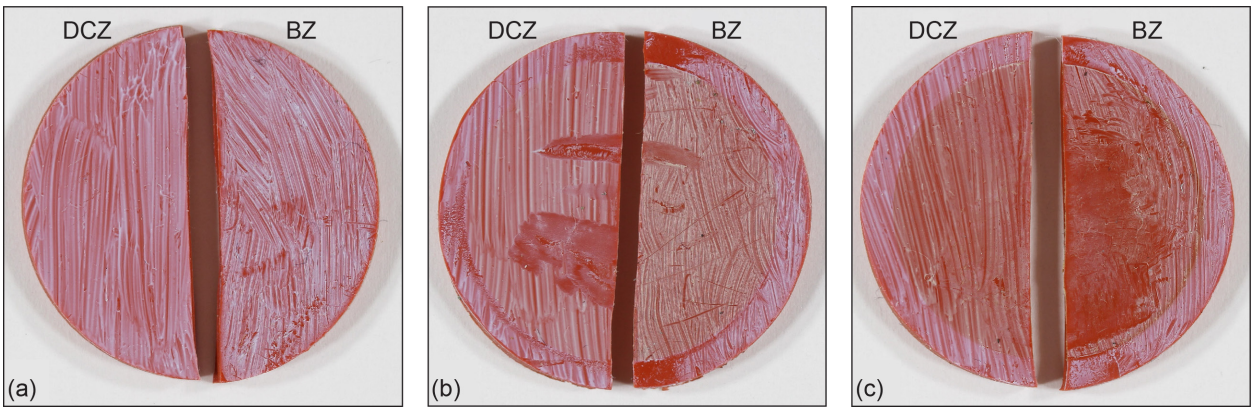

Figure 25.—Postflight MISSE–12 BZ-coated (right half) and DCZ-coated (left half) test articles. (a) Unexposed. (b) Wake facing. (c) Ram facing.

Figure 26.—Postflight MISSE–13 DCZ-coated test article assemblies. (a) Unexposed. (b) Wake facing. (c) Zenith facing.

The test article assemblies were also photographed in 365-nm-wavelength UV light with the DSLR camera. When the baseline material, the 1.5% TiO_2, and the Braycote® 601EF-coated assemblies were exposed to the UV light, the surfaces of the flight assemblies fluoresced a pink color, whereas the outer rings and the control assemblies did not (Figure 27 through Figure 30). The fluorescence of the flight test articles indicated some change in the silicone S0383–70 compound occurred as a result of exposure to UV radiation and/or AO during the MISSE flights. The same change in fluorescence has been observed for the S0383–70 and 1.5% TiO_2 materials after terrestrial exposures to UVA, UVB, and UVC radiation at atmospheric and vacuum pressure conditions, indicating that exposure to UV radiation changes the material. Terrestrial exposures of S0383–70 to AO also resulted in a change in the material fluorescence; however, during terrestrial AO exposure, some amount of exposure to UV radiation occurs, and these AO exposures could not be decoupled from the UV radiation exposure to determine the contribution or effect of AO exposure individually on the change in fluorescence. Both the BZ and DCZ coatings fluoresce in UV light due to the ZnO in the mixtures; however, a difference was still observed between the flight test articles and the control test articles when exposed to 365-nm UV light. The color of the unexposed coatings (i.e., the surfaces of the control test articles) had a green hue in the UV light, whereas the color of the exposed coatings did not; it was white with a pinkish tint (Figure 31 through Figure 33). Upon closer inspection of the photographs, the coating looked more like a mix of pink and white stripes that matched the application pattern. Based on the additive mixing color chart for light, which shows that white is generated in the overlap region of green and magenta (i.e., pink) light, the white color observed was attributed to the additive mixing of the green light from the ZnO fluorescence and the pink light from the fluorescence of the grease (Braycote® 601EF and DC7) exposed to space environments. Further investigation is required to determine what changes in molecular structure at the surface of the test articles were responsible for the change in fluorescence.

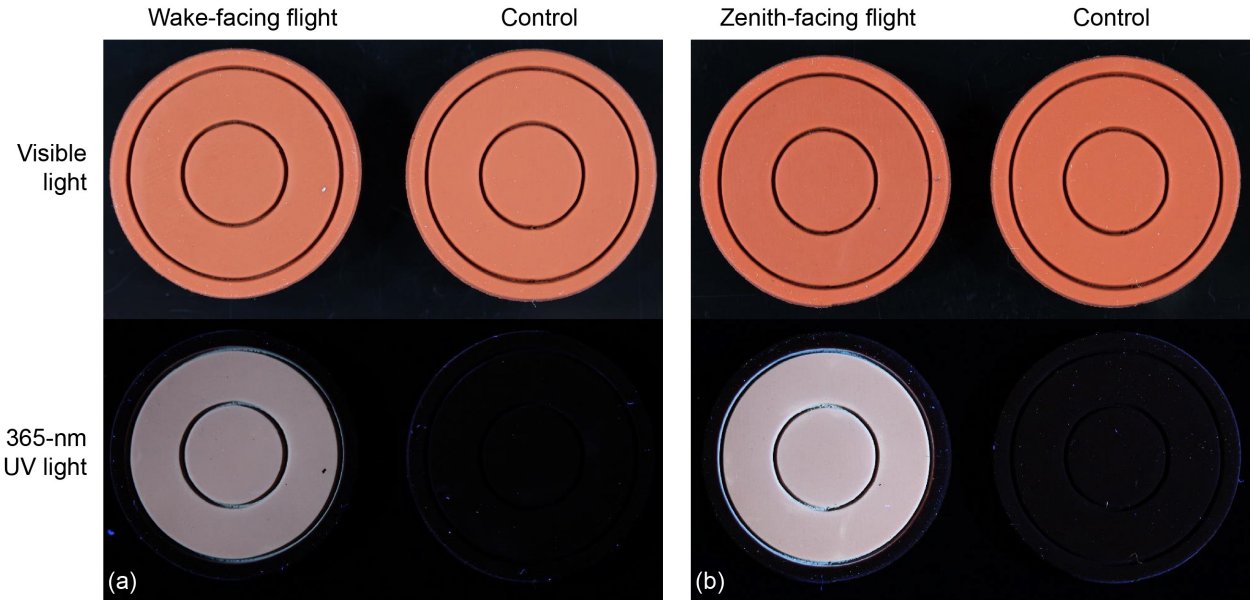

Figure 27.—Baseline material S0383–70 MISSE–13 flight and control test article assemblies under visible light (top) and 365-nm-wavelength UV light (bottom). (a) Wake facing. (b) Zenith facing.

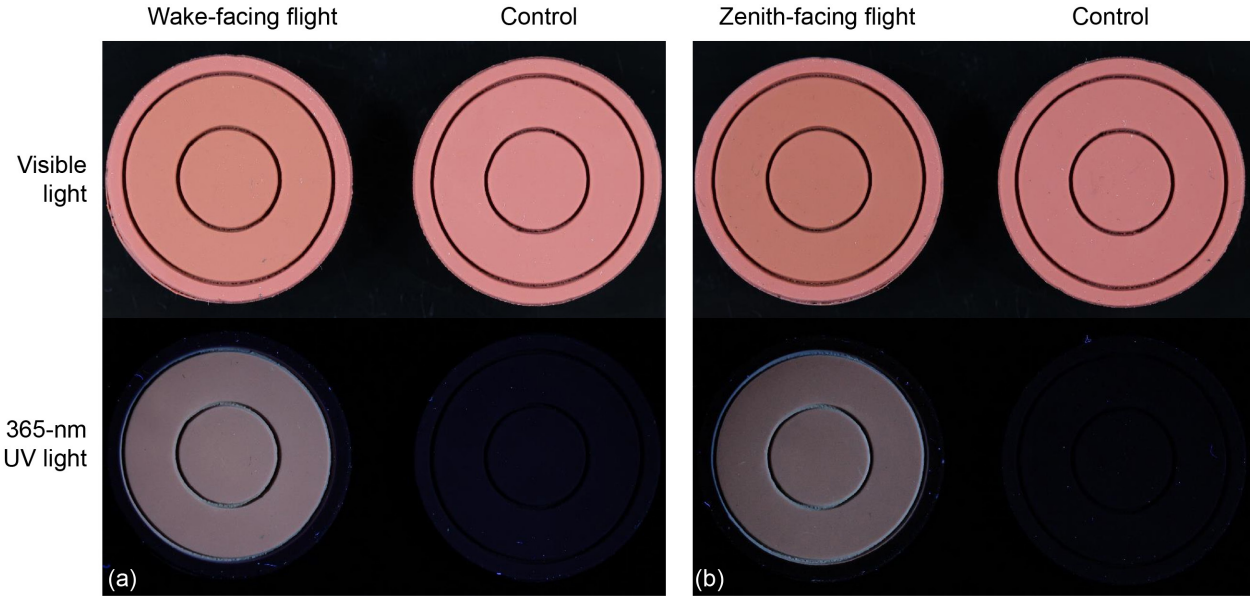

Figure 28.—1.5% TiO_2 MISSE–13 flight and control test article assemblies under visible light (top) and 365-nm-wavelength UV light (bottom). (a) Wake facing. (b) Zenith facing.

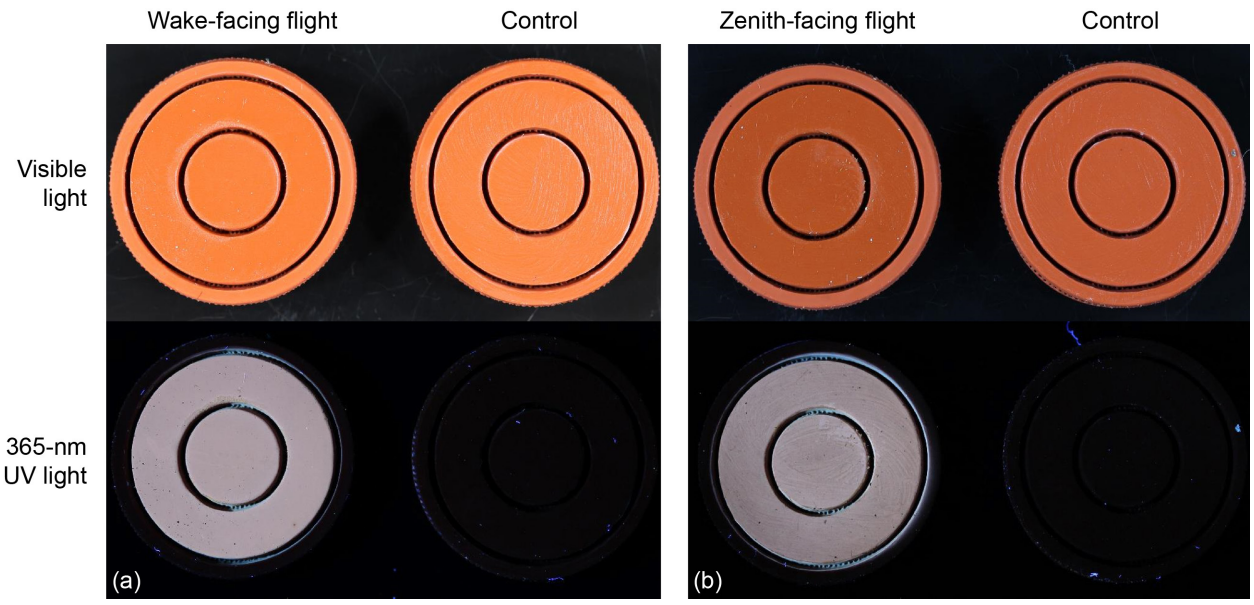

Figure 29.—Braycote® 601EF-coated MISSE–13 flight and control test article assemblies under visible light (top) and 365-nm-wavelength UV light (bottom). (a) Wake facing. (b) Zenith facing.

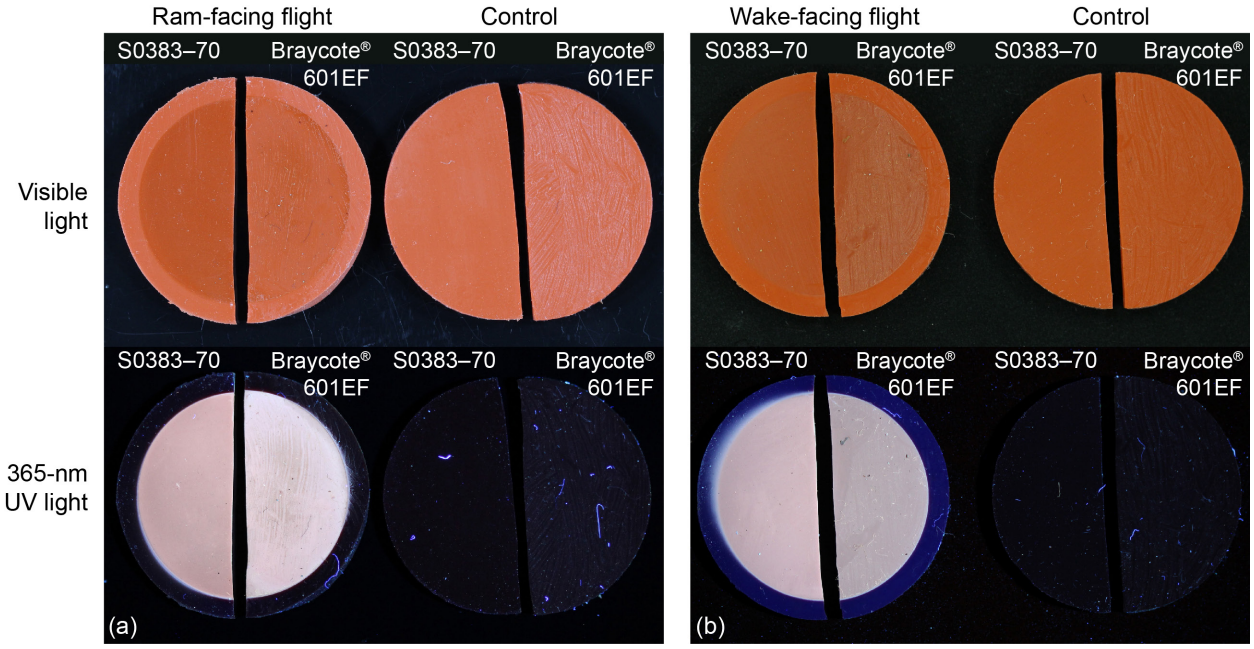

Figure 30.—Baseline material S0383–70 and Braycote® 601EF-coated MISSE–12 flight and control test articles under visible light (top) and 365-nm-wavelength UV light (bottom). (a) Ram facing. (b) Wake facing.

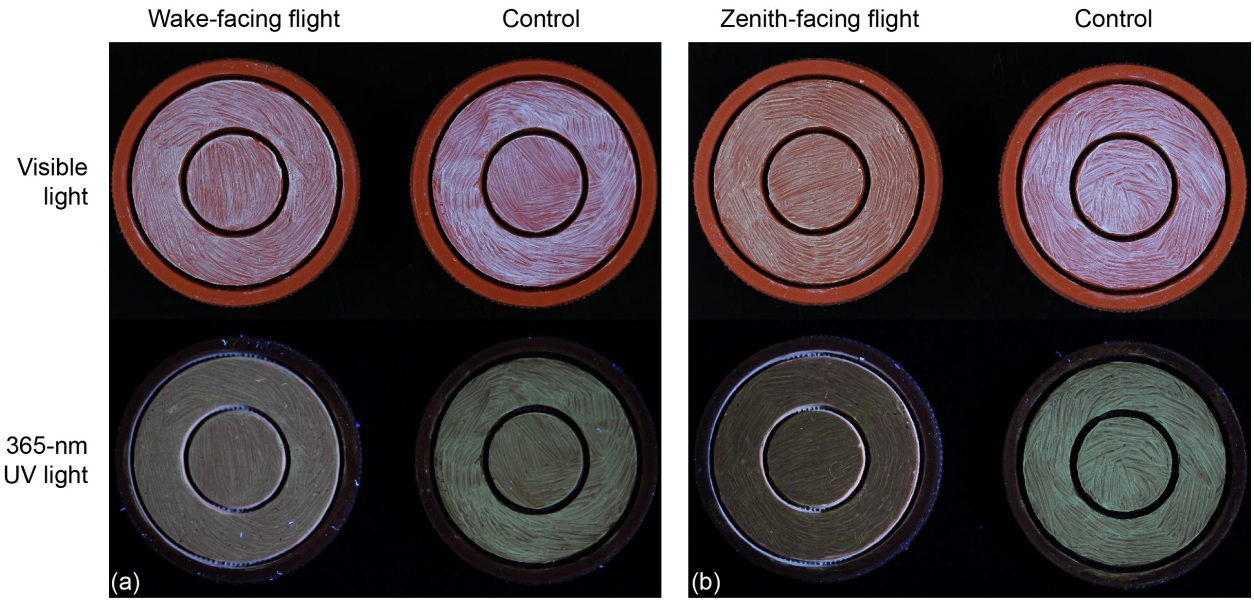

Figure 31.—BZ-coated MISSE–13 flight and control test article assemblies under visible light (top) and 365-nm-wavelength UV light (bottom). (a) Wake facing. (b) Zenith facing.

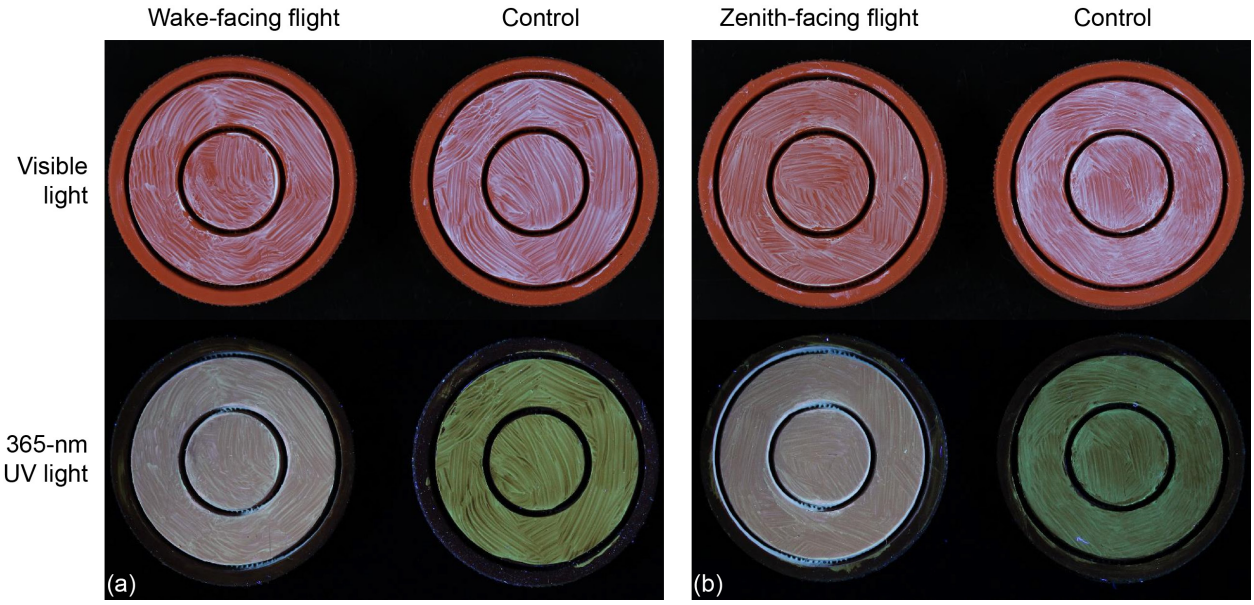

Figure 32.—DCZ-coated MISSE–13 flight and control test article assemblies under visible light (top) and 365-nm-wavelength UV light (bottom). (a) Wake facing. (b) Zenith facing.

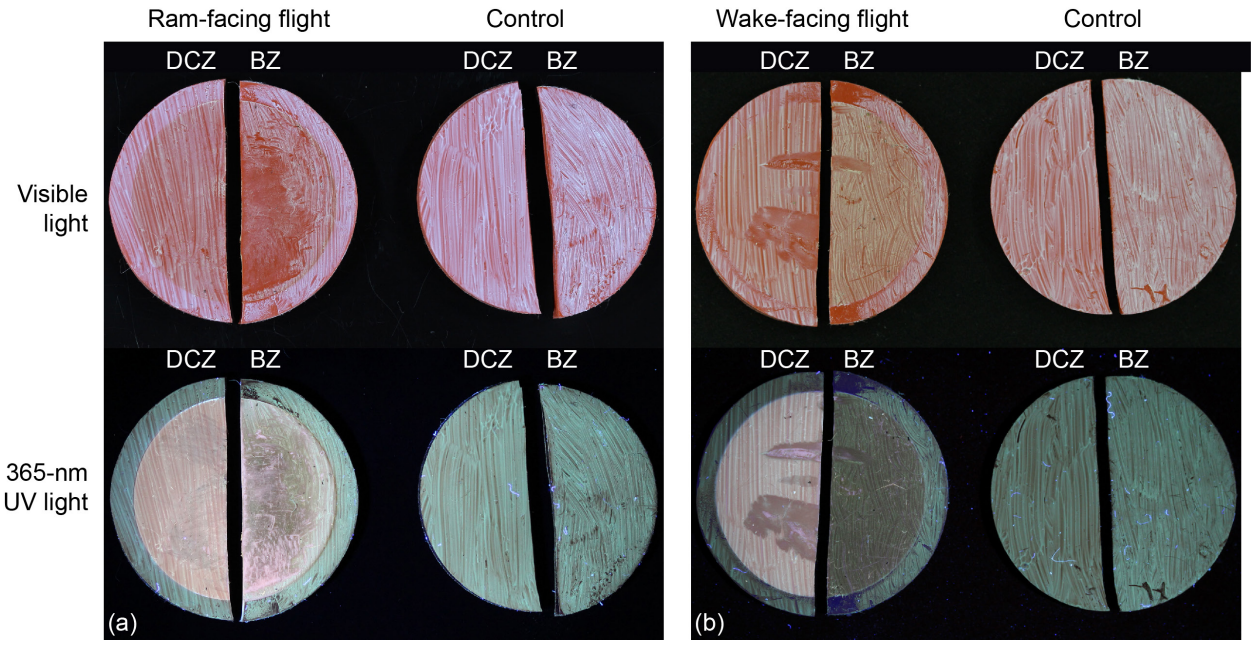

Figure 33.—DCZ- and BZ-coated MISSE–12 flight and control test articles under visible light (top) and 365-nm-wavelength UV light (bottom). (a) Ram facing. (b) Wake facing.

Next, the surfaces were examined at a 20× magnification. A representative 2- by 2-mm area of each semicircle, flat ring, and button surface was examined. At this magnification, the features from the tooling marks on the unexposed S0383–70 baseline material were clearly visible (Figure 34(a) and Figure 35(a)), and the S0383–70 wake-facing and zenith-facing surfaces from MISSE–13 looked like the baseline material (Figure 34(b) and Figure 34(c)). On the MISSE–12 wake-facing surface, the tooling marks were visible along with additional perpendicular lines (Figure 35(b)), whereas on the ram-facing surface, the tooling marks were not visible and the surface was covered with nonuniform horizontal, vertical, and diagonal lines (Figure 35(c)). Like the macro photographs, the surfaces of the 1.5% TiO_2 test articles did not show the tooling mark features (Figure 36); all imaged surfaces had a uniform textured look, with no differences between the unexposed, wake-facing, or zenith-facing test articles. However, the tooling mark features were observed on the backside of the test article (Figure 37(a)) and on the sheet material used to cut out the test articles (Figure 37(b) and Figure 37(c)) confirming a change in the surface from the laser-cutting process. The Braycote® 601EF coating and BZ coating on the unexposed test articles looked the same. On the surfaces, the application pattern was observed, along with what looked like bubbles in the coating (Figure 38(a), Figure 39(a), Figure 40(a), and Figure 41(a)). In the images of the MISSE–13 Braycote® 601EF-coated articles that had been exposed to space environments, the coating in sections of the observed areas appeared to have spalled from the surface. The arrows in Figure 38(b) and Figure 38(c) indicate the sections without coating due to spalling. The areas on the surface where the coating remained looked similar to the unexposed surface with the application pattern and bubbles in the coating. This was the same for the wake-facing MISSE–12 surface (Figure 39(b)); however, the Braycote® 601EF coating on the MISSE–12 ram-facing surface lacked the bubble features in the application pattern (Figure 39(c)). Unlike the Braycote® 601EF coating, the BZ coating did not show spalling. For the BZ coating, the wake-facing surfaces looked like the unexposed surfaces (Figure 40(b) and Figure 41(b)), but differences were observed on the zenith-facing and ram-facing surfaces. The MISSE–13 zenith-facing surface was smoother and lacked the bubbles seen on the unexposed and wake-facing surfaces, although the application pattern was still visible (Figure 40(c)). As noted in the first inspection results and shown in

Figure 17, the BZ coating on the MISSE–12 ram-facing test article was disturbed. The magnified image of the surface was taken in what appeared to be a nondisturbed or minimally disturbed area; however, most of the exposed surface was disturbed, and the image may not be truly representative of the postflight coating condition (Figure 41(c)). The lack of spalling in the space-exposed BZ articles indicates that the addition of ZnO to the Braycote® 601EF enhanced the grease's durability in low Earth orbit.

Compared to the coatings with Braycote® 601EF grease, the silicone-based DCZ coating was smoother, had a less distinctive application pattern, and lacked bubbles (Figure 42 and Figure 43). The unexposed and wake-facing surfaces appeared similar (Figure 42(a), Figure 42(b), Figure 43(a), and Figure 43(b)), whereas the zenith-facing surface appeared more textured, with a mud-tiling look in some areas (Figure 42(c)), and the ram-facing surface was completely different. The surface appeared textured and, in the image, ridges from top to bottom were seen (Figure 43(c)). Compared to the other exposed surfaces, the ram-facing surface was exposed to up to twice as much UV radiation and significantly more AO exposure.

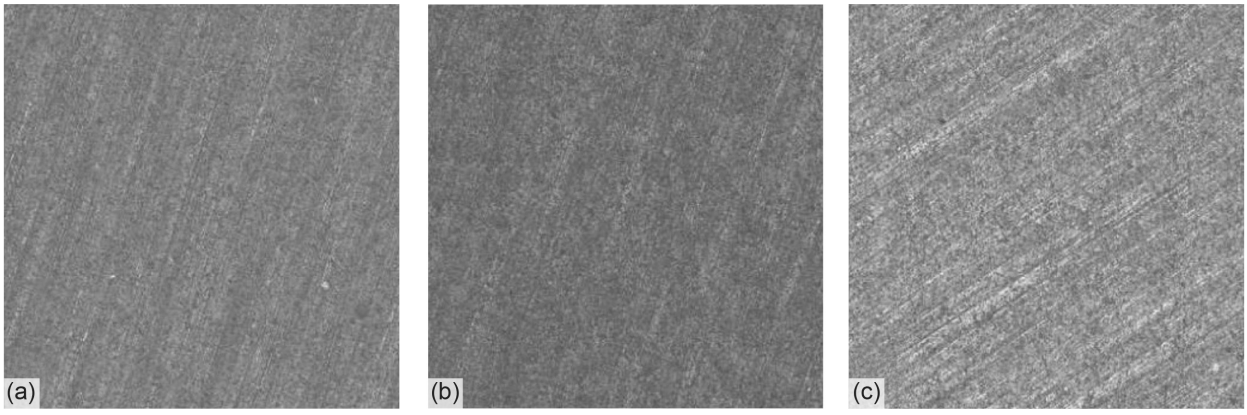

Figure 34.—Postflight images of MISSE–13 baseline material S0383–70 test article assemblies at 20× magnification. (a) Unexposed. (b) Wake facing. (c) Zenith facing.

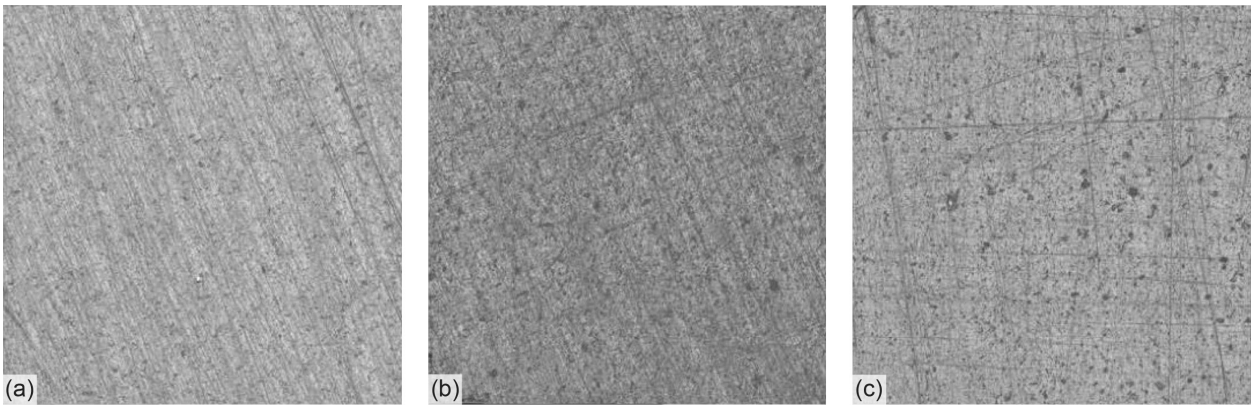

Figure 35.—Postflight images of MISSE–12 baseline material S0383–70 test articles at 20× magnification. (a) Unexposed. (b) Wake facing. (c) Ram facing.

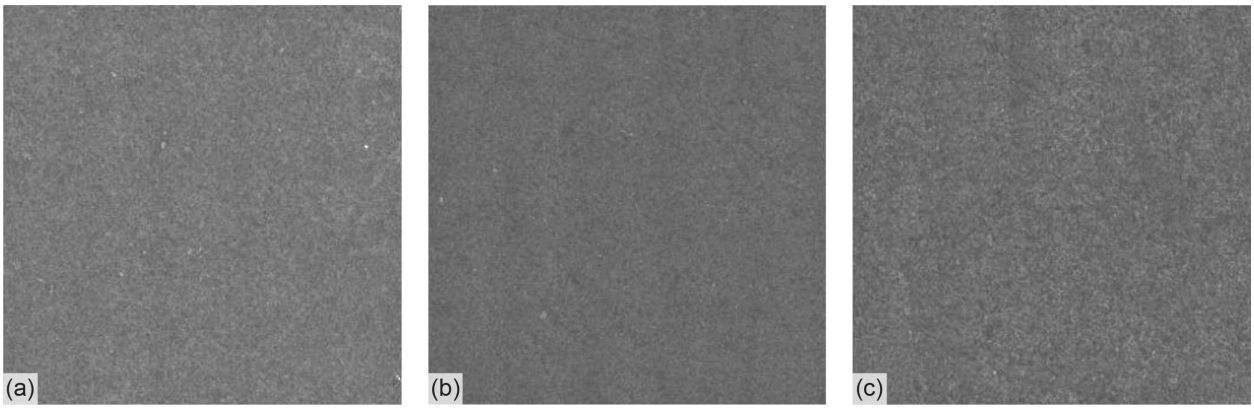

Figure 36.—Postflight images of MISSE–13 1.5% TiO_2 test article assemblies at 20× magnification. (a) Unexposed. (b) Wake facing. (c) Zenith facing.

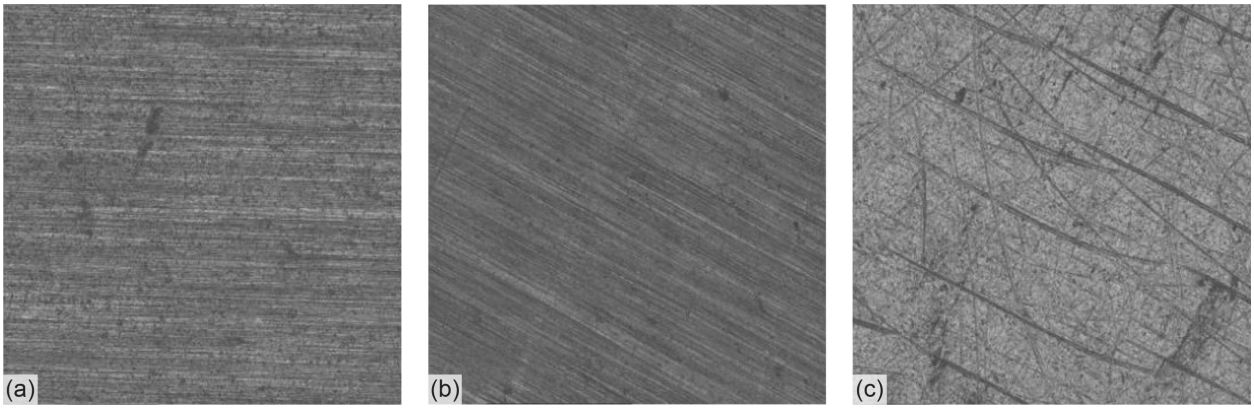

Figure 37.—1.5% TiO_2 material at 20× magnification. (a) Unexposed MISSE–13 test article backside. (b) Sheet material backside. (c) Sheet material top side.

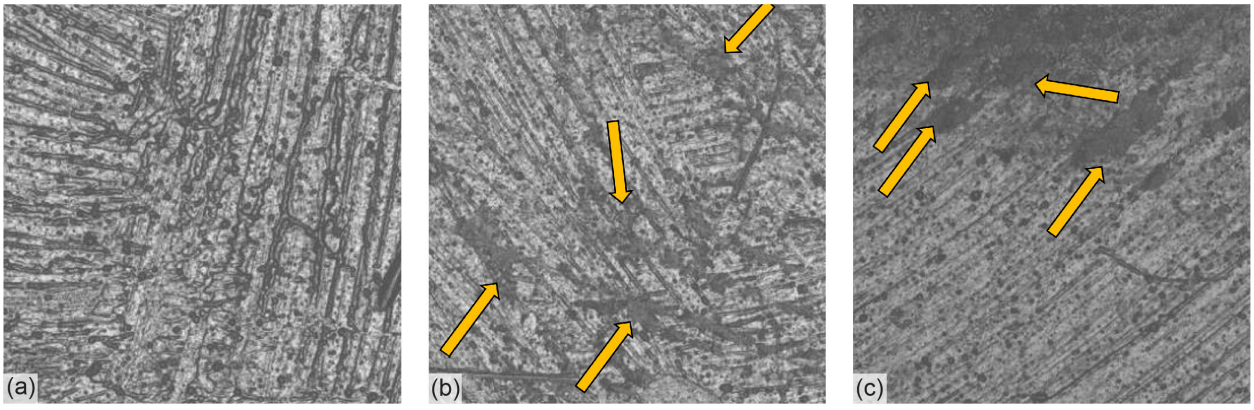

Figure 38.—Postflight images of MISSE–13 Braycote® 601EF-coated test article assemblies at 20× magnification. (a) Unexposed. (b) Wake facing. (c) Zenith facing.

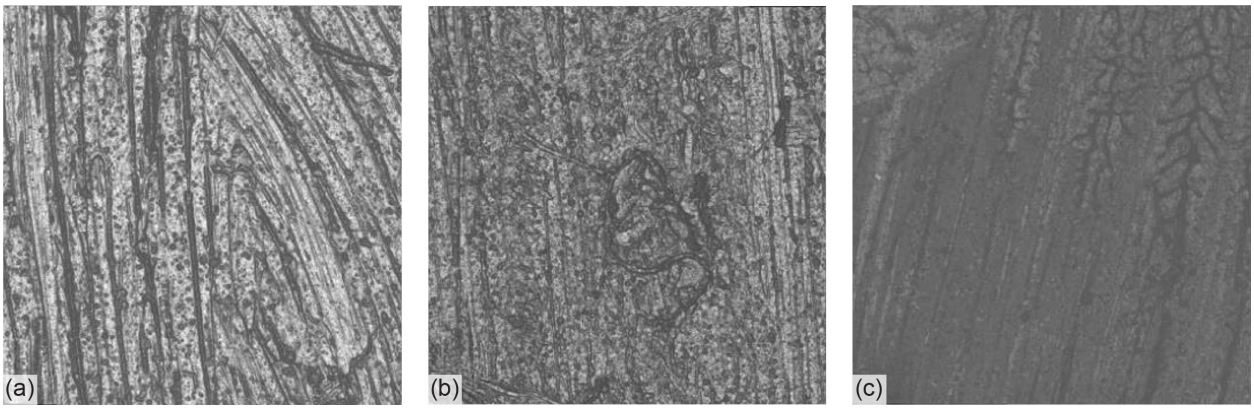

Figure 39.—Postflight images of MISSE–12 Braycote® 601EF-coated test articles at 20× magnification. (a) Unexposed. (b) Wake facing. (c) Ram facing.

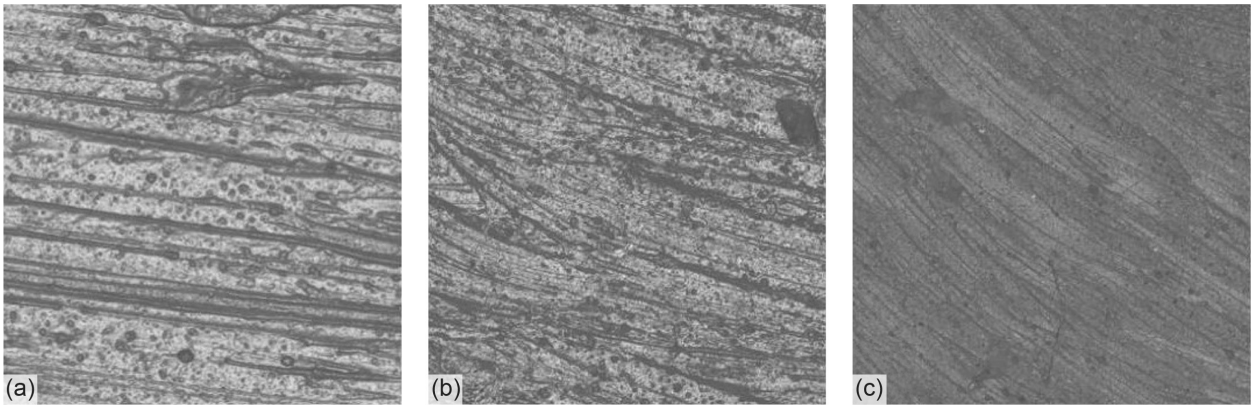

Figure 40.—Postflight images of MISSE–13 BZ-coated test article assemblies at 20× magnification. (a) Unexposed. (b) Wake facing. (c) Zenith facing.

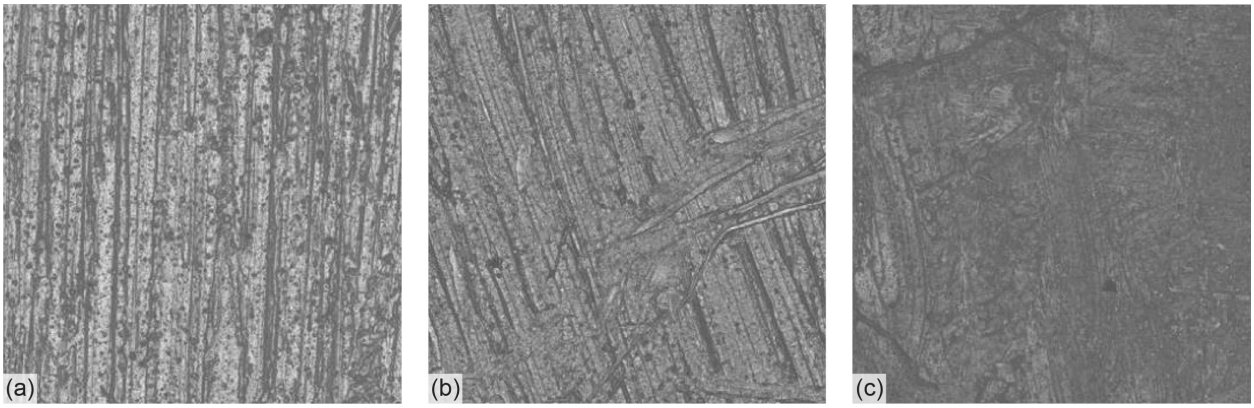

Figure 41.—Postflight images of MISSE–12 BZ-coated test articles at 20× magnification. (a) Unexposed. (b) Wake facing. (c) Ram facing.

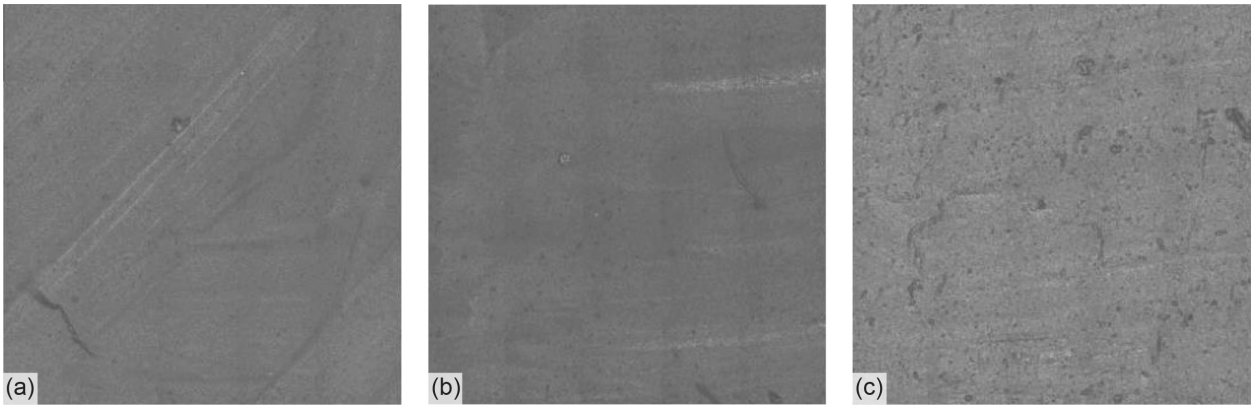

Figure 42.—Postflight images of MISSE–13 DCZ-coated test article assemblies at 20× magnification. (a) Unexposed. (b) Wake facing. (c) Zenith facing.

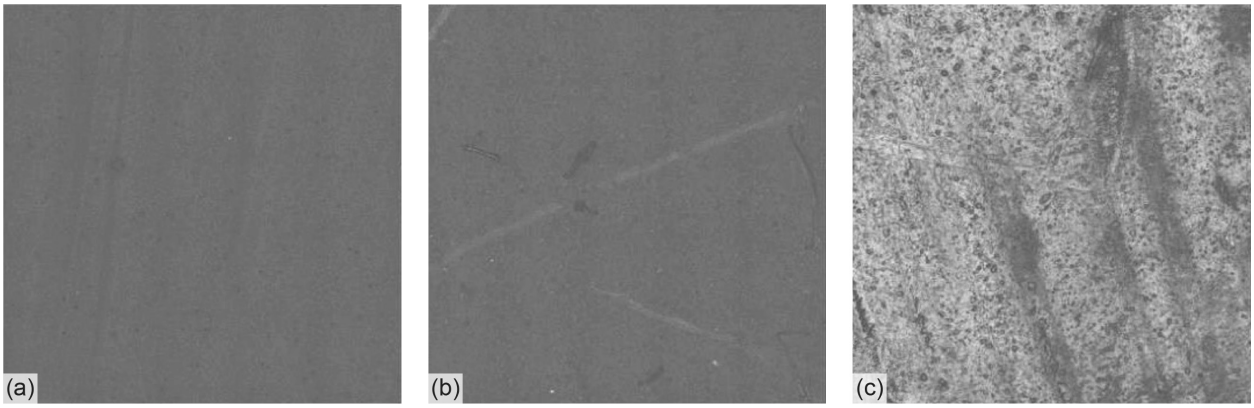

Figure 43.—Postflight images of MISSE–12 DCZ-coated test articles at 20× magnification. (a) Unexposed. (b) Wake facing. (c) Ram facing.

The top surface of the MISSE–13 button portion of the test article assembly was also examined with a scanning electron microscope (SEM) (Hitachi 4700). Images were taken at 1.0 kV and 300× or 500× magnification. The sample surfaces were examined without the use of a conductive sputter coating. Features in the images of the unexposed baseline S0383–70 material were the same as those observed in the images at 20× magnification (Figure 44(a)). The S0383–70 wake-facing and zenith-facing surfaces were imaged at 500×, and these two surfaces had the same uniform appearance (Figure 44(b) and Figure 44(c)). Unlike the images at 20× magnification (Figure 34(b) and Figure 34(c)), the SEM images of the exposed surfaces looked different than the unexposed surface; the tooling marks were not evident on the wake or zenith surfaces. The lack of tooling marks can be attributed to the increased magnification and/or the specific location on the surface selected for imaging. The S0383–70 surfaces (unexposed, wake facing, and zenith facing) were then compared to the surface of a S0383–70 O-ring exposed to space environments in the wake direction on the MISSE–6 flight (Ref. 13).

During MISSE–6, the UV radiation exposure was approximately 3 to 4 times the UV radiation exposure for the MISSE–13 wake direction and 1.5 to 4 times for the zenith direction. The AO exposure was 49 to 58 times as great, as noted in Table V. Like the MISSE–13 test articles, the MISSE–6 O-ring surface had visible tooling mark features (Figure 45). Unlike the MISSE–13 surfaces, the MISSE–6 surface had developed a brittle crust due to the prolonged exposures. The arrows in Figure 45 point to the cracks on the surface. The crack lines in Figure 45(a) were on the as-exposed postflight surface, whereas

the surface crack in Figure 45(b) was formed when a durometer hardness indenter contacted the exposed surface. The insert in the figure showing the cracked surface at 500× magnification clearly demonstrates the brittleness of the crust that formed on the surface of the O-ring. Although no clear indications of surface damage were observed on the S0383–70 material after MISSE–13 exposure levels, continued exposure to higher exposure levels, as seen during the MISSE–6 flight, result in damage to the elastomer surface.

The 1.5% TiO_2 material showed no difference between the unexposed, wake-facing, or zenith-facing surfaces. The uniform textured surface of the unexposed test article button and the uniform textured surfaces of the exposed test article buttons were the same (Figure 46).

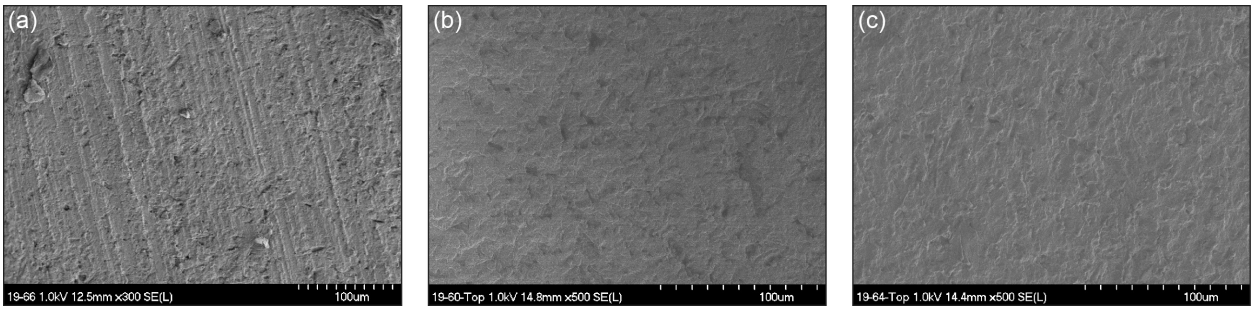

Figure 44.—Postflight SEM images of MISSE–13 baseline material S0383–70. (a) Unexposed at 300× magnification. (b) Wake-facing surface at 500× magnification. (c) Zenith-facing surface at 500× magnification.

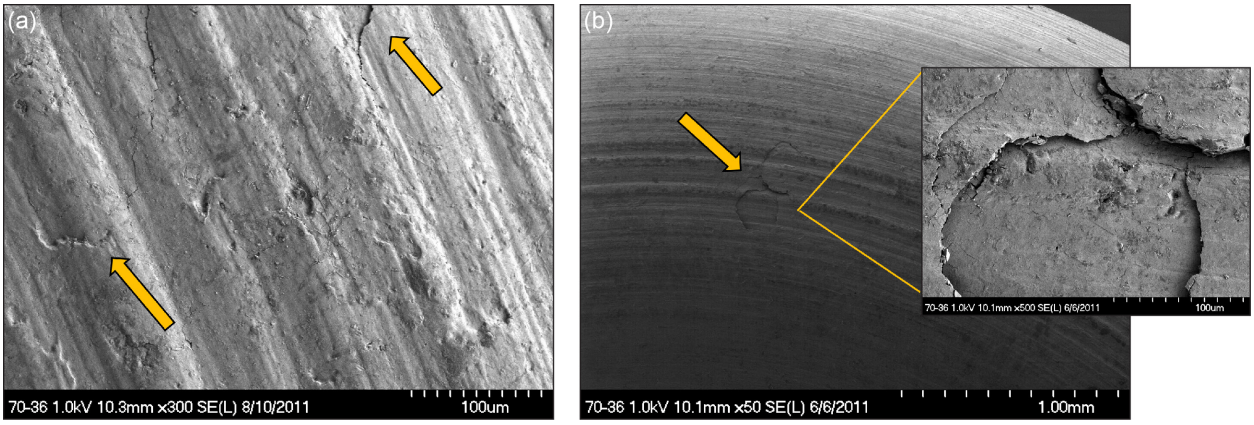

Figure 45.—MISSE–6 postflight SEM images of wake-facing S0383–70 O-ring surface. (a) At 300× magnification. (b) At 50× magnification with 500× magnification insert.

TABLE V.—INCREASE IN UV RADIATION EXPOSURE AND AO EXPOSURE OF MISSE–6 TEST ARTICLES COMPARED TO MISSE–13 TEST ARTICLES

MISSE–13	Wake-facing MISSE–6	
	UV	AO
Wake facing	3.3 to 3.8 times	49 times
Zenith facing	1.5 to 4.2 times	58 times

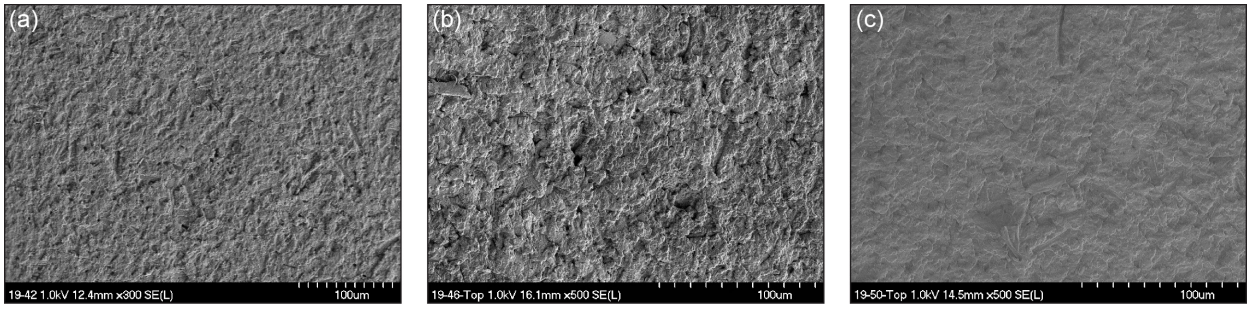

Figure 46.—Postflight SEM images of MISSE–13 1.5% TiO_2 material. (a) Unexposed at 300× magnification. (b) Wake-facing surface at 500× magnification. (c) Zenith-facing surface at 500× magnification.

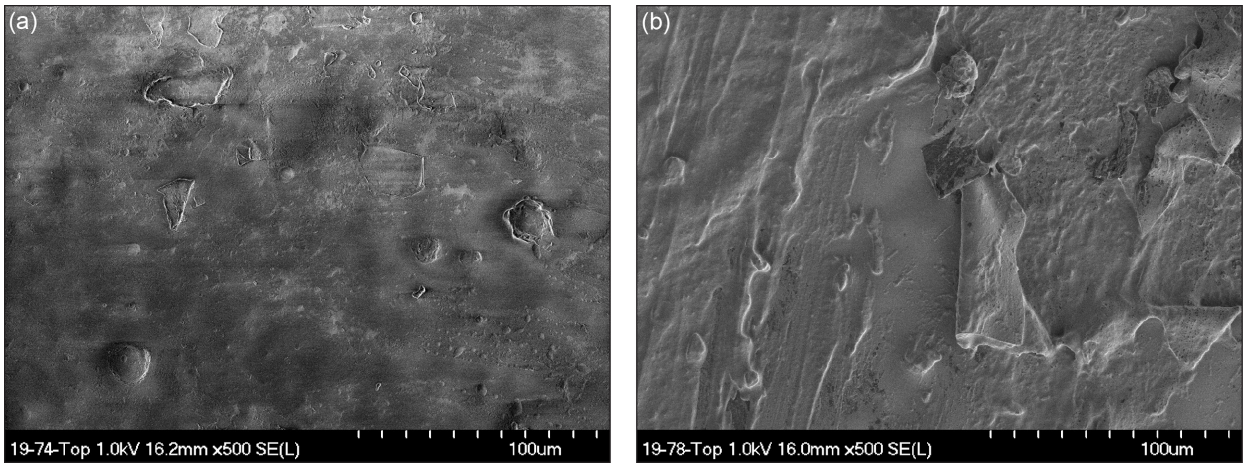

Figure 47.—Postflight SEM images of MISSE–13 Braycote® 601EF-coated surface at 500× magnification. (a) Wake facing. (b) Zenith facing.

The wake-facing and zenith-facing button surfaces of the coated test articles were imaged to evaluate the condition of the coating. For each coating type, the coating remained on the surface in some form; it was not removed or volatilized by the space exposures. The Braycote® 601EF surfaces were imaged at 500× magnification (Figure 47). In the wake-facing image (Figure 47(a)), the coating looked more smooth and more uniform than the coating on the zenith-facing image (Figure 47(b)); this was most likely simply due to the locations selected for imaging. The BZ coating on both the wake-facing and zenith-facing buttons looked like it was layered (Figure 48), similar to the zenith-facing coating seen in Figure 47(b). The top layer of the BZ coating had fold-like features, similar to folds in a fabric cloth, which separated from the bottom layer in some areas. The bottom layer had the imprint of the contours from the top layer but did not have any of the folded-fabric features. The DCZ coating was different than the Braycote® 601EF or BZ coating in that it was dried and cracked (Figure 49). The mud-tiling effect observed at 20× magnification was clearly visible at 300× magnification. This effect is likely due to the formation of a passivating silicon oxide layer created when AO reacted with the Si in the silicone-based DCZ grease.

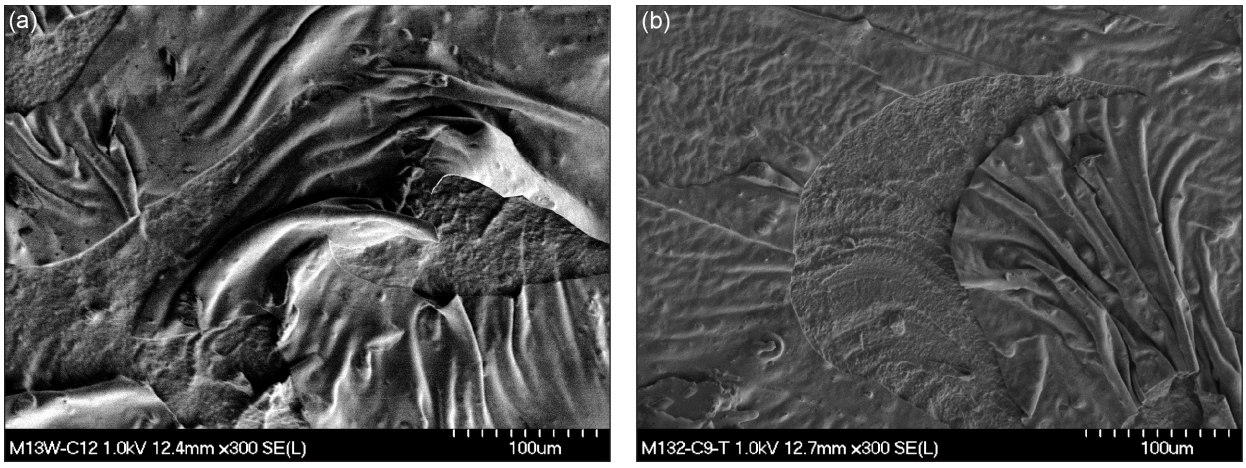

Figure 48.—Postflight SEM images of MISSE–13 BZ-coated surface at 300× magnification. (a) Wake facing. (b) Zenith facing.

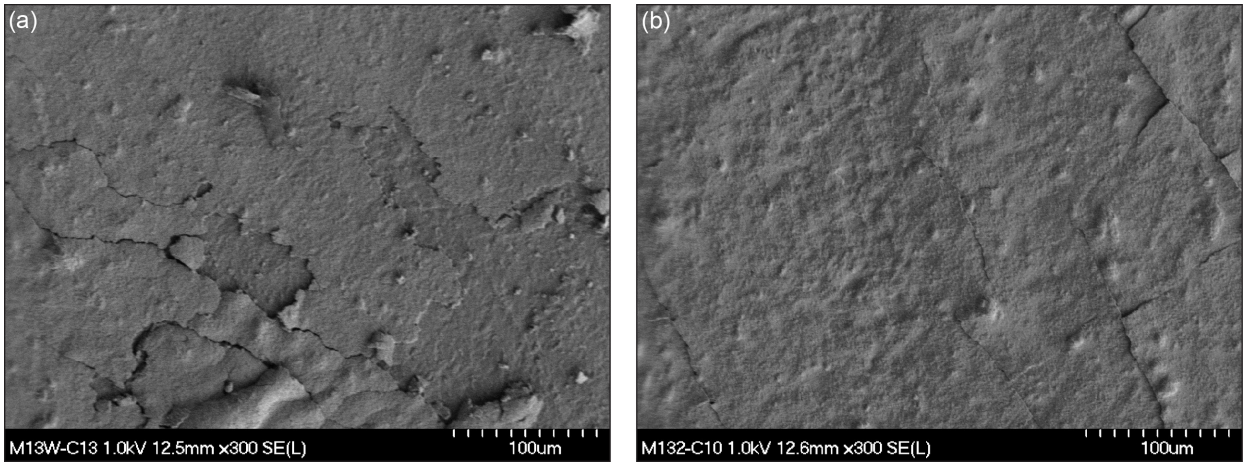

Figure 49.—Postflight SEM images of MISSE–13 DCZ-coated surface at 300× magnification. (a) Wake facing. (b) Zenith facing.

5.2 Inspection of the Cross Section Surface

In addition to images of the top surface, images of the MISSE–13 button cross section were taken with the SEM. The cross section images of both the unexposed S0383–70 baseline material and the unexposed 1.5% TiO_2 material were uniform in appearance (Figure 50). This same uniformity was not observed in all the cross sections of the exposed buttons. The S0383–70 wake-facing and zenith-facing buttons had a layer of material at the exposed surface that was different than the remaining bulk material. For the wake-facing button, the thickness of the layer was measured as 31 μm, and the layer on the zenith-facing button was 21 μm (Figure 51). These layers were about half the thickness of the MISSE–6 wake-facing O-ring (Figure 52) that was exposed to 49 to 58 times the AO (wake-facing and zenith-facing directions, respectively). In the MISSE–6 SEM image, the thickness of the layer was not uniform, which was attributed to the nonuniformity of exposure along the curved surface of the O-ring. The exposed surfaces of the MISSE–13 buttons, in contrast, were flat, resulting in a more uniform exposure across the surface and a more uniform layer. A difference was also seen at the surface of the Braycote® 601EF-coated wake-facing and zenith-facing buttons (Figure 53). On the wake-facing button

(Figure 53(a)), the thickness of the layer was 24 μm, and on the zenith-facing button (Figure 53(b)), the thickness was 29 μm. The cross section images of the exposed TiO_2 buttons (Figure 54) looked slightly different than the unexposed cross section images (Figure 50(b)). Both the wake-facing and zenith-facing TiO_2 buttons had a thin layer at the top that appeared different than the bulk material, although it was not as pronounced as on the other test articles. In-depth analyses are required to determine the differences in chemical structure of the surface layer and bulk material of the test articles. These analyses were beyond the scope of this study and were relegated to recommended future work. In contrast to the TiO_2 buttons, the wake-facing and zenith-facing cross sections of the BZ- and DCZ-coated buttons appeared uniform (Figure 55 and Figure 56, respectively). The layer observed in the S0383–70, Braycote® 601EF, and TiO_2 buttons was not observed in the BZ and DCZ cross sections, providing evidence that the BZ and DCZ coatings protected the S0383–70 material.

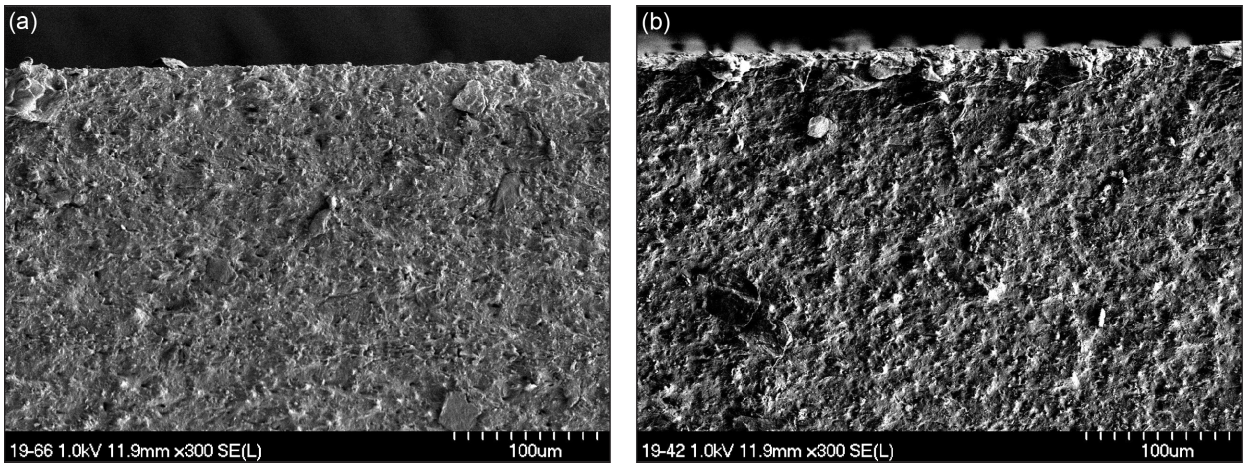

Figure 50.—Postflight SEM cross section images of unexposed material at 300× magnification. (a) S0383–70. (b) 1.5% TiO_2.

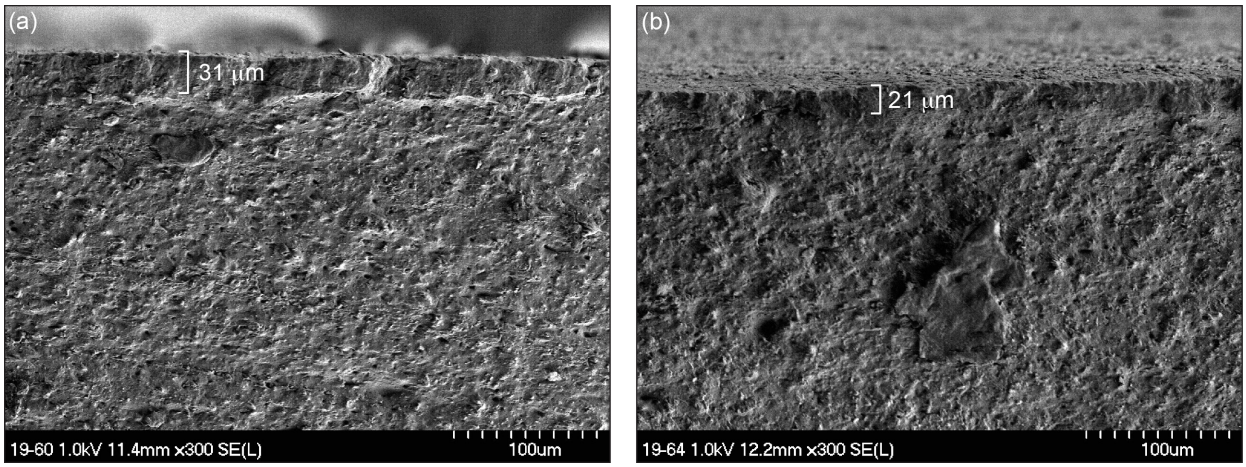

Figure 51.—Postflight SEM images of MISSE–13 S0383–70 test articles at 300× magnification. (a) Wake-facing cross section. (b) Zenith-facing cross section.

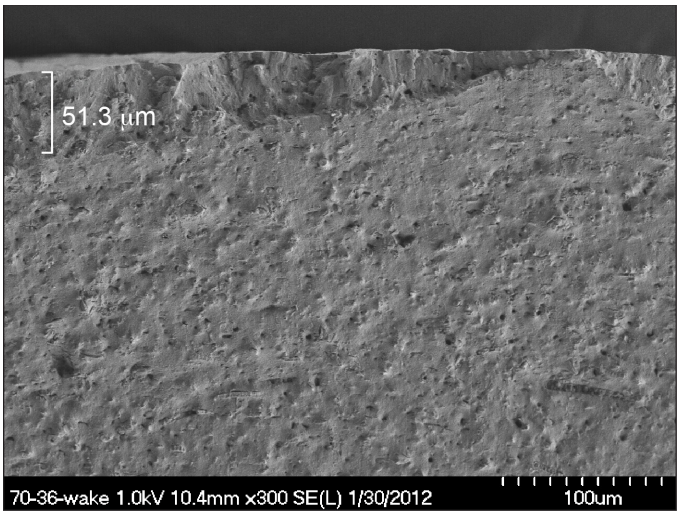

Figure 52.—Postflight SEM image of MISSE–6 S0383–70 wake-facing O-ring cross section at 300× magnification.

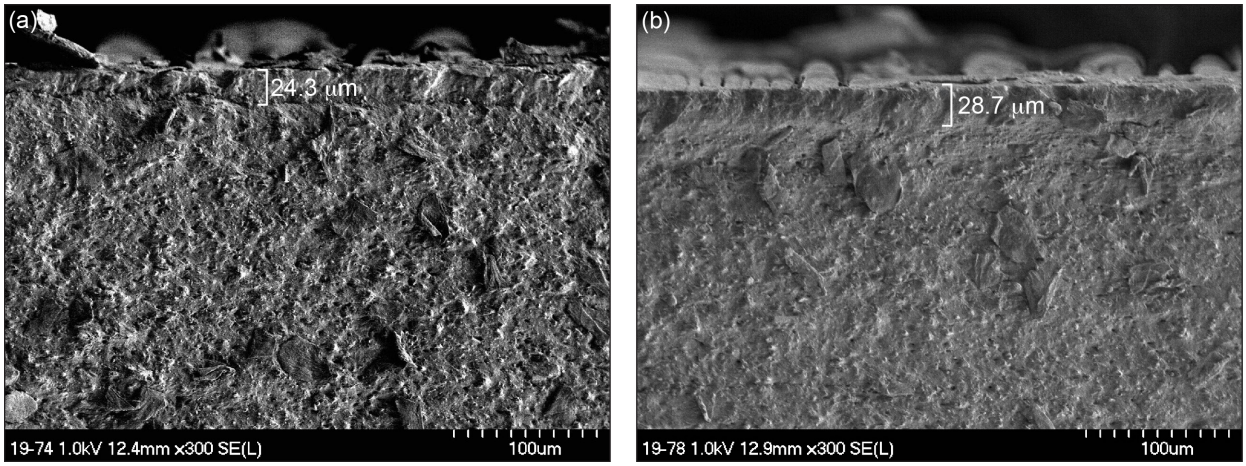

Figure 53.—Postflight SEM images of MISSE–13 Braycote® 601EF-coated test articles at 300× magnification. (a) Wake-facing cross section. (b) Zenith-facing cross section.

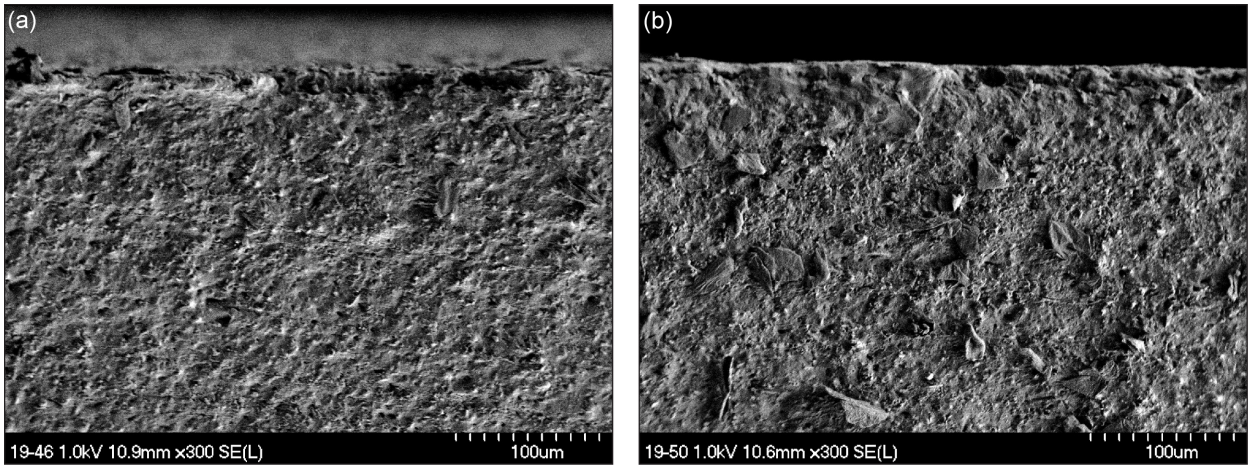

Figure 54.—Postflight SEM images of MISSE–13 1.5% TiO_2 test articles at 300× magnification. (a) Wake-facing cross section. (b) Zenith-facing cross section.

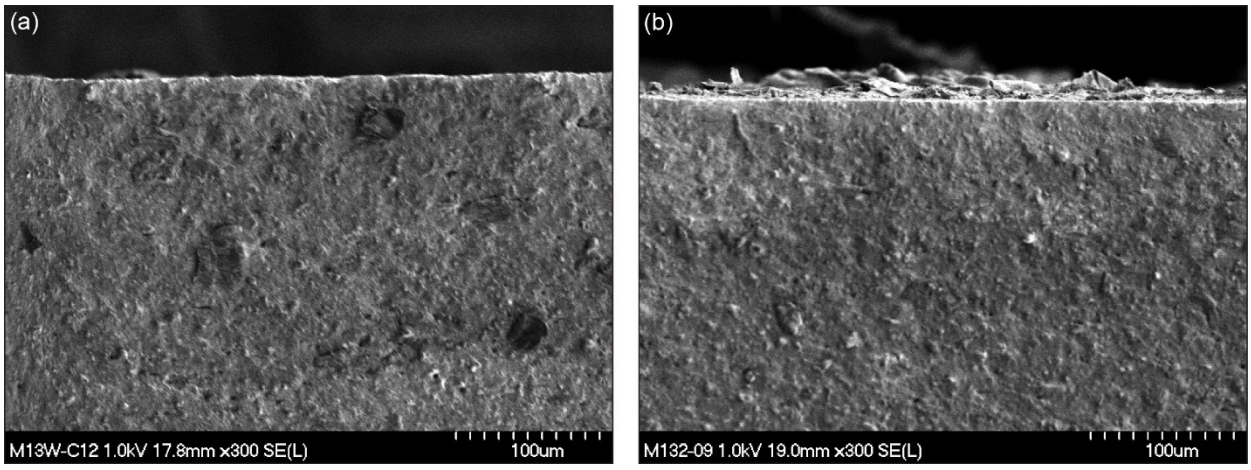

Figure 55.—Postflight SEM images of MISSE–13 BZ-coated test articles at 300× magnification. (a) Wake-facing cross section. (b) Zenith-facing cross section.

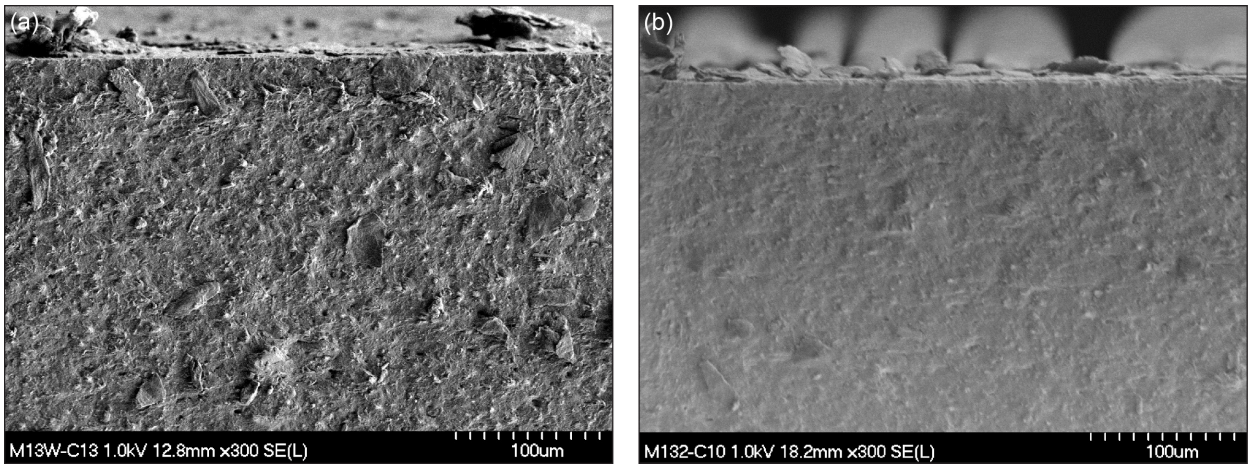

Figure 56.—Postflight SEM images of MISSE–13 DCZ-coated test articles at 300× magnification. (a) Wake-facing cross section. (b) Zenith-facing cross section.

5.3 Inspection of Surfaces After Leak Rate Testing

The MISSE–13 test articles were fabricated to evaluate both the physical effects and performance effects of space environment exposures. The flat rings were leak rate tested (Section 6.0) and the surfaces were reinspected, photographed, and imaged at 20× magnification. No differences from the postflight photographs and images were observed for the S0383–70 material or the 1.5% TiO_2 material after leak rate testing. For the Braycote® 601EF surfaces, no differences were observed visually or in the macro photographs; however, the images at 20× magnification showed differences for the unexposed and zenith-facing surfaces. On the unexposed surface, the application lines of the coating were no longer visible, the coating appeared to have fewer peaks and valleys, and there were areas without coating (Figure 57(a)). This was an expected result from compressing the grease during the leak rate test, and due to the thinness and transparency of the Braycote® 601EF coating, these changes were not visible in the macro photographs. The wake-facing surface (Figure 57(b)) was similar to that seen in the postflight image (Figure 38(b)), with sections of spalled coating. After the leak rate test, the zenith-facing surface had more areas without coating (Figure 57(c)) than were seen in the postflight images (Figure 38(c)). The

changes in the BZ coating from compression during the leak rate tests were visible in the macro photographs (Figure 58) and magnified images (Figure 59). The distinct pattern in the coating from the application process was no longer visible. The coating on the unexposed surface became uniform across the flat ring, and some of the coating from the wake-facing and zenith-facing surfaces was no longer present, particularly on the wake-facing surface. The DCZ coating, in contrast, still had the visible pattern of lines from the application process even though the lines were less distinct. Of the three surfaces with DCZ coating, the unexposed surface showed the most change from the postflight condition to the post-leak-rate-test condition (Figure 26 compared to Figure 60). Again, it was expected for a compliant coating to move when compressed. In the magnified images, the unexposed surface looked less uniform after leak rate testing, whereas the wake-facing and zenith-facing surfaces showed no changes (Figure 61).

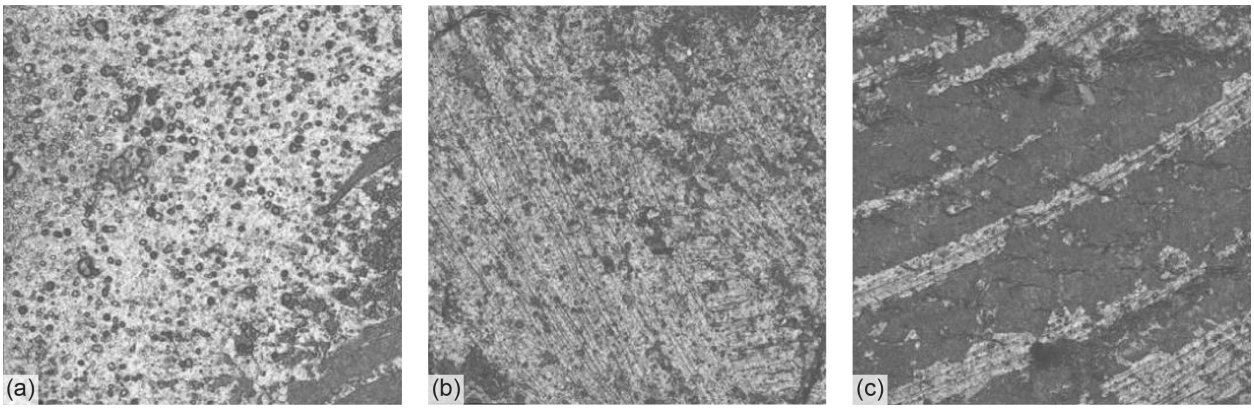

Figure 57.—Post-leak-rate-test images of MISSE–13 Braycote® 601EF-coated flat ring surfaces at ×20 magnification. (a) Unexposed. (b) Wake facing. (c) Zenith facing.

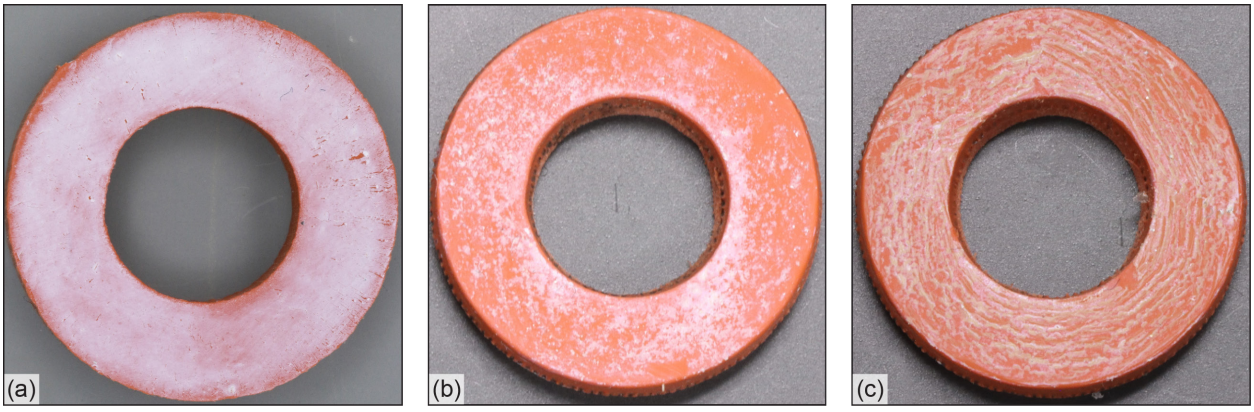

Figure 58.—Post-leak-rate-test photographs of MISSE–13 BZ-coated flat rings. (a) Unexposed. (b) Wake facing. (c) Zenith facing.

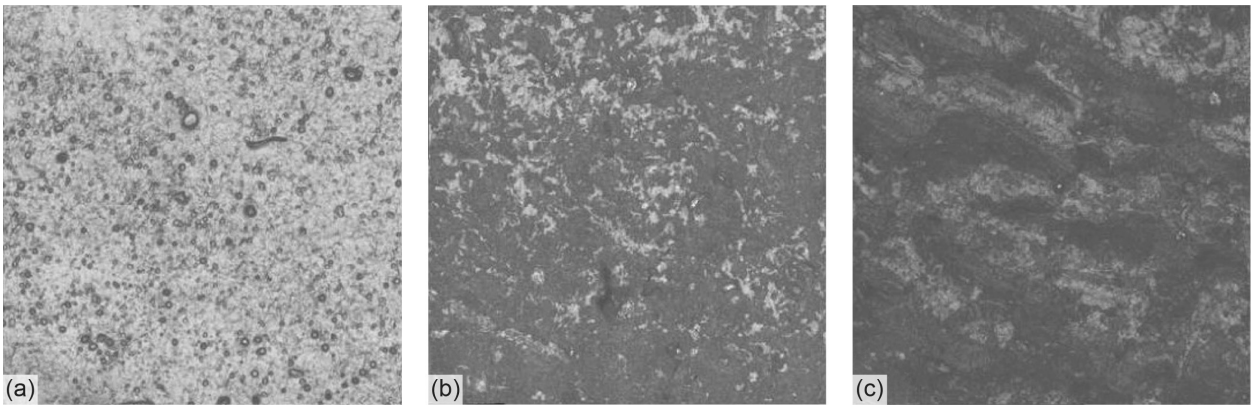

Figure 59.—Post-leak-rate-test images of MISSE–13 BZ-coated flat ring surfaces at 20× magnification. (a) Unexposed. (b) Wake facing. (c) Zenith facing.

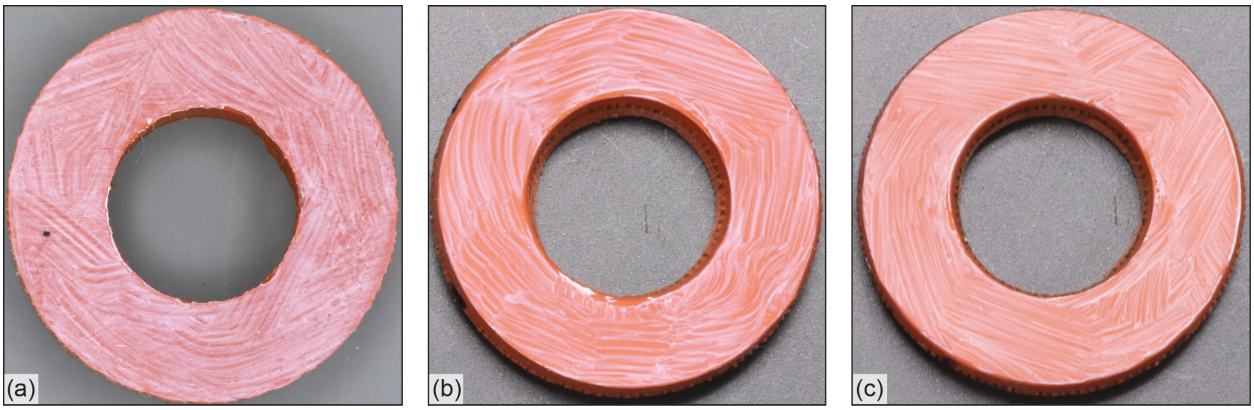

Figure 60.—Post-leak-rate-test photographs of MISSE–13 DCZ-coated flat rings. (a) Unexposed. (b) Wake facing. (c) Zenith facing.

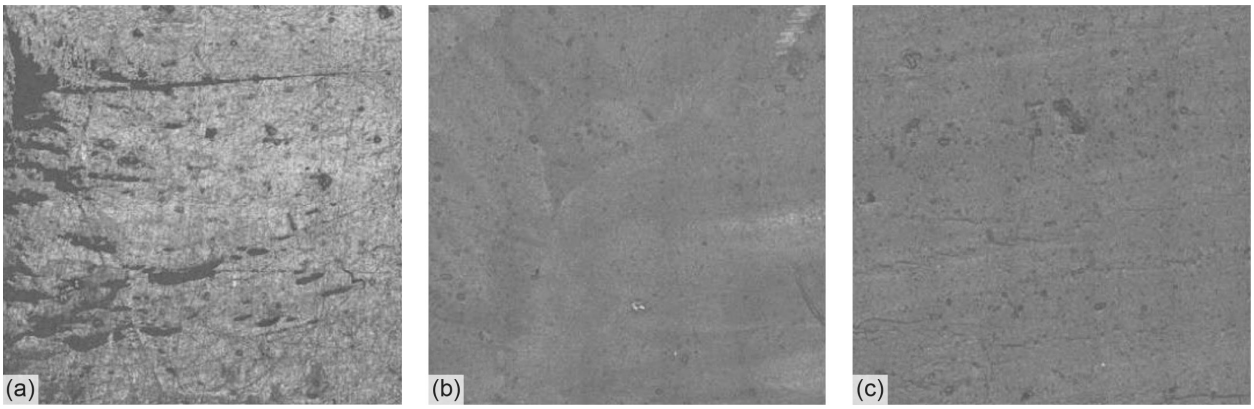

Figure 61.—Post-leak-rate-test images of MISSE–13 DCZ-coated flat ring surfaces at 20× magnification. (a) Unexposed. (b) Wake facing. (c) Zenith facing.

5.4 Inspection of the Cleaned Surfaces

To evaluate the durability of the coatings, the test article surfaces were cleaned. For the MISSE–13 test articles, the flat rings were cleaned after leak rate testing was performed. A solvent-soaked, lint-free task wipe was used to clean the surface. The coated surfaces were cleaned with Fluoroclean HE™ (Castrol Ltd.), the recommended solvent for removing Braycote® 601EF grease, and the uncoated surfaces were cleaned with isopropanol. The cleaned surfaces were reinspected, photographed, and imaged at 20× magnification, and the flat rings were leak rate tested again (results in Section 6.0). Very little to no difference was observed with the S0383–70 and 1.5% TiO_2 test articles.

As expected, differences in the photographs and magnified images of the test articles with coatings were seen. The Braycote® 601EF coating was completely removed from the unexposed surface, with the resulting surface looking like the unexposed S0383–70 baseline material (Figure 62(a) and Figure 63(a)). At 20× magnification, the features in the elastomer from the tooling marks were visible (Figure 64(a) and Figure 65(a)). After cleaning, a nonuniform thin film remained on the surfaces of the test articles (Figure 62(b) and (c) and Figure 63(b) and (c)). On the MISSE–13 wake-facing surface, a small area with a thicker film was visible at the 9 o'clock position in Figure 62(b). In the magnified images, the thin film on the MISSE–13 wake-facing and zenith-facing surfaces and the MISSE–12 ram-facing surface had a uniform textured appearance. On the MISSE–12 wake-facing surface, some tooling mark features were observed, indicating the Braycote® 601EF coating was removed from this section of the test article surface. Also, a brown residue remained on the task wipe used to clean the flight surfaces that was not observed on the task wipe used to clean the unexposed Braycote® 601EF surfaces, indicating that a change occurred in the Braycote® 601EF coating when it was exposed to space environments.

The BZ-coated surfaces also had a thin film remaining on the surface after the cleaning procedure. As shown in Figure 66, some of the BZ coating remained on the unexposed, wake-facing, and zenith-facing surfaces at the 6 o'clock (Figure 66(a)), 5 and 11 o'clock (Figure 66(b)), and 3 and 7 o'clock positions (Figure 66(c)), respectively. When the test articles were photographed under UV light (365-nm wavelength), the coating remaining on the surface was more apparent, as shown in Figure 67. In addition, the areas on the surfaces where the coating was removed during cleaning of the wake-facing and zenith-facing test articles did not fluoresce in the UV light, providing evidence that the BZ coating protected the S0383–70 silicone from the on-orbit UV exposure. In Figure 68, the residual BZ coating can be seen toward the bottom right edge of the wake-facing test article (Figure 68(b)) and on the upper half of the ram-facing test article (Figure 68(c)). Again, the coating remaining on the surfaces was easily seen under UV light (Figure 69), and the areas where the coating was removed did not fluoresce. The magnified images showed uniform textured surfaces, and the tooling mark features in the elastomer material were not visible on the MISSE–13 wake-facing and zenith-facing test articles (Figure 70(b) and Figure 70(c)) or the MISSE–12 ram-facing test article (Figure 71(c)). Tooling mark features were visible on the MISSE–12 wake-facing test article (Figure 71(b)).

The DCZ coating (Figure 72 through Figure 77) was the most durable; it was not easily removed from the surface, although it was more easily removed from the unexposed surface than from the exposed surfaces (Figure 72 and Figure 74). An interesting observation was made of the MISSE–12 wake-facing test article after cleaning: In Figure 74(b), areas where the coating was not removed when the surface was cleaned match the areas of the disturbed coating observed at deintegration (Figure 17(b)). Like the BZ-coated test articles, the cleaned DCZ test articles were photographed under UV light (Figure 73 and Figure 75). The areas where the coating was removed from the surface did not fluoresce, indicating the coating protected the S0383–70 silicone surface from on-orbit UV exposure. In the magnified images, the tooling mark features were visible on the unexposed cleaned surface of the MISSE–12 test article (Figure 77(a)).

Tooling mark features were also visible on the unexposed MISSE–13 flat ring along with some scratches (Figure 76(a)). The wake-facing surfaces had indications of the applied coating where it was not completely removed from the surface (Figure 76(b) and Figure 77(b)). In addition, the MISSE–12 surface had a hatch-like pattern in the areas where the coating was removed that was similar to the pattern observed on the S0383–70 wake-facing postflight surface (Figure 35(b)). The dried coating on the zenith-facing surface had a cracked appearance (Figure 76(c)), and the dried coating on the ram-facing surface appeared rough, without a particular pattern (Figure 77(c)).

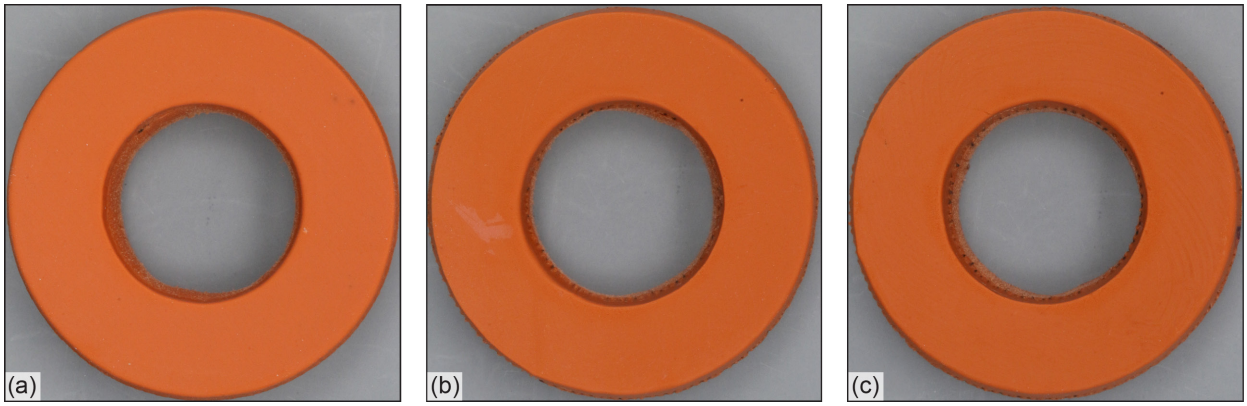

Figure 62.—Cleaned MISSE–13 Braycote® 601EF-coated flat rings. (a) Unexposed. (b) Wake facing. (c) Zenith facing.

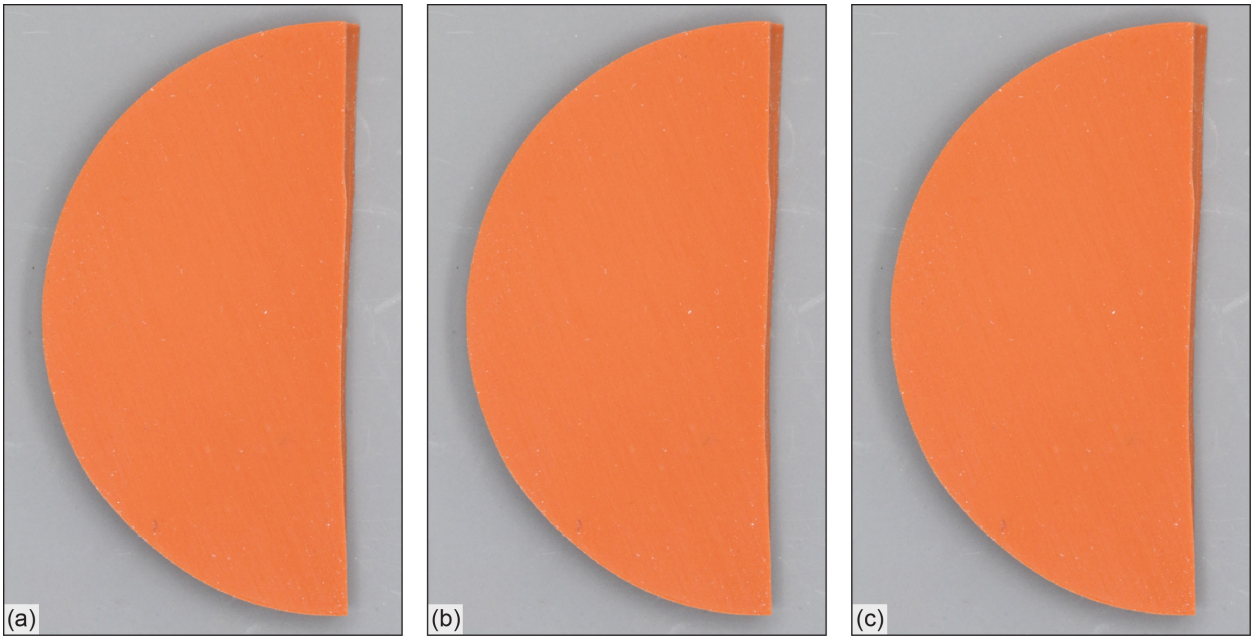

Figure 63.—Cleaned MISSE–12 Braycote® 601EF-coated test articles. (a) Unexposed. (b) Wake facing. (c) Ram facing.

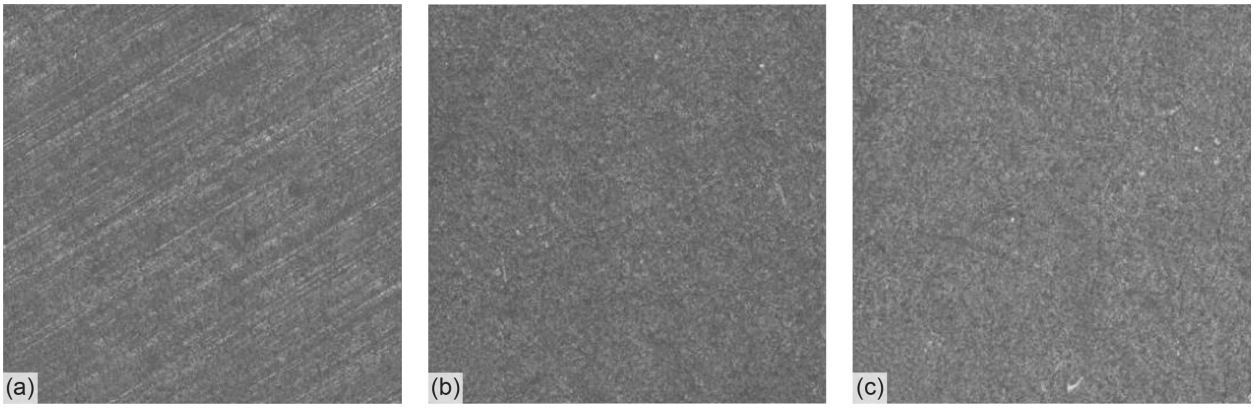

Figure 64.—Images of cleaned MISSE–13 Braycote® 601EF-coated flat ring surfaces at 20× magnification. (a) Unexposed. (b) Wake facing. (c) Zenith facing.

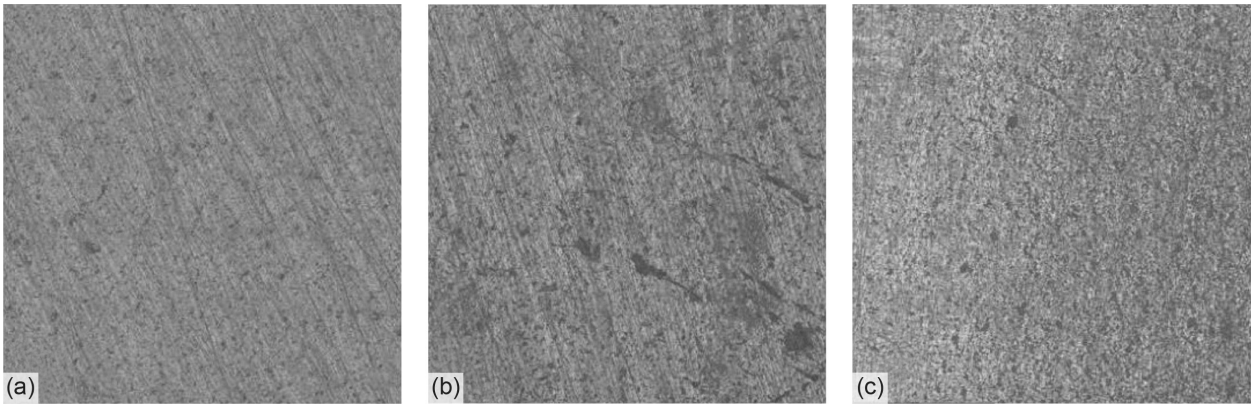

Figure 65.—Images of cleaned MISSE–12 Braycote® 601EF-coated test article surfaces at 20× magnification. (a) Unexposed. (b) Wake facing. (c) Ram facing.

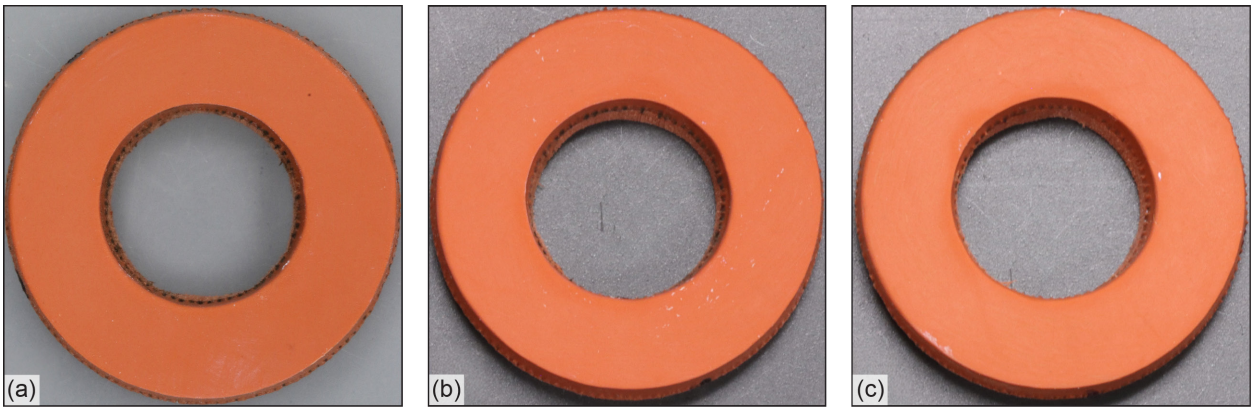

Figure 66.—Cleaned MISSE–13 BZ-coated flat rings. (a) Unexposed. (b) Wake facing. (c) Zenith facing.

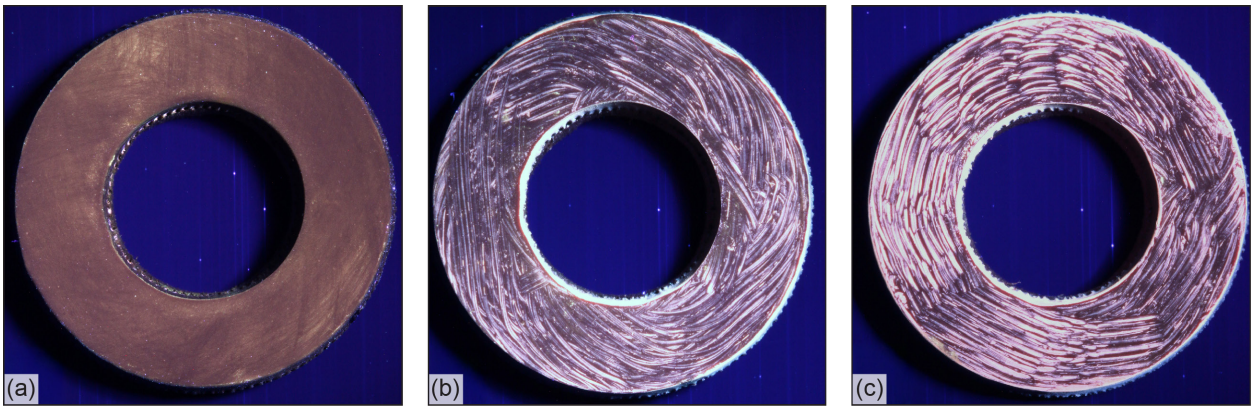

Figure 67.—Cleaned MISSE–13 BZ-coated flat rings illuminated with 365-nm-wavelength UV light. (a) Unexposed. (b) Wake facing. (c) Zenith facing.

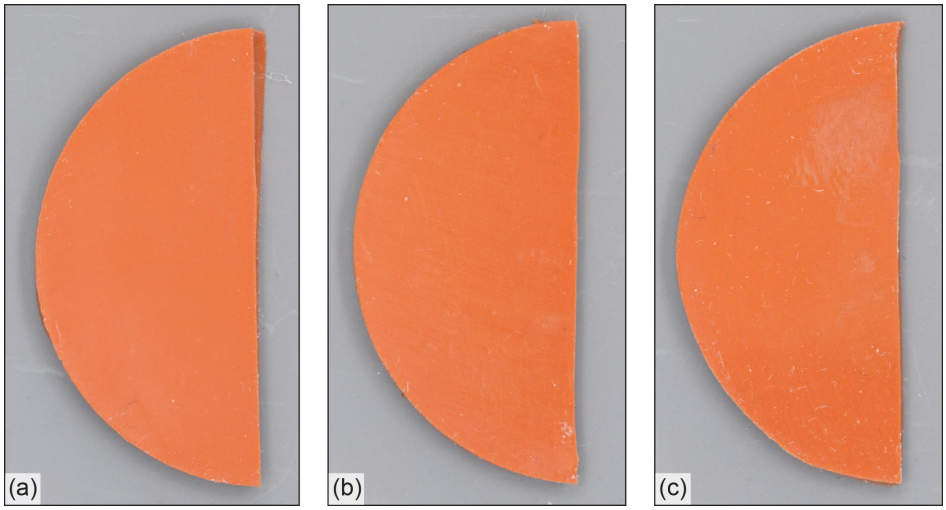

Figure 68.—Cleaned MISSE–12 BZ-coated test articles. (a) Unexposed. (b) Wake facing. (c) Ram facing.

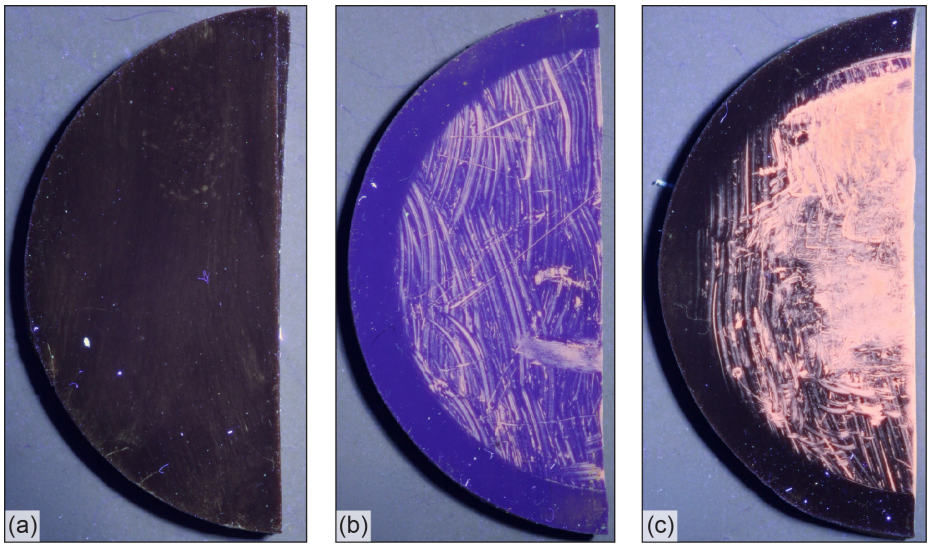

Figure 69.—Cleaned MISSE–12 BZ-coated test articles illuminated with 365-nm-wavelength UV light. (a) Unexposed. (b) Wake facing. (c) Ram facing.

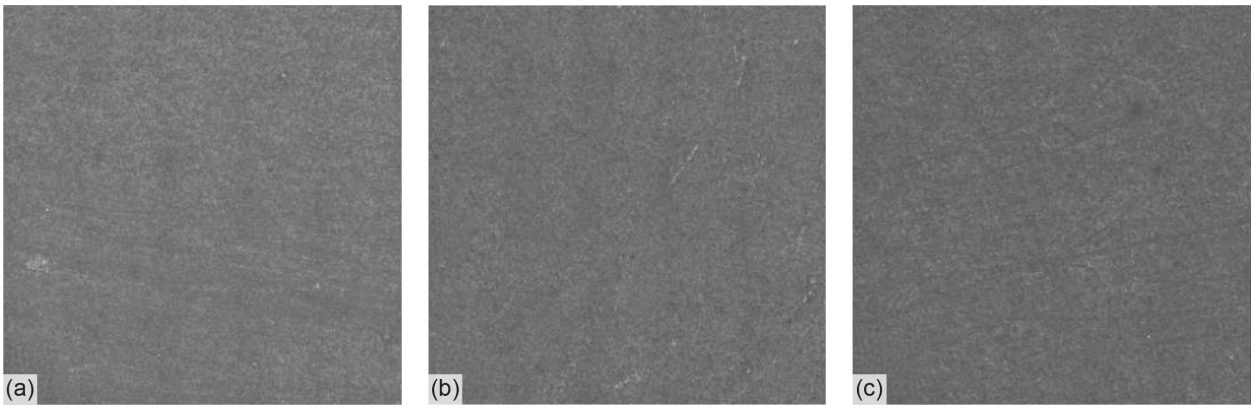

Figure 70.—Cleaned MISSE–13 BZ-coated flat ring surfaces at 20× magnification. (a) Unexposed. (b) Wake facing. (c) Zenith facing.

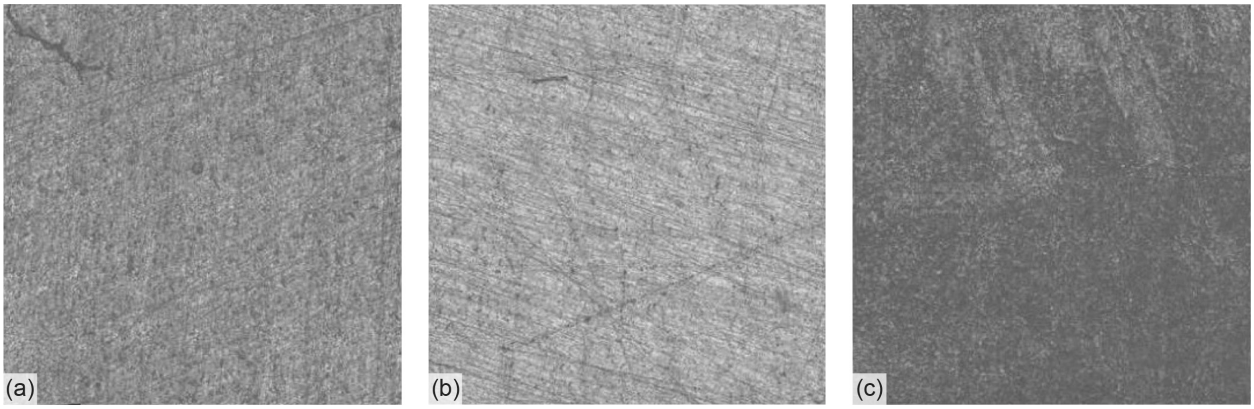

Figure 71.—Cleaned MISSE–12 BZ-coated test article surfaces at 20× magnification. (a) Unexposed. (b) Wake facing. (c) Ram facing.

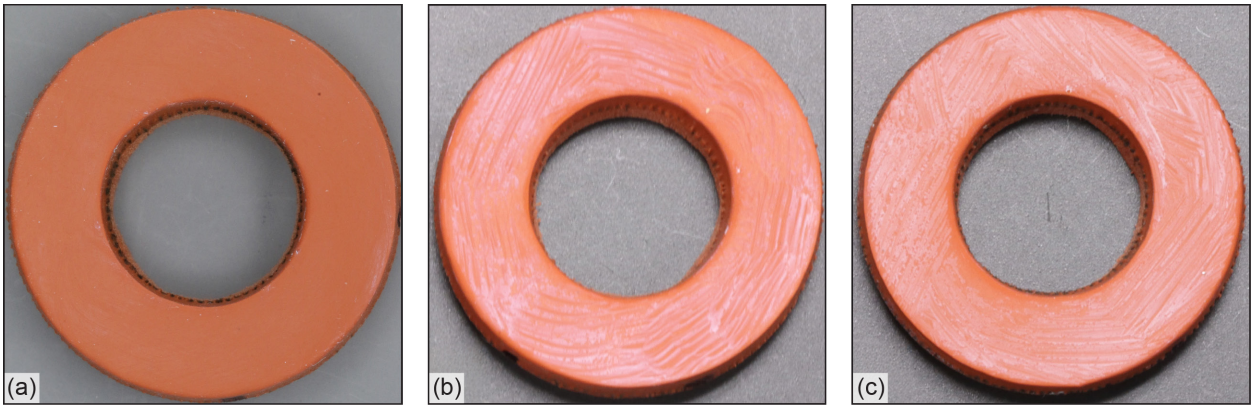

Figure 72.—Cleaned MISSE–13 DCZ-coated flat rings. (a) Unexposed. (b) Wake facing. (c) Zenith facing.

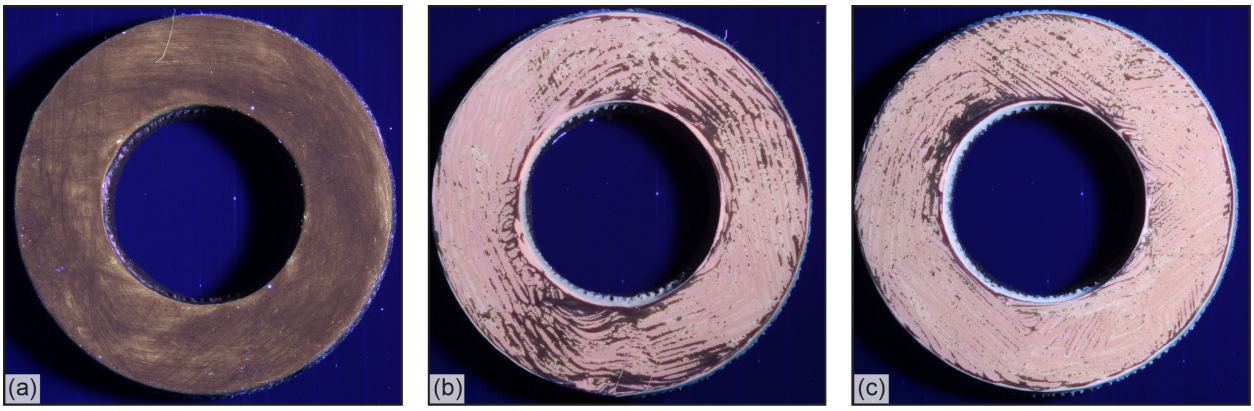

Figure 73.—Cleaned MISSE–13 DCZ-coated flat rings illuminated with 365-nm-wavelength UV light. (a) Unexposed. (b) Wake facing. (c) Zenith facing.

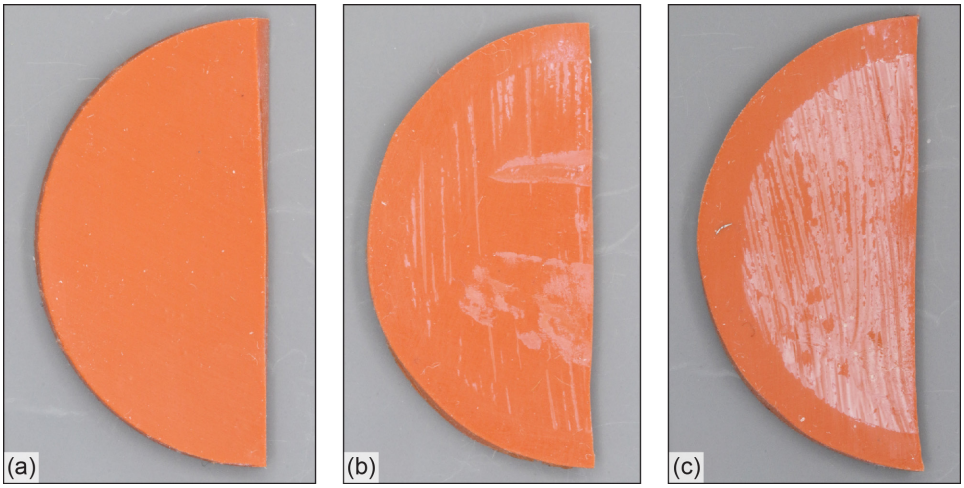

Figure 74.—Cleaned MISSE–12 DCZ-coated test articles. (a) Unexposed. (b) Wake facing. (c) Ram facing.

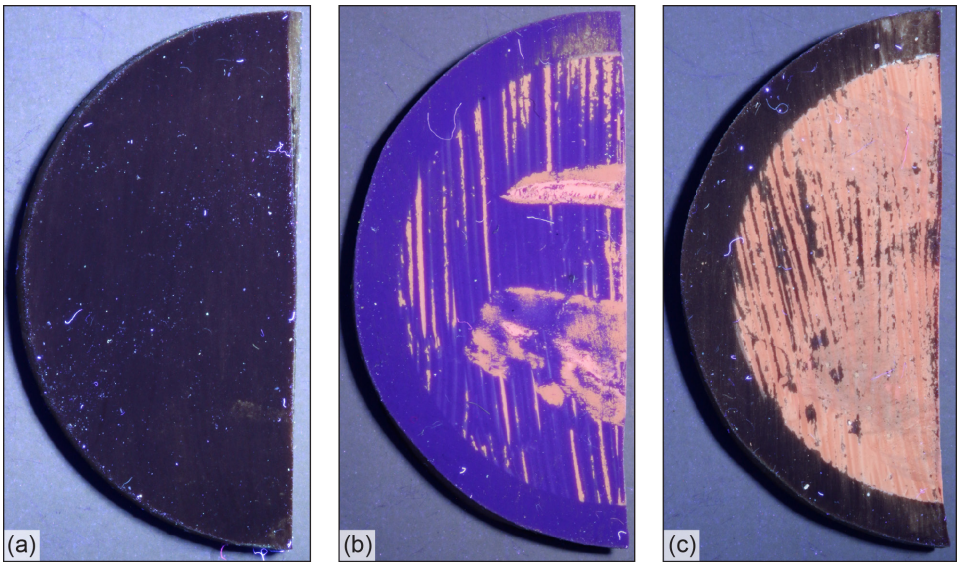

Figure 75.—Cleaned MISSE–12 DCZ-coated test articles illuminated with 365-nm-wavelength UV light. (a) Unexposed. (b) Wake facing. (c) Ram facing.

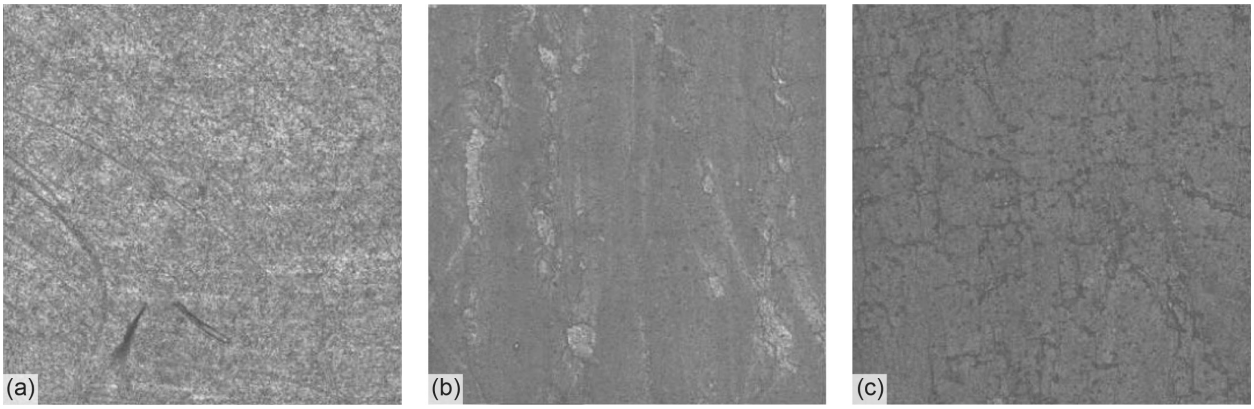

Figure 76.—Images of cleaned MISSE–13 DCZ-coated flat ring surfaces at 20× magnification. (a) Unexposed. (b) Wake facing. (c) Zenith facing.

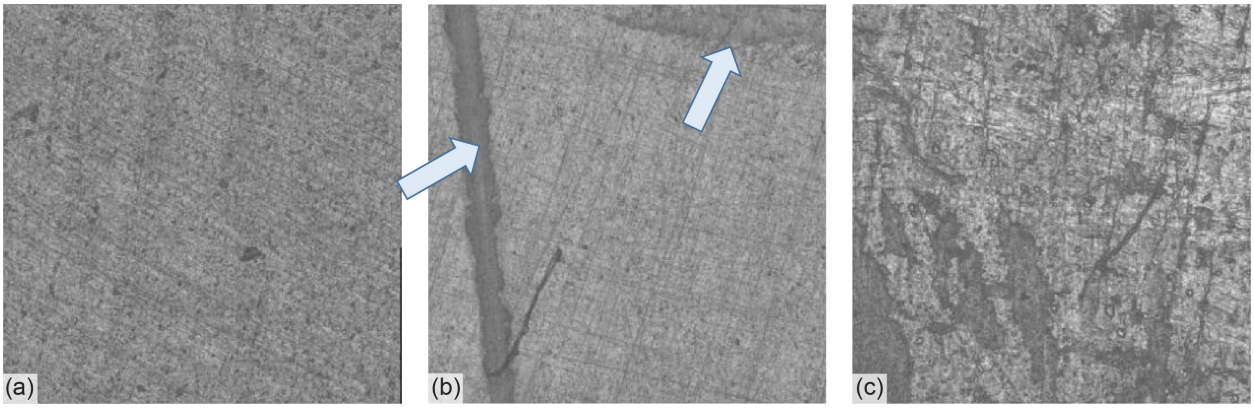

Figure 77.—Images of cleaned MISSE–12 DCZ-coated test articles surfaces at 20× magnification. (a) Unexposed. (b) Wake facing. (c) Ram facing.

5.5 Mass

The mass of the backup controls and flight test articles was measured when the test articles were prepared and again upon receipt postflight. The time between measurements was 3.5 yr (MISSE–13 test article assemblies) and 4 yr (MISSE–12 test articles). Caution should be exercised when comparing mass differences for the coated test articles, because any inadvertent disturbance (i.e., wiping off) of the coating skews the results. As shown in Table VI, the measured mass-loss range was 0 to 0.5% for all test articles (controls and flight), and any change in mass was deemed insignificant. The absence of mass loss was expected for the S0383–70 elastomer, as it has been successfully used in space programs for a docking seal.

5.6 Durometer Hardness

One ground-control button of each of the following test article types was used for durometer hardness testing: S0383–70, 1.5% TiO_2, and Braycote® 601EF. The standard followed for measuring the durometer hardness was ASTM D2240 (Ref. 14), and a Rex Gauge instrument that reported M-scale durometer hardness was used, as Type M is intended for materials with a thickness of 0.050 in. or greater. As specified in the standard, five measurements were taken of each button, with the average reported as the durometer hardness and the standard deviation as the error. Three sets of measurements were taken for

TABLE VI.—MASS LOSS OF MISSE–13 TEST ARTICLES AS PERCENTAGE OF INITIAL MASS

Test article type	Flight	Mass loss, %				
		Backup controls		Wake	Zenith	Ram
S0383–70	MISSE–13	0.2	0.2	0.3	0.2	---
	MISSE–12	0.0	0.1	0.2	---	0.0
1.5% TiO_2	MISSE–13	0.1	0.2	0.2	0.2	---
		0.2	0.1			
Braycote® 601EF-coated	MISSE–13	0.0	0.0	0.2	0.1	---
	MISSE–12	0.2	0.1	0.3	---	0.5
BZ coated	MISSE–13	0.1	0.1	0.2	0.2	---
	MISSE–12	0.0	0.1	0.2	---	0.5
DCZ coated	MISSE–13	0.1	0.1	0.2	0.2	---
	MISSE–12	0.1	0.1	0.1	---	0.0

each of the test control articles. The first set was taken on October 11, 2019; these were the preflight values. The second and third sets of measurements were taken after the flight test articles returned to NASA Glenn 3.5 yr later. These measurements were taken on April 11, 2023, and January 12, 2024. As shown in Figure 78, there was no significant difference in the measured durometer hardness for the unexposed controls between the preflight and postflight conditions, indicating that the factor of time, by itself, did not affect the surface durometer.

In addition to the measurements taken of the ground controls on January 12, 2024, measurements of the flight test article buttons were taken. The flight test articles were the same half of the button that was used for the SEM imaging. The durometer hardness of the exposed surface was measured after the SEM imaging was completed, and the surfaces were wiped with solvents to explore the durability of the coating. The unexposed buttons for the S0383–70, 1.5% TiO_2, and Braycote® 601EF surfaces were from the ground control test articles; the BZ and DCZ buttons were from the wake backup test articles. As shown in Figure 79, the surfaces exposed to space environments (wake facing and zenith facing) had a small increase in durometer hardness. The same trend was observed with the MISSE–12 test articles (Figure 80); the measured durometer hardness of the exposed test articles was slightly greater than that of the unexposed control test articles. Of the space-exposed test articles, the durometer hardness of the Braycote® 601EF-coated surfaces increased the most for the MISSE–13 specimens and the MISSE–12 ram-facing specimen. The MISSE–12 baseline material for both the ram-facing and wake-facing test articles had increases in durometer hardness similar to those for the MISSE–12 ram-facing Braycote® 601EF-coated test article. The smallest increase in durometer hardness was the MISSE–13 DCZ wake-facing test article. From these results, it appears the DCZ coating provided some protection from the space environment. Caution should be used when comparing increases in durometer hardness observed for MISSE–12 test articles with those observed for MISSE–13 test articles for the same coatings, because the MISSE–12 test articles were 2.75 times thinner than the MISSE–13 test articles. However, it can be stated that the increase in durometer hardness was an indication that some change to the surface material occurred because of space environments exposure.

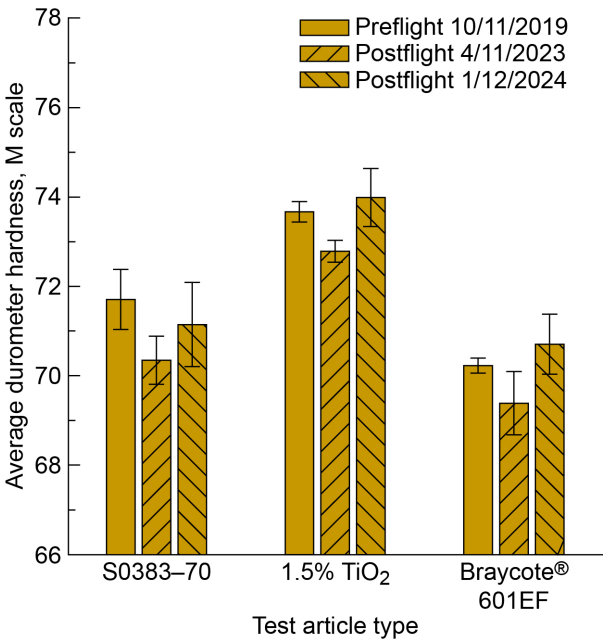

Figure 78.—Durometer hardness measurements of MISSE–13 ground control test articles preflight and unexposed postflight.

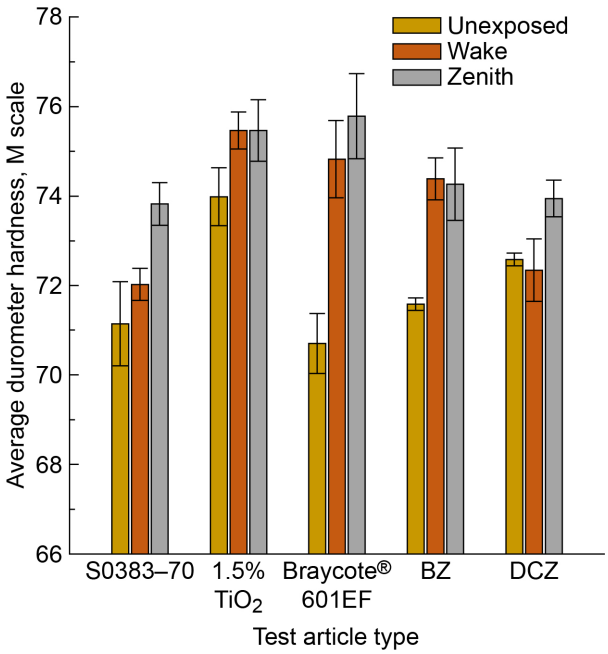

Figure 79.—Durometer hardness measurements of MISSE–13 test article surfaces postflight.

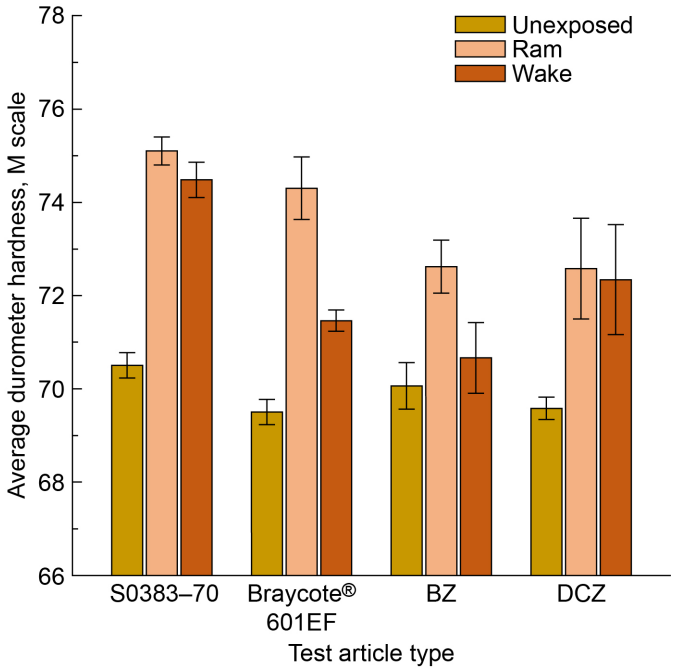

Figure 80.—Durometer hardness measurements of MISSE–12 test articles surfaces postflight.

6.0 Results—Leak Rate Tests

To characterize the performance of the materials, leak rate tests with the flat rings of the MISSE–13 test assemblies were performed using a pressure decay method with a mass-point leak rate analysis (Refs. 15 and 16). For a given test, the test article was installed between two flat plates, with shim stacks

at each fastener location. The height of the shim stacks was set to achieve a nominal 20% compression of the flat ring. The volume upstream of the test article was pressurized to approximately 2 atm with dry air, which decayed as the air permeated through the material and flowed across the sealing interfaces to ambient pressure. The leak rate tests were conducted at a controlled temperature of 21.6 °C (preflight) and 21.3 °C (postflight) in a Tenney® (TPS, LLC) environmental chamber, model BTRC. The gas pressure and temperature were recorded over time, and the ideal gas law was used to calculate the mass in the system at each time step. From the first-order linear regression of the mass–time data set, the leak rate was calculated for a nominal differential pressure of 14.7 psid across the test article.

6.1 Preflight and Unexposed Test Articles

The leak rates of the ground control test articles were measured prior to MISSE–13 flight in November 2019. The results showed that regardless of the surface condition (i.e., coated or uncoated), there was no difference in leak rate among the ground control test articles, indicating that the coatings did not increase or decrease the leakage at the mating interface; the leak rate was dominated by permeation through the elastomer. The initial average measured leak rate was 6.75±0.18 ng/s. The same test articles were retested after the MISSE–13 flight in April and July 2023. The average postflight leak rate of the ground control test articles was 6.87±0.06 ng/s, and as shown in Figure 81, there was no difference in leak rate from the preflight measurements. There was a difference in the magnitude of the measurement uncertainties (i.e., error bars) between 2019 and 2023, which was directly related to the test volume. In most of the 2023 leak rate tests, the test volume was approximately one-fourth of the test volume in 2019. Figure 82 groups the leak rate measurements by test article type (e.g., S0383–70 baseline material, Braycote® 601EF-coated, etc.) and includes the unexposed flight backup test articles along with the ground control test articles. The average leak rate for each test article type is listed in Table VII. Given that the coating did not affect the leak rate of the flat ring, the average leak rate measured for all unexposed test articles (preflight, postflight, and all test article types) was calculated. The average leak rate measured for all unexposed test articles was 6.77±0.07 ng/s.

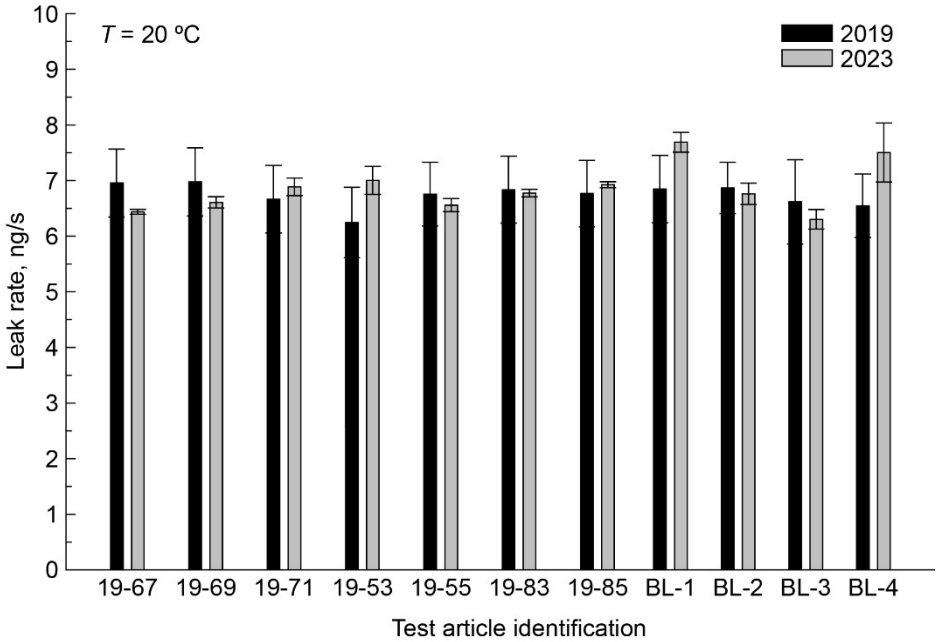

Figure 81.—Leak rates from ground control test articles measured in 2019 and 2023.

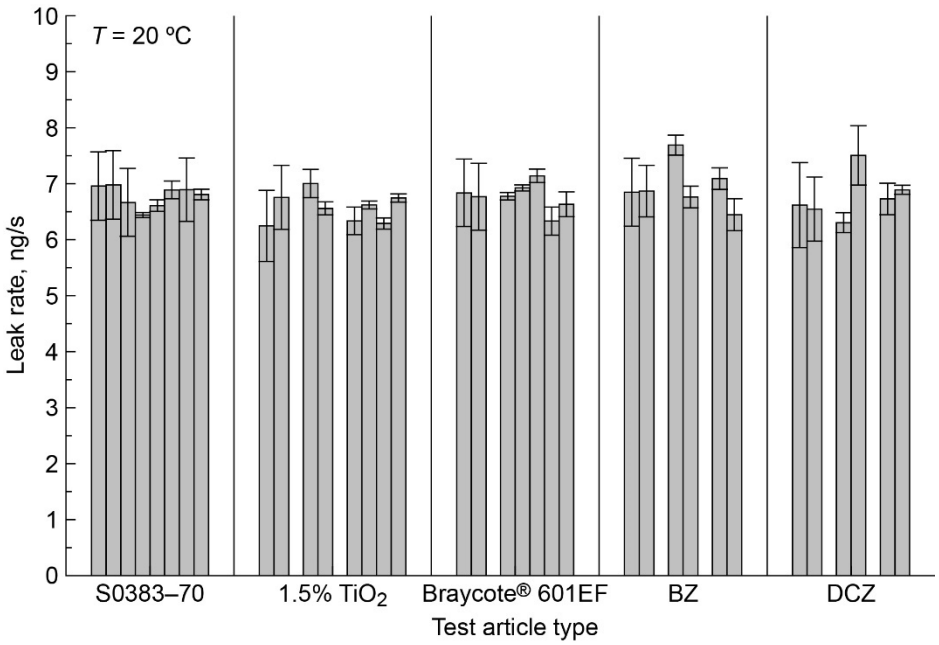

Figure 82.—Leak rates of ground control and backup test articles grouped by test article type.

TABLE VII.—AVERAGE LEAK RATES FOR UNEXPOSED TEST ARTICLES BY TEST ARTICLE TYPE

Test article type	Leak rate, ng/s
S0383–70 baseline material	6.79±0.15
1.5% TiO_2	6.58±0.12
Braycote® 601EF coating	6.79±0.13
BZ coating	6.96±0.15
DCZ coating	6.78±0.19

6.2 Postflight Leak Rate Measurements

Postflight leak rate tests of the exposed test articles were completed in June and July 2023. Figure 83 compares the leak rates of the test articles exposed to space environments in the wake-facing direction, and Figure 84 compares the leak rates of the test articles exposed in the zenith-facing direction. As shown in the figures, the leak rates of the S0383–70 and 1.5% TiO_2 test articles were significantly greater than the leak rate for an unexposed test article—840 to 1,360 times as great. For both exposure directions, the 1.5% TiO_2 test articles had the largest measured leak rates, with the zenith-facing test article having a leak rate greater than that of the wake-facing test article. Exposure to UV radiation is known to cause damage to silicone elastomers, and the increase in leak rate from the baseline values was attributed to this exposure. In addition, the larger leak rates for the zenith-facing test articles provided more evidence that the Aegis-reported values for UV exposure were probably low. The leak rates for all coated space-exposed test articles were not significantly different from the leak rates for the unexposed baseline material. Leak rates for the Braycote® 601EF-coated and BZ-coated zenith-facing test articles were only 3 to 6% greater than the average unexposed test article leak rate. In the wake-facing direction, the

DCZ-coated and Braycote® 601EF-coated test articles had leak rates slightly less (approx. 10%) than the average leak rate of the unexposed test articles. The leak rate of the BZ-coated test article was slightly more than the unexposed average leak rate value (approx. 7%). For each material type, the leak rates for the different exposure conditions were compared (Figure 85 through Figure 89). As shown in the figures, the coated test articles outperformed the S0383–70 baseline material and 1.5% TiO_2 material.

During a leak test, the coating on the test article was disturbed due to the mating interface plate contacting and compressing the test article. For this reason, three coated test articles were selected and subjected to additional leak rate tests to evaluate the effect of multiple mating sequences. Two Braycote® 601EF-coated test articles were selected because (1) the use of this grease is typical for space vehicle applications and (2) the coatings were thinly applied. A DCZ test article was selected because (1) the DCZ coating (and BZ coating) was intended to act as a sunscreen, and therefore a thicker coating was applied, and (2) the zenith-facing test article had a greater leak rate than the DCZ wake-facing test article and the BZ-coated test articles (wake facing and zenith facing). The Braycote® 601EF-coated wake-facing and zenith-facing test articles were retested 22 and 21 days, respectively, after the first leak rate tests. The DCZ-coated test article was retested 11 days later. There was no difference in the measured leak rate of the Braycote® 601EF-coated test articles; however, the leak rate of the DCZ-coated test article increased from 14.9 to 95.4 ng/s. The increase in leak rate was attributed to an increase in the interface leakage from the disturbance of the coating.

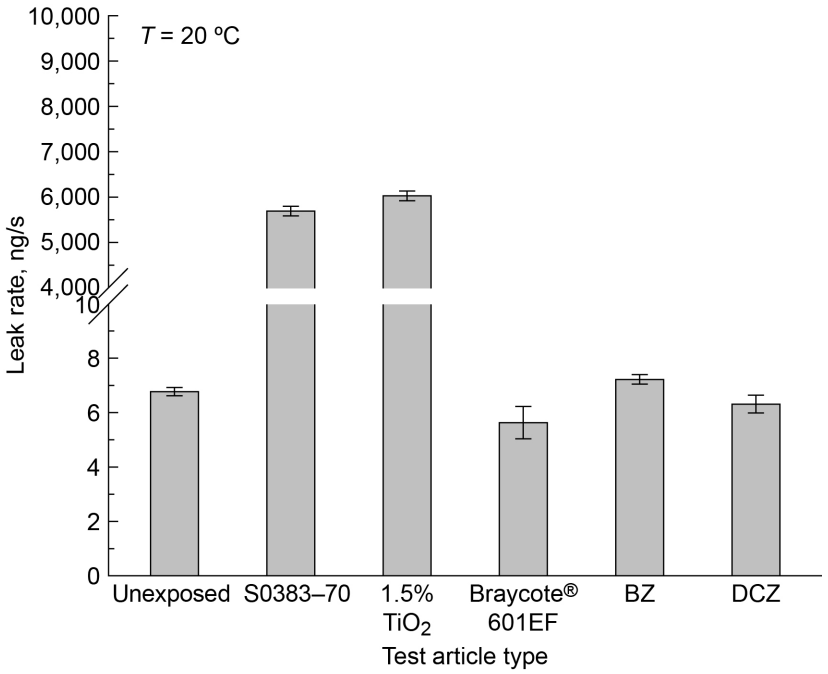

Figure 83.—Leak rates for unexposed baseline material test article and wake-facing test articles.

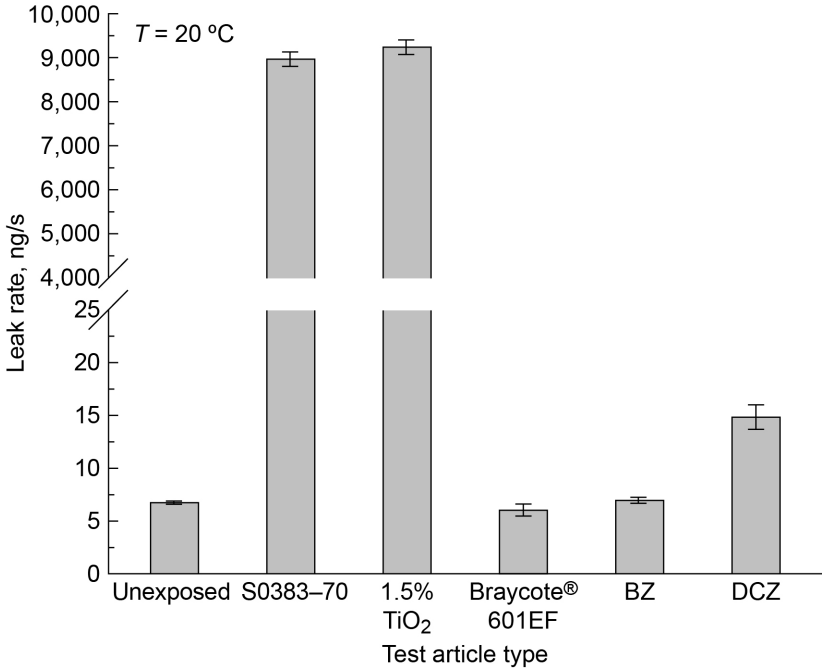

Figure 84.—Leak rates for unexposed baseline material test article and zenith-facing test articles.

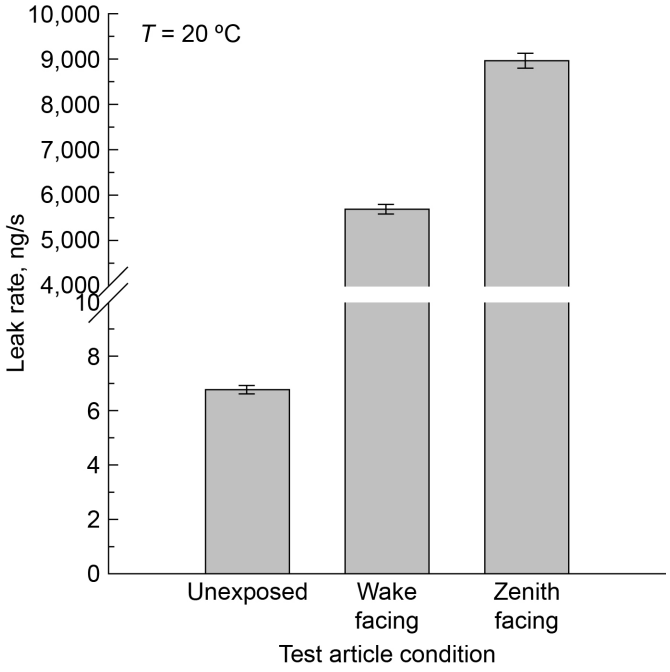

Figure 85.—Leak rates for unexposed baseline material, wake-facing baseline material, and zenith-facing baseline material test articles.

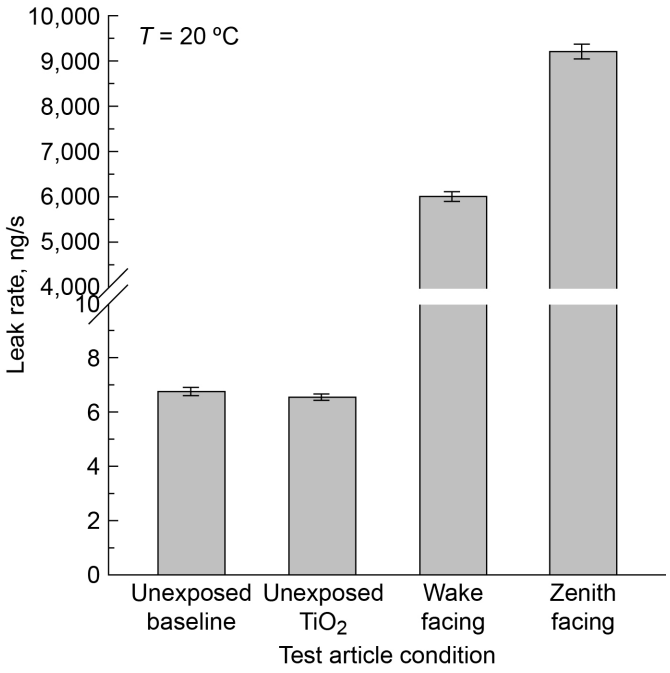

Figure 86.—Leak rates for unexposed baseline material, unexposed 1.5% TiO_2 material, wake-facing TiO_2 material, and zenith-facing 1.5% TiO_2 material test articles.

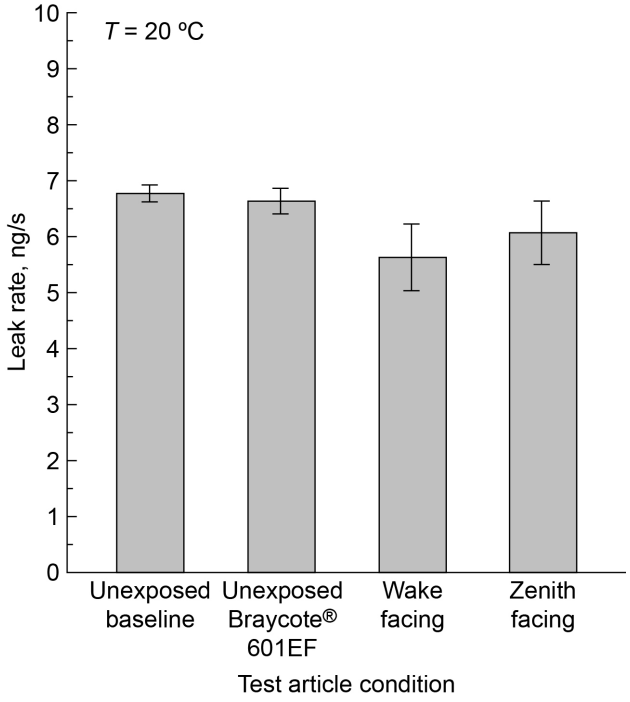

Figure 87.—Leak rates of unexposed baseline material, unexposed Braycote® 601EF-coated, wake-facing Braycote® 601EF-coated, and zenith-facing Braycote® 601EF-coated test articles.

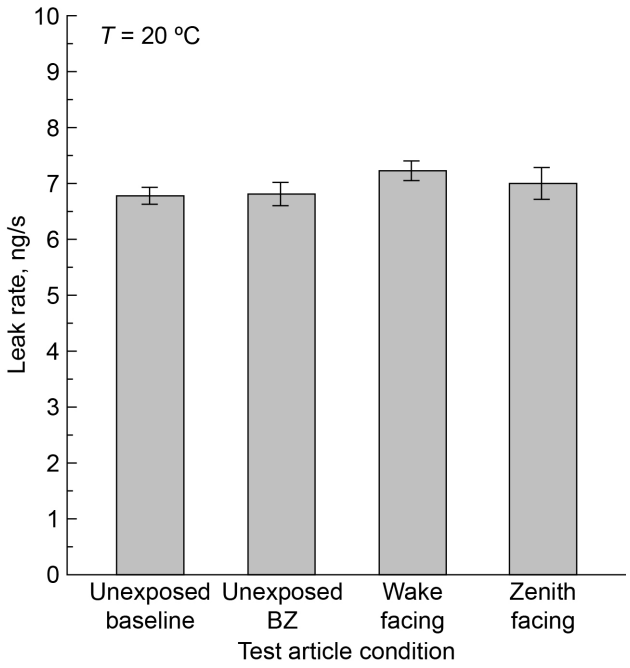

Figure 88.—Leak rates of unexposed baseline material, unexposed BZ-coated, wake-facing BZ-coated, and zenith-facing BZ-coated test articles.

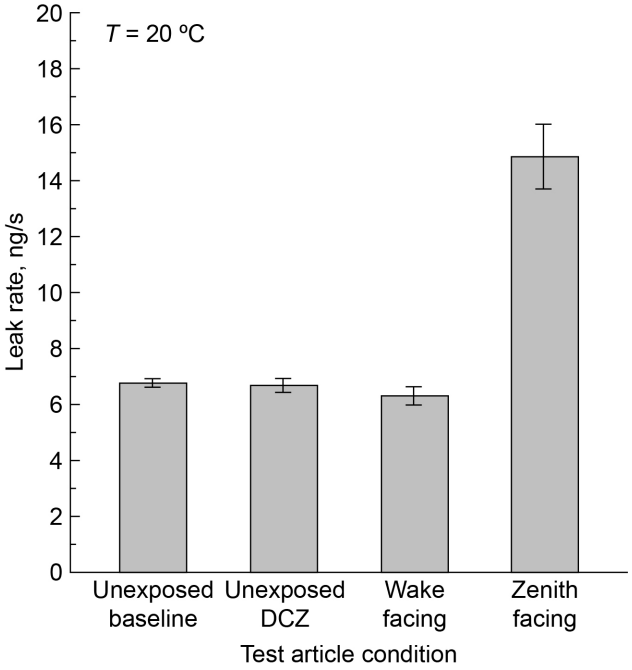

Figure 89.—Leak rates of unexposed baseline material, unexposed DCZ-coated, wake-facing DCZ-coated, and zenith-facing DCZ-coated test articles.

6.3 Postflight Leak Rate Measurements After Surface Cleaning

After the postflight leak rate tests, the coatings were cleaned from the flat ring surfaces to evaluate (1) the durability of the coating, (2) whether the underlying material was damaged, and (3) if the leak rate of the cleaned flat ring was in-family with the leak rate of the unexposed uncoated baseline material. Refer to Section 5.0 for the evaluation of the coating and inspection of the cleaned surfaces. As shown in Figure 90 and Figure 91 for the S0383–70 and 1.5% TiO_2 materials, respectively, the leak rates for the cleaned surfaces were less than the postflight leak rates for both the wake-facing and zenith-facing test articles. However, the leak rates were still significantly greater than those measured for the unexposed test articles. In other studies of S0383–70 exposed to UV radiation, it was observed that as the damaged elastomer surface remained compressed, the leak rate decreased until it reached some steady-state value. Therefore, it was not surprising to see decreases in the leak rates of the cleaned flat rings. The measured leak rates for the cleaned wake-facing and zenith-facing Braycote® 601EF flat rings (approx. 1,600 and 1,900 ng/s, respectively) were unexpected given that the postflight leak rates were in-family with leak rates of the unexposed test articles (Figure 92). Each flat ring and leak test system was inspected at the end of the test; no gross physical damage (e.g., cuts or scratches) or FOD was found. The flat rings were retested, and the second leak rate results were in-family with the first measurements (1,600 and 1,900 ng/s). Because no damage or FOD was found, the increase in leak rates was attributed to damage to the elastomer material that resulted in interface leak paths. The leak rates of the cleaned BZ and DCZ flat rings were in-family with the postflight leak rates, as shown in Figure 93 and Figure 94.

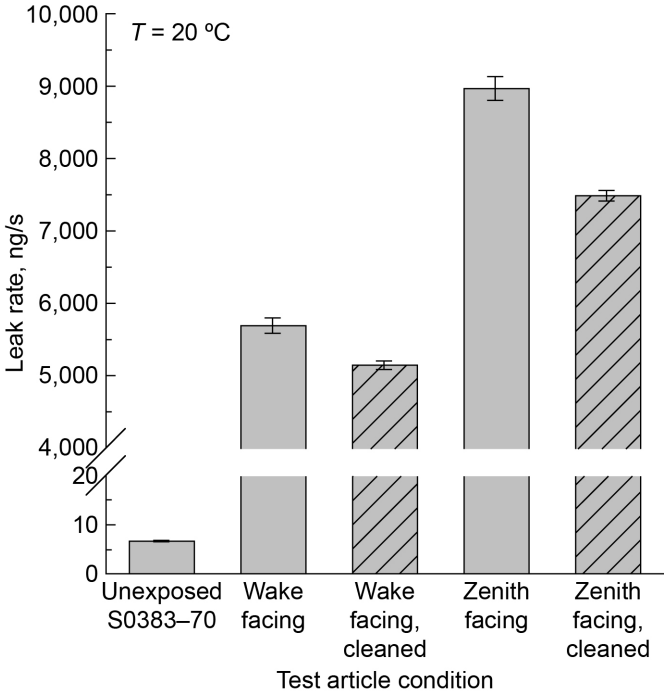

Figure 90.—Leak rates from wake-facing and zenith-facing baseline material S0383–70 test articles postflight and after surface cleaning.

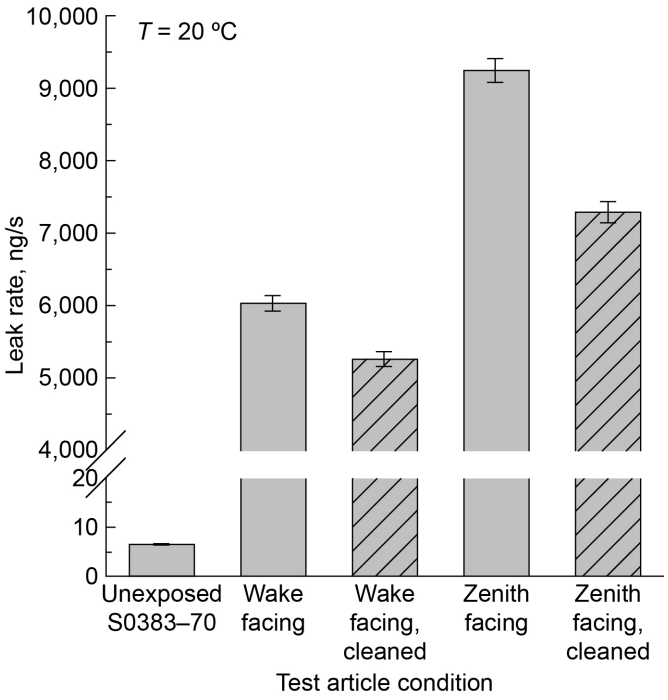

Figure 91.—Leak rates from wake-facing and zenith-facing 1.5% TiO_2 test articles postflight and after surface cleaning.

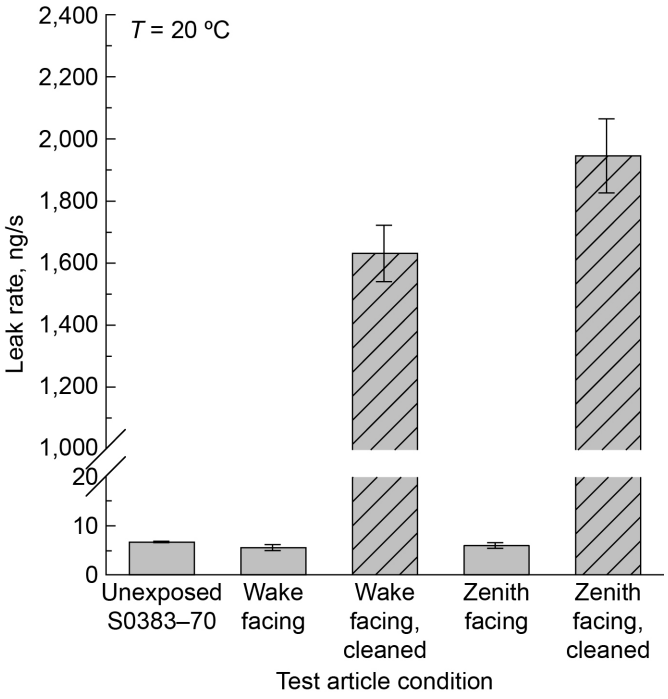

Figure 92.—Leak rates from wake-facing and zenith-facing Braycote® 601EF-coated test articles postflight and after surface cleaning.

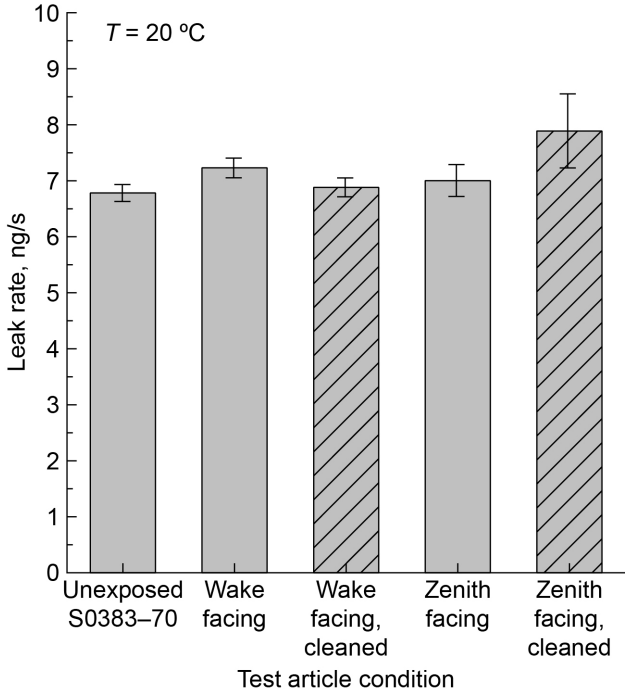

Figure 93.—Leak rates from wake-facing and zenith-facing BZ-coated test articles postflight and after surface cleaning.

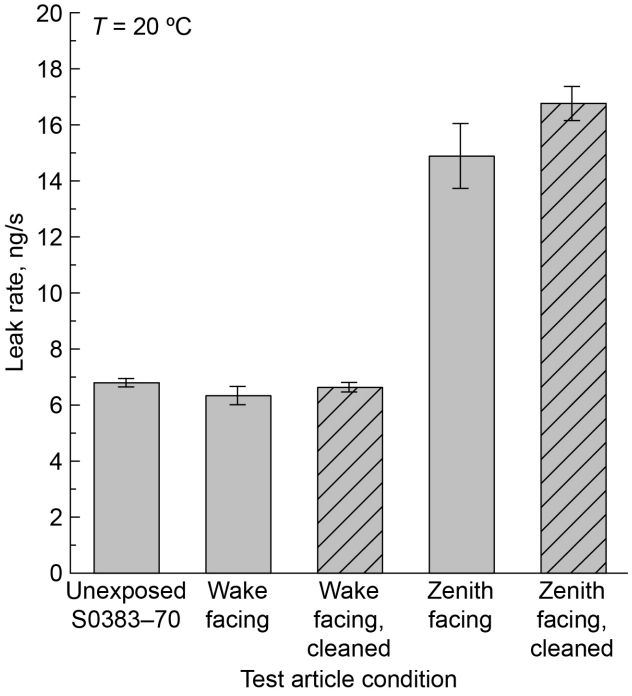

Figure 94.—Leak rates from wake-facing and zenith-facing DCZ-coated test articles postflight and after surface cleaning.

7.0 Summary of Results

The silicone compound S0383–70 is a space-rated material used on space vehicles in sealing applications (e.g., NASA Docking System docking hatch seals). Often the seals are directly exposed to the space environment. Using the Materials International Space Station Experiment Flight Facility (MISSE–FF), S0383–70 test articles were exposed to space environments as part of the MISSE–12 and MISSE–15 Polymers and Composites Experiments 3 (PCE–3) and the MISSE–13 PCE–4 experiments. The effects of simultaneous exposure to space environments (temperature, vacuum pressure, atomic oxygen (AO), and ultraviolet (UV) radiation) on the silicone compound were explored for test articles fabricated from S0383–70 with coatings applied to the surface. The following three coatings were tested: Braycote® (BP Lubricants USA Inc.) 601EF grease, Braycote® 601EF plus Z–COTE® (designated as BZ), and Dow Corning® 7 (DC7) grease (Dow Corning Corp.) plus Z–COTE® (designated as DCZ). In addition, test articles fabricated from a reformulated silicone compound (S0383–70 plus 1.5% TiO_2) were part of the investigation. The Braycote® 601EF-coated test articles represented current-use configuration of the S0383–70 material as a docking seal. The other two coatings were sunscreens developed at the NASA Glenn Research Center to prevent damage to the elastomer from UV radiation. Like the sunscreen coatings, the reformulated compound was designed to minimize the effects of UV radiation. Instead of a coating, the UV-blocking material (TiO_2) was incorporated into the baseline material (S0383–70), thus eliminating the potential unfavorable characteristics that come along with a coating, namely, application uniformity, foreign object debris (FOD) collector, and reduction or removal of the coating over time or through multiple mating and unmating sequences.

Semicircular test articles and test article assemblies, each composed of a button and flat ring, were flown facing the ram, wake, or zenith direction. In the ram direction, the AO exposure was two orders of magnitude greater than that of the other directions, and the UV radiation exposure was approximately twice as great. In the wake and zenith directions, the AO exposure was comparable; however, the UV exposure for the zenith direction was greater than the UV exposure for the wake direction. All test articles showed some effect from the space environment exposures, as seen in the fluorescence change, durometer hardness change, the formation of a layer of material at the exposed surface, and change in sealing capability.

When comparing the exposed surfaces with the unexposed control surfaces, a change in fluorescence was observed, indicating some change at the molecular level. The unexposed S0383–70, 1.5% TiO_2, and Braycote® 601EF test articles did not fluoresce in 365-nm-wavelength UV light; however, the surfaces exposed to space environments did. The exposed surfaces fluoresced pink light. The unexposed BZ-coated and DCZ-coated surfaces fluoresced green light from the ZnO in the coating under 365-nm UV light, and the exposed coatings fluoresced white with a pinkish tint. This showed a change in fluorescence after exposure to space environments.

In general, the durometer hardness of the exposed material was greater than that of the unexposed material; however, durometer increases were small and inconsistent. The average increase for the uncoated S0383–70 baseline material after space exposure was approximately 5% as measured on the M-scale. The average durometer hardness increase for the Braycote® 601EF-coated test articles was slightly more than the baseline material average increase, indicating that UV radiation may have passed through the coating, causing damage to the elastomer. On average, the durometer hardness increase for the test articles with the ZnO coatings and the TiO_2 was less than the baseline material increase, indicating that these coatings provided some protection to the elastomer.

Evidence of changes or damage to the surface was also observed in the photographs and scanning electron microscopy (SEM) images of the unexposed and exposed test articles. Photographs and visual

inspection of the test articles showed that the coatings on the exposed surfaces appeared more dried out and cracked than the unexposed coatings. Despite these observed changes, the coatings still provided protection to the underlying material. In addition, SEM images of the surface showed areas where the coating was removed or spalled from the surface. SEM images of button cross sections showed that the baseline S0383–70 and Braycote® 601EF-coated buttons had a 21- to 31-μm layer at the surface that appeared to be different than the remaining bulk material. A thinner layer was observed in the 1.5% TiO_2 test article. This layer was not seen in the BZ or DCZ images, thereby providing evidence of the utility of these coatings.

Leak rate performance results showed that the coatings protected the S0383–70 material. The leak rate of the baseline material exposed to space environments significantly increased to an unacceptable level, from 6.79±0.15 to 5700±110 ng/s (wake-facing direction) and 8980±160 ng/s (zenith-facing direction). The leak rates of the exposed BZ flat rings were no different than the leak rates of the unexposed BZ flat rings for both the wake-facing and zenith-facing directions. Likewise, the wake-facing flat ring coated with DCZ showed no difference in leak rate compared to the unexposed DCZ-coated flat ring. There was a measurable increase in leak rate for the DCZ zenith-facing flat ring, from 6.71±0.25 to 14.89±1.16 ng/s. The reformulated silicone compound with TiO_2 embedded in the material to block the UV radiation was not successful at eliminating or minimizing damage. The leak rates of the 1.5% TiO_2 test articles were in-family with the uncoated exposed baseline material (6,040±110 and 9,250±170 ng/s for wake facing and zenith facing, respectively); the concentration of the TiO_2 particles was not great enough to protect the material.

The durability of the coatings was evaluated in two ways. First, the leak rate tests were repeated to simulate multiple mating and unmating sequences. The Braycote® 601EF-coated test articles and a DCZ-coated test article were selected for repeat tests. There was no difference measured in leak rate between the initial and repeated test for the Braycote® 601EF wake-facing and zenith-facing test articles, whereas the leak rate of the zenith-facing DCZ-coated flat ring increased by a factor of approximately 6. The repeated tests demonstrated that the thin coating of Braycote® 601EF was not affected by the mating and unmating sequence, whereas the thicker DCZ coating was. The second evaluation of the coating was based on the ease of cleaning the coating from the surface. The coatings on the unexposed surfaces were easily removed with the solvent-soaked wipe. Most of the Braycote® 601EF and BZ coating from the exposed test articles was removed with a thin film remaining. The DCZ coating, in contrast, was not easily removed. The DCZ coating exposed to space environments was the most durable with respect to removal by mechanical wiping. After the surfaces were cleaned of the coatings, the leak rate tests were repeated. The leak rates of the baseline S0383–70, 1.5% TiO2, BZ-coated, and wake-facing DCZ-coated test articles remained the same as the postflight leak rates. The leak rates of the Braycote® 601EF-coated test articles significantly increased by 270 and 320 times, wake facing and zenith facing, respectively, thereby confirming indications of damage seen in durometer and SEM analyses. The leak rate of the cleaned zenith-facing DCZ-coated flat ring decreased from 6 times as great after the repeat test to approximately the same as the initial postflight leak rate. The leak rate of the DCZ test article after repeated testing and cleaning was on the order of the initial postflight results and unexposed baseline leak rates, indicating good protection of the elastomer.

Overall, the BZ and DCZ coatings provided protection to the S0383–70 elastomer from the damaging effects of space environments. The leak rates of the flat rings exposed to vacuum, AO, and UV radiation in both the wake-facing and zenith-facing directions were comparable to the leak rate for an uncoated unexposed S0383–70 flat ring. The coatings were durable and still intact at the end of the mission. The positive results obtained from the MISSE–12 and MISSE–13 test articles will aid in the continued advancement of the BZ and DCZ coatings as viable options for silicone space seals.

Based on the results and findings from the MISSE–12 and MISSE–13 test articles, the following forward work was identified:

1. Investigate what changes occur in the molecular structure of silicone elastomer compound S0383–70 after exposure to UV radiation that results in the material fluorescing.
2. Investigate the chemical structure of the exposed surface layer compared to the bulk material of S0383–70.
3. Conduct additional MISSE–FF space environment exposures with BZ- and DCZ-coated test articles in the wake-facing and zenith-facing directions to confirm leak rate results and physical property findings.
4. Conduct MISSE–FF space environment exposures with BZ- and DCZ-coated test articles in the ram-facing and nadir-facing directions to evaluate the effects of different AO and UV radiation exposure levels on sealing performance (i.e., leak rate).
5. Evaluate the effect of multiple mating and unmating sequences, coupled with intermittent exposure to UV radiation, on BZ- and DCZ-coated test articles and their subsequent leak rates and adhesion force values.

References

1. de Groh III, Henry C., et al.: Anti-adhesion Elastomer Seal Coatings for Ultraviolet and Atomic Oxygen Protection. J. Appl Polym. Sci., vol. 132, no. 11, 2015.
2. Imka, Emily C., et al.: Effects of Low Earth Orbit on Docking Seal Materials. NASA/TM—2014-218435, 2014. https://ntrs.nasa.gov
3. de Groh III, Henry C., et al.: Effects of Atomic Oxygen and Grease on Outgassing and Adhesion of Silicone Elastomers for Space Applications. NASA/TM—2012-217263, 2012. https://ntrs.nasa.gov
4. de Groh, Henry C., et al.: Space Environment Effects on Silicone Seal Materials. NASA/TM—2010-216332, 2010. https://ntrs.nasa.gov
5. de Groh, Kim K.; and Banks, Bruce A.: Space Environmental Exposure of the MISSE 9-15 Polymers and Composites Experiment 1-4 (PCE 1-4). NASA/TM-20240000755, 2024. https://ntrs.nasa.gov
6. de Groh, Kim K.; and Banks, Bruce A.: MISSE-Flight Facility Polymers and Composites Experiment 1-4 (PCE 1-4). NASA/TM-20205008863, 2021. https://ntrs.nasa.gov
7. International Organization for Standardization: Space Environment (Natural and Artificial)—Process for Determining Solar Irradiances. ISO Standard 21348:2007, 2007.
8. ASTM E490–22: Standard Solar Constant and Zero Air Mass Solar Spectral Irradiance Tables. ASTM International, West Conshohocken, PA, 2022.
9. Aegis Aerospace: MISSE MSC UV Equivalent Sun Hours Calculation. Report (A. Goode, MEMO-MISSE-0004 Rev C03, August 17, 2022).
10. de Groh, Kim K., et al.: Erosion Results of the MISSE 7 Polymers Experiment and Zenith Polymers Experiment After 1.5 Years of Space Exposure. NASA/TM—2016-219167 (Corrected Copy), 2017. https://ntrs.nasa.gov
11. de Groh, Kim K.; Whitt, Austin; and Banks, Bruce A.: Effect of Space Exposure on the Tensile Properties of MISSE Teflon Flight Samples. NASA/TM-20250003725, 2025. https://ntrs.nasa.gov
12. de Groh, Kim K., et al.: Erosion Results of the MISSE 8 Polymers Experiment After 2 Years of Space Exposure on the International Space Station. NASA/TM—2017-219445, 2017. https://ntrs.nasa.gov

13. Wasowski, Janice L.; and Daniels, Christopher C.: Comparison of Leak Rates of In-Flight and Ground Based Exposed Silicone Elastomer Seals. Presented at the 2012 National Space and Missile Materials Symposium, Tampa, FL, 2012.
14. ASTM D2240–05: Standard Test Method for Rubber Property—Durometer Hardness. ASTM International, West Conshohocken, PA, 2005.
15. Garafolo, Nicholas G.; and Daniels, Christopher C.: Comprehensive Mass Point Leak Rate Technique. Part I: Methodology With Uncertainty and Experimental Error Analysis. Presented at the JSNDI/ASNT Fourth Japan-US Symposium on Emerging NDE Capabilities for a Safer World, Maui, HI, 2010.
16. Daniels, Christopher C.; and Garafolo, Nicholas G.: Comprehensive Mass Point Leak Rate Technique. Part II: Application of Methodology and Variable Influences. Presented at the JSNDI/ASNT Fourth Japan-US Symposium on Emerging NDE Capabilities for a Safer World, Maui, HI, 2010.